




2023

## How to Build a Cortex: Coordinated Assembly of Cortical Septins and Actomyosin in the Leader Bleb

Asia Marie Paguntalan

Follow this and additional works at: [https://ecommons.luc.edu/luc\\_theses](https://ecommons.luc.edu/luc_theses)

 Part of the [Cell Biology Commons](#)

---

### Recommended Citation

Paguntalan, Asia Marie, "How to Build a Cortex: Coordinated Assembly of Cortical Septins and Actomyosin in the Leader Bleb" (2023). *Master's Theses*. 4483.

[https://ecommons.luc.edu/luc\\_theses/4483](https://ecommons.luc.edu/luc_theses/4483)

This Thesis is brought to you for free and open access by the Theses and Dissertations at Loyola eCommons. It has been accepted for inclusion in Master's Theses by an authorized administrator of Loyola eCommons. For more information, please contact [ecommons@luc.edu](mailto:ecommons@luc.edu).



This work is licensed under a [Creative Commons Attribution-Noncommercial-No Derivative Works 3.0 License](#).  
Copyright © 2023 Asia Marie Paguntalan

LOYOLA UNIVERSITY CHICAGO

HOW TO BUILD A CORTEX:  
COORDINATED ASSEMBLY OF CORTICAL SEPTINS AND  
ACTOMYOSIN IN THE LEADER BLEB

A THESIS SUBMITTED TO  
THE FACULTY OF THE GRADUATE SCHOOL  
IN CANDIDACY FOR THE DEGREE OF  
MASTER OF SCIENCE  
PROGRAM IN BIOCHEMISTRY AND MOLECULAR BIOLOGY

BY  
ASIA MARIE PAGUNTALAN

CHICAGO, IL

AUGUST 2023

Copyright by Asia Paguntalan, 2023  
All rights reserved.

## ACKNOWLEDGEMENTS

I would like to acknowledge all those who contributed to this thesis, starting with my directors, Dr. Patrick W. Oakes and Dr. Jordan R. Beach, without whose mentorship and insight this work would not be possible. Thank you both for the endless encouragement, support, and patience.

I want to thank all members of the Oakes and Beach labs at Loyola University Chicago for their technical guidance, thoughtful feedback, and daily camaraderie. I especially want to thank Dr. Alexia Caillier and Dr. Lee Troughton, who contributed invaluable insight and instruction throughout the course of this project. I would also like to acknowledge the chair of my committee, Dr. Jonathan Kirk, as well as Mel Bollnow and Anna Dauzvardis, for their help in the preparation of this thesis.

To my brother, Tim, thank you for being my biggest cheerleader. To my parents, John and Carol, thank you for your limitless love and support. For the sacrifices you have made, I can never repay you.

For my Lola.

## TABLE OF CONTENTS

ACKNOWLEDGEMENTS .....	iii
LIST OF FIGURES.....	vi
LIST OF TABLES.....	viii
LIST OF ABBREVIATIONS.....	ix
ABSTRACT .....	x
CHAPTER 1: PURPOSE AND INTRODUCTION .....	1
CHAPTER 2: BACKGROUND .....	4
Plasticity of Cell Migration .....	4
Molecular Machines of Cell Migration.....	17
The Cortical Septin Cytoskeleton .....	22
Project Aims.....	28
CHAPTER 3: MATERIALS AND METHODS .....	29
Experimental Methods.....	29
Image and Data Analysis.....	38
CHAPTER 4: MAIN RESULTS.....	43
Fibroblast Migration Behavior Depends on Adhesion & Contractility .....	43
Cortical Dynamics Mediate Migration Mode Switching.....	53
Septins Associate with Actomyosin in the Stable Bleb Cortex .....	64
Global Septin Depletion Alters Cortical Dynamics.....	68
CHAPTER 5: DISCUSSION.....	74
Bleb Formation: Balancing Polymerization, Adhesion, and Contractility .....	75
Bleb Shape and Stabilization: When Contractility Breaks Symmetry .....	78
Consequences of Septin Depletion on Bleb Dynamics .....	87
Conclusions & Future Directions .....	90
REFERENCE LIST.....	92
VITA .....	99

## LIST OF FIGURES

Figure 1. Actin Networks in Mesenchymal Migration. ....	8
Figure 2. Amoeboid Modes of Migration. ....	12
Figure 3. Transient Bleb Life Cycle. ....	13
Figure 4. Elongation of a Stable Bleb.....	14
Figure 5. Cytoskeletal Components of the Cell Cortex .....	20
Figure 6. NMII-Dependent Contractile Force Generation .....	22
Figure 7. Septin Domains and Filament Assembly .....	25
Figure 8. Cell Confinement System Overview .....	44
Figure 9. Confinement Alters MEF Protrusion and Morphology.....	46
Figure 10. Adhesion Inhibition Drives Rounding and Transient Blebbing under Confinement.....	47
Figure 11. High NMII Activity Drives Migration Mode Switching .....	49
Figure 12. Effects of Contractility and Substrate Adhesion on MEF Migration Behavior	53
Figure 13. Leader Bleb-Based Migration Does Not Require Focal Adhesions or Stress Fibers. ....	55
Figure 14. Loss of Stress Fibers Coincides with Cortical Actomyosin Enrichment. ....	56
Figure 15. Non-Adhesive Confinement Generates Two Types of Blebs.....	58
Figure 16. MEFs using Leader Bleb-Based Migration Display a Cortical Actin Density Gradient .....	59
Figure 17. Retrograde Flow Maintains a Cortex-Depleted Distal Membrane in Stable Blebs .....	60
Figure 18. Stable and Transient Bleb Display Distinct NMII Profiles .....	62

Figure 19. Non-Adhesive Confinement Alters Cortical Septin Dynamics.....	65
Figure 20. Septins and Actin Undergo Coordinated Flows in the Bleb Cortex.....	67
Figure 21. Overview of shRNA-Mediated Septin Knockdown Experiments.....	69
Figure 23. SEPT7 Depletion Disrupts Septin Filament Assembly.....	71
Figure 24. Septin Depletion Increases Cell Rounding and Transient Blebbing .....	72
Figure 25. Septin Depletion Correlates to Increased NMIIA/B Expression .....	73
Figure 26. Different Types of Blebs in Confined MEFs. ....	75
Figure 27. Detachment of Motile Bleb Fragments from the Uropod.....	83
Figure 28. Circus Blebbing Often Precedes Leader Bleb Elongation. ....	85



## LIST OF TABLES

Table 1. shRNA Construct Information .....	32
Table 2. Fixation Reagents and Buffers .....	36
Table 3. Antibodies and Stains .....	37

## LIST OF ABBREVIATIONS

<b>ABP</b>	actin-binding protein
<b>BSA</b>	bovine serum albumin
<b>CalA</b>	calyculin A
<b>CRISPR</b>	clustered regularly interspaced short palindromic repeats
<b>DMSO</b>	dimethylsulfoxide
<b>ECM</b>	extracellular matrix
<b>ERM</b>	ezzrin, radixin, moesin
<b>FA</b>	focal adhesion
<b>FACS</b>	fluorescence-activated cell sorting
<b>FN</b>	fibronectin
<b>GFP</b>	green fluorescent protein
<b>HEK</b>	human embryonic kidney
<b>iRFP</b>	infrared fluorescent protein
<b>LBB</b>	leader bleb-based
<b>MAT</b>	mesenchymal-to-amoeboid migration
<b>MEF</b>	mouse embryonic fibroblast
<b>MLCK</b>	myosin light chain kinase
<b>MLCP</b>	myosin light chain phosphatase
<b>MMP</b>	matrix metalloprotease
<b>MRLC</b>	myosin regulatory light chain
<b>NMII</b>	non-muscle myosin
<b>NT</b>	non-targeting
<b>PDMS</b>	poly(dimethylsiloxane)
<b>PEG</b>	poly(ethylene glycol)
<b>PFA</b>	paraformaldehyde
<b>PLL</b>	poly(L-lysine)
<b>PMOXA</b>	poly(2-methyl-2-oxazoline)
<b>ROI</b>	region of interest
<b>SF</b>	stress fiber
<b>shRNA</b>	small hairpin RNA
<b>WT</b>	wildtype

## ABSTRACT

In confined spaces, migrating cells can undergo mesenchymal-to-amoeboid transitions by altering their cortical dynamics and adhesion with the environment. Septins frequently associate with cortical actin and non-muscle myosin (NMII), but the functional nature of these interactions remains unclear.

Upon non-adhesive confinement and NMII enrichment, fibroblasts can switch to a fast, leader bleb-based mode of motility, characterized by the absence of adhesions and stress fibers and formation of a single, elongated leader bleb. During this transition, cortical actin remodeling and polarized NMII contractility drive leader bleb stabilization by generating long-range cortical flows, in coordination with changes in septin localization and assembly dynamics. Meanwhile, septin depletion increases global NMII expression, promoting cellular rounding and transient blebbing under non-adhesive confinement.

These findings demonstrate the plasticity of fibroblast migration behavior, mediated by cortical septin-actomyosin remodeling and, further, open the door for future studies on the functional relationship between septins and NMII at the cortex.

## CHAPTER 1

### PURPOSE AND INTRODUCTION

Many highly motile cell types display strong morphological and migratory plasticity and can switch between multiple modes of migration, allowing for optimal navigation of diverse tissue environments *in vivo* (Wolf et al., 2003; Tozluoglu et al., 2013; Diz-Munos et al., 2010). Modulating the chemical and mechanical properties of the extracellular environment *in vitro*, can induce cells to undergo significant changes in morphology and migration behavior, even without any direct alteration to gene expression (Bergert et al., 2012; 2015; Wolf et al., 2003; Balzer et al., 2012). This is most easily seen using mechanical compression, which causes mesenchymal cells – such as fibroblast – to readily transition to an amoeboid-like motility program by altering their adhesion with the substrate and the dynamics of their cortical cytoskeleton (Liu et al., 2015; Ruprecht et al., 2015).

The cell cortex is primarily composed of filamentous actin, or F-actin, while additional actin-binding proteins regulate filament turnover, orientation, and connectivity (Ennomani et al., 2016; Krueger et al., 2018). Properties of the cortex, especially contractility, depend on both the organization of F-actin and the generation of forces by non-muscle myosin II (NMII) motors (Shutova & Svitkina, 2018; Chugh & Paluch, 2018). Because cortical mechanics provide the driving force for many cellular processes

including cell-matrix adhesion, membrane dynamics, cortical flows, and more, understanding how the cortex is dynamically assembled is fundamentally important. Furthermore, to identify perturbations of the cortex that may compromise these essential processes, we must first expand our understanding of cortical network organization and mechanics.

Septins are a family of highly conserved filament-forming GTP-binding proteins that often serve as molecular scaffolds for cytoskeletal organization (Mostowy & Cossart et al., 2012; Kinoshita, 2006; Spiliotis & Gladfelter, 2012). Septin-family proteins contribute to the stabilization of cytoskeletal structures, often in response to external mechanical cues (Caudron & Barral, 2009; Gildea & Krummel, 2010). Individual septins can assemble into higher-order structures, such as linear filaments and bundles or rings, which bind actin and NMII to provide structural stability (Bridges & Gladfelter, 2015; Zhovmer et al., 2022). The precise mechanisms, however, by which the mammalian septin cytoskeleton contributes to the organization of cortical actomyosin networks and, by extension, migration mode plasticity, remain unclear.

Because examination of cortical networks is often obscured by high network density and internal cytoskeletal structures, a simplified model of the mammalian cortex, amenable to high-resolution molecular imaging, is required. As noted, upon compression, cells of mesenchymal origin can take on amoeboid-like modes of migration. One such mode, leader bleb-based migration, depends on high cortical contractility and is characterized by the elongation of a single stable bleb, aptly termed

the “leader bleb,” at the cell’s anterior face (Liu et al., 2015; Logue et al., 2015). Notably, this stable bleb is devoid of internal cytoskeletal structures, such as stress fibers and focal adhesion complexes, that frequently limit visualization of discrete molecular events at the cortex (Liu et al., 2015; Bergert et al., 2015; Ruprecht et al, 2015). The stable bleb also maintains a steady retrograde flow of actomyosin in coordination with continuous network turnover (Logue et al., 2015; Bergert et al., 2015). Together, the dynamic architecture of the cortical network and lack of internal structures make the stable bleb a minimalist, yet relevant, model of the cell cortex and, more broadly, allows for examination of the molecular mechanisms driving migration plasticity and leader bleb-based migration.

Using a specialized micropillar confinement system in combination with high resolution fluorescence microscopy, I investigated the coordination of septin-actomyosin assembly in the cortex of stable bleb-induced fibroblasts and evaluated the consequences of septin depletion on cellular contractility and migration behavior. Overall, the primary goal of this master’s thesis is to understand how the mammalian septin cytoskeleton contributes to the organization and assembly of cortical actomyosin networks and, by extension, fibroblast migration mode plasticity.

## CHAPTER 2

### BACKGROUND

#### **Plasticity of Cell Migration**

Cell migration is a fundamental property of cells in nearly every physiological niche and involves complex mechanical interactions that range from tissue-level dynamics down to individual molecular-scale events (Lauffenberger & Horwitz, 1996; Trepats et al., 2012). This process of directed cell movement, often in response to chemical or mechanical signals, drives tissue morphogenesis during development (Simske et al. 2001), allows for an effective immune response (Lammermann et al., 2008) and maintains tissue integrity and organization (Gurtner et al., 2008). Dysregulation of motility mechanisms can have detrimental medical outcomes, such as autoimmune and inflammatory diseases and, most notably, the progression of metastatic cancers. Therefore, migration mechanisms must be tightly regulated in both space and time to preserve healthy physiology.

In cells, the actin cytoskeleton is the primary regulator of cell shape and motility (Svitkina, 2018; Friedl & Wolf, 2009). Almost all modes of single-cell migration heavily rely on the dynamic organization and properties of actin (Salbreux et al., 2012). The actin cytoskeleton consists of actin filaments (F-actin) that interact with and are regulated by a diverse array of actin-binding proteins (ABPs). These include filament

nucleators, crosslinkers, regulators of assembly/disassembly, and molecular motors such as NMIIA/B (Pollard & Borisy, 2003). One of the most important functions of actin is to generate force, including the pushing (protrusive) and pulling (contractile) forces required for migration (Shutova & Svitkina, 2018). The actin cytoskeleton is also an important regulator of cell shape, largely mediated by interactions between the cell cortex and the plasma membrane (Chugh & Paluch, 2018).

Depending on the forces used for locomotion and cytoskeletal organization, single-cell motility can be divided into two broad categories: mesenchymal or amoeboid migration (Friedl & Wolf, 2003; 2010). Mesenchymal migration generally relies on high matrix-metalloprotease (MMP) activity, actin polymerization-driven protrusions, and strong traction forces, facilitated by complex cell-matrix adhesions and actomyosin stress fibers (Treat et al., 2012; Pollard & Borisy, 2003; Wolf et al., 2003). Meanwhile, amoeboid motility is less clearly defined, but can be broadly characterized by fast migration speeds, rounder cell bodies and protrusions, low MMP activity, and a lack of specific cell-matrix adhesion (Yoshida & Soldati, 2006; Friedl & Wolf, 2003). Migrating amoeboid cells also display greater overall reliance on cell contractility, largely mediated by properties of the actin-based cell cortex (Bergert et al., 2012; 2015; Ruprecht et al., 2015). This section introduces the complex cytoskeletal structures and mechanisms of force generation required by different modes of migration.

### **Mesenchymal Migration**

Mesenchymal motility is best exemplified by the lamellipodial mode of migration,



which is the default motility mechanism employed by fibroblasts that migrate throughout nearly all tissues in the human body (Treat et al., 2012). Unlike epithelial cells, which maintain apical-basal polarity, the asymmetric cytoskeletal arrangement of mesenchymal cells generates their distinct front-end to back-end polarity, enabling motility (Vicente-Manzanares et al., 2007). Mesenchymal cells rely on several distinct cytoskeletal structures for migration: 1) an actin-rich lamellipodium at the cell's leading edge, 2) thin filopodial protrusions of tightly bundled actin, 3) stress fibers – strong, contractile bundles of actomyosin, and 4) focal adhesion complexes that mechanically link the intracellular cytoskeleton to the extracellular matrix (ECM) (Figure 1; Alberts et al., 2007). The follow section highlights these key structures and provide insight to the molecular mechanisms powering mesenchymal cell migration.

**Actin-rich protrusions.** The lamellipodium is a flat, undulating protrusion that forms at the leading edge of migrating mesenchymal cells and consists of a thin meshwork of branched F-actin and ABPs, which regulate network assembly and disassembly (Figure 1A; Pollard & Borisy, 2003). During lamellipodial expansion, F-actin polymerization at the leading edge pushes on the plasma membrane to extend the cell's anterior margin (Mogilner & Oster, 1996). Many functionally distinct ABPs contribute to the assembly and organization of the lamellipodial actin network. The most important of these is the Arp2/3 complex, a branch nucleator, which facilitates the nucleation of new F-actin branches on preexisting filaments (Amann & Pollard, 2001; Wu et al., 2012). The Arp2/3 complex is indispensable for lamellipodial formation, but other ABPs also

contribute to filament length, network density, and turnover dynamics (Wu et al., 2012).

These include filament nucleation and elongation machinery, such as formins and Ena/VASP (Bear et al., 2002; Dominguez et al., 2009), while actin capping proteins regulate filament length by blocking barbed end growth (Mejillano et al., 2004).

Meanwhile, actin-depolymerizing factors, such as ADF/cofilin, coordinate with filament nucleators to regulate the dynamic turnover of the lamellipodial network (Plastino & Blanchoin, 2018). As cells travel, actin treadmilling maintains the lamellipodial network, where filament polymerization at the anterior margin is coupled with depolymerization at the base of the lamellipodium (Pollard & Borisy, 2003). Network disassembly releases globular actin (G-actin) monomers to be recycled and re-integrated into expanding actin arrays, either in the lamellipodium or elsewhere in the cell (Pollard & Borisy, 2003).

In contrast to the branched, disordered architecture of the lamellipodial actin network, filopodia contain tight parallel actin bundles (Figure 1B). Unidirectional polymerization of filopodial actin filaments at the leading edge drives extension of these thin, elongated protrusions (Pollard & Borisy, 2003; Svitkina et al., 2003). Like in lamellipodia, formins nucleate new actin filaments, formins and Ena/VASP proteins facilitate nucleation and barbed end elongation (Svitkina et al., 2003; Young et al., 2015), and ADF/cofilin mediate filament severing and depolymerization at the base (Breitsprecher et al., 2011). In filopodia, fascin binds and crosslinks actin filaments into tight, parallel bundles that are bound to the plasma membrane by ERM – ezrin, radixin,

moesin – family proteins (Vignjevic et al., 2006; Diz-Munos et al., 2010). In short, ABPs are indispensable for lamellipodial migration and play essential roles in regulating motility and polarity.

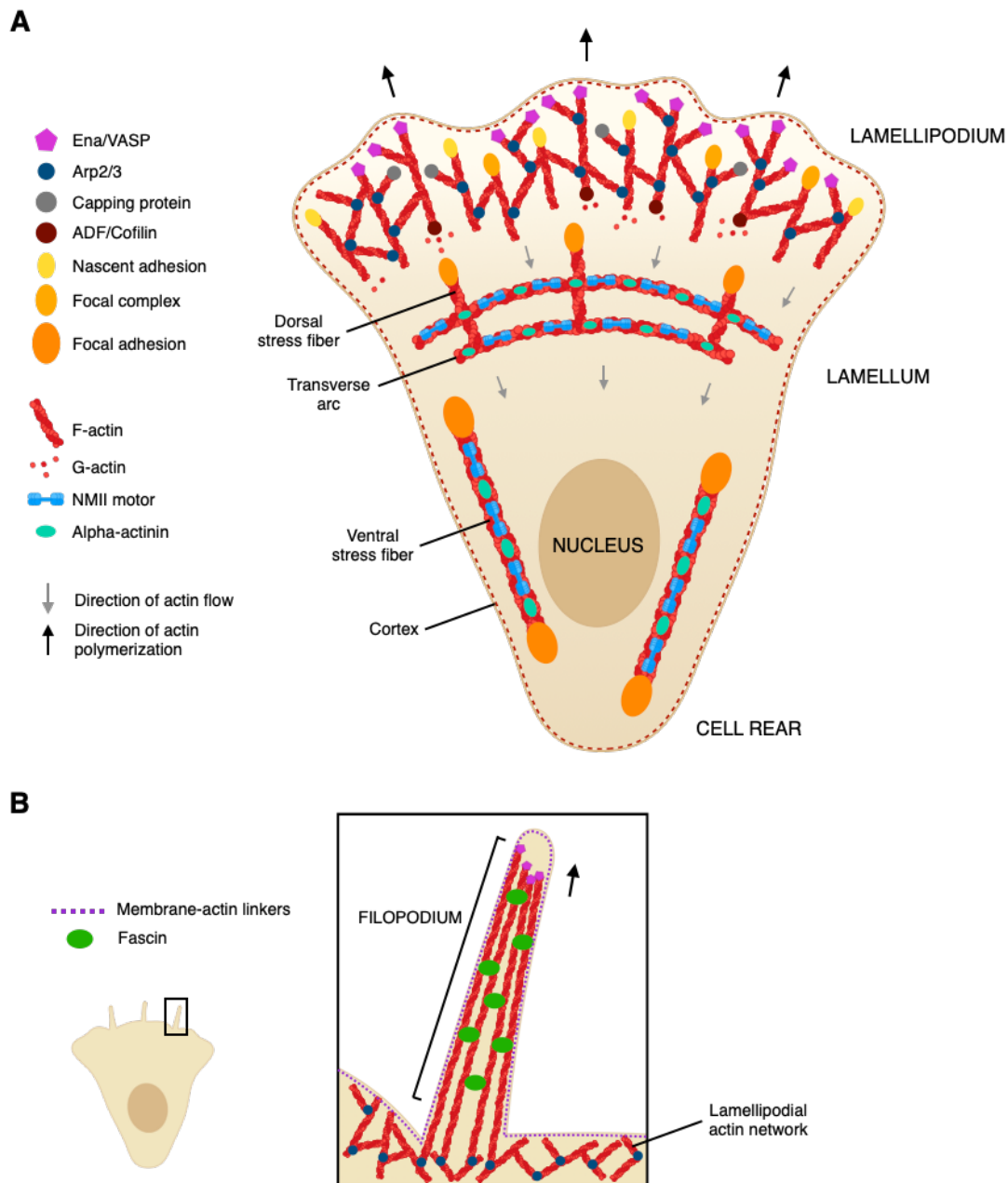


**Figure 1. Actin Networks in Mesenchymal Migration.** **A)** The main actomyosin machinery in fibroblasts includes the branched lamellipodial network and SFs, regulated by various ABPs and NMII motors. **B)** Filopodial networks consist of tightly bundled actin and ABPs such as fascin.

**Stress Fibers and Focal Adhesions.** While lamellipodial and filopodial actin networks maintain uniform polarity, stress fibers (SFs) are highly ordered mixed-polarity cables of tightly-bundled F-actin (Burrige & Wittchen, 2013). NMII-associated SFs represent the main contractile machinery in migrating mesenchymal cells, responsible for the transmission of traction forces that power locomotion (Livne & Geiger, 2016). SFs are classified into three major groups based on their location, composition, and association with focal adhesions (FAs): dorsal SFs, transverse arcs, and ventral SFs (Figure 1A; Hotulainen & Lappalainen, 2006; Tojkander et al., 2012).

Dorsal SFs are non-contractile actin cables that extend inward from maturing FA complexes near the base of the lamellipodium (Hotulainen & Lappalainen, 2006). Transverse arcs are curved actomyosin SFs that are not directly bound to FAs but can transmit contractile forces to the cell's surroundings via their association with dorsal SFs (Hotulainen & Lappalainen, 2006; Tojkander et al., 2012). Ventral SFs arise along the mid-body and posterior of the cell, parallel to the direction of migration. These are anchored to FA complexes at both ends and represent important contractile machinery for mesenchymal migration (Tojkander et al., 2012). Similarly, contractile perinuclear cap fibers are also anchored to FAs at both ends. They help regulate nuclear shape and positioning during migration and may function in mechanotransduction by transmitting forces from the cell's environment to the nucleus (Tojkander et al., 2012; Khatau et al., 2009). This is important for cell migration, as nuclear deformation is an important determinant of cell shape and migration (Venturini et al., 2020; Lomakin et al., 2019).

To convert actin-generated forces into mechanisms of whole-cell migration, mesenchymal cells require traction. When cells migrate through their ECM, this traction is provided by strong cell-matrix contacts, called focal adhesions (FAs), which link actin SFs to the ECM (Figure 1A; Zamir & Geiger, 2001). Integrin-family cell adhesion molecules facilitate these interactions, providing strong anchorage to the internal actin cytoskeleton (Zaidel-Bar et al., 2003). Integrin-actin interactions are mediated by adaptor proteins that form the adhesion plaque at the cytoplasmic face of the plasma membrane (Zaidel-Bar et al., 2003; 2004).

NMII-mediated contractile forces along adhesion-associated SFs generates traction, which is transmitted via integrins to the ECM (Schwarz & Gardel, 2012). The recruitment of mechanosensitive proteins, like zyxin, in response to tensile strain helps stabilize the linkage between integrin-bound plaque proteins and actin SFs (Colombelli et al., 2009). Zyxin is often considered a marker for mature FAs, as it is typically excluded from younger nascent adhesions and focal complexes (Beningo et al., 2001). FAs are also important signaling hubs for information exchange between the cytoplasm and the extracellular environment and play a role in mechanotransduction of information about the ECM, like substrate stiffness for example, to the internal cytoskeleton (Dupont et al., 2011). These mechanical signals can be important determinants of cell migration behavior and plasticity (Tozluoglu et al., 2013; Barnhart et al., 2011).

Overall, mesenchymal migration requires the dynamic assembly and disassembly of complex actin networks, highly regulated in both space and time.

Therefore, the coordinated regulation of actin network contractility, architecture, and turnover dynamics is essential for efficient, processive mesenchymal motility.

### **Amoeboid Migration**

In comparison to mesenchymal migration, amoeboid modes of motility are less clearly defined. Based on original observations of free-living amoebae, the amoeboid migration is typically associated with the formation of rounded and poorly attached membrane protrusions that are not necessarily rich in F-actin (Yoshida & Soldati, 2006; Paluch et al., 2016). In higher eukaryotes, similar amoeboid-like features of cell migration have been described in leukocytes, tumor cells, and even some stem cells (Friedl et al., 2001; Lammermann et al., 2008; Sahai and Marshall, 2003; Wolf et al., 2003). In general, the criteria used to define amoeboid migration has come to include fast migration speed, strong reliance on cell contractility, the absence of specific adhesion with the ECM, and a lack of MMP activity (Paluch & Raz, 2013; Lammermann & Sixt, 2006; Wolf et al., 2003). Morphologically, amoeboid cells have much rounder cell bodies with blunt protrusions that are often mediated by pressure-driven flow, like in blebs (Paluch & Raz, 2013; Berget et al., 2012; 2015).

It is important to note, however, that most cells using “amoeboid” modes of migration usually only exhibit a subset of these traits. For example, neutrophils, which are considered typical amoeboid cells, can form actin-rich protrusions that have a more lamella-like shape, rather than the blunt pseudopods usually associated with amoeboid motility (Fritz-Laylin et al., 2007). While mechanisms of mesenchymal migration are

fairly consistent and well defined, some modes of amoeboid migration seem to represent intermediate or transitional modes between lamellipodial and bleb-based migration.

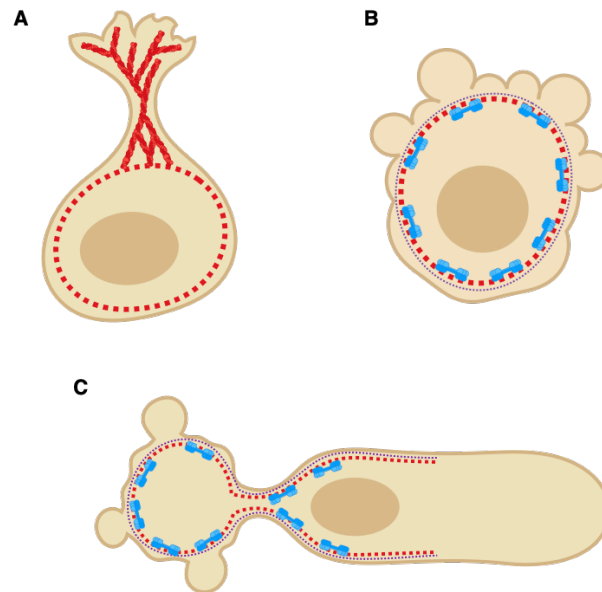


**Figure 2. Amoeboid Modes of Migration.** **A)** Pseudopodal-amoeboid migration is driven by actin polymerization at the leading edge. **B)** Intermittent bleb-based migration involves repeated blebbing at the leading edge. **C)** Leader bleb-based migration requires rear-directed NMII contractility and retrograde flows.

Bleb-based motility is perhaps most extreme mechanism of amoeboid migration and exhibits nearly all of the categorical “amoeboid” motility traits (Paluch et al., 2016). Bleb-based migration requires cell contractility to power locomotion, rather than actin-driven protrusions at the leading edge, and also does not appear to rely on specific adhesion with the external environment (Figure 2; Paluch & Raz, 2013; Bergert et al., 2012; 2015; Liu et al., 2015). Blebs are a hallmark of amoeboid migration and are nucleated by the detachment of the membrane from the underlying cortical network (Charras et al., 2006; Diz-Munos et al., 2010). Blebs expansion is driven by high intracellular pressure and typical stalls when the pressure within the protrusion

equilibrates with the cytoplasmic pressure in the cell body (Charras et al., 2008; Tinevez et al., 2009). Mechanisms of blebbing and bleb-based motility rely on high contractility generated by NMII motor activity within the cortical actin network, which are essential for the initial detachment of the membrane (Tinevez et al., 2009; Bergert et al., 2012). In short, increasing cortical contractility correlates with increased blebbing events (Charras & Coughlin et al., 2008; Liu et al., 2015).

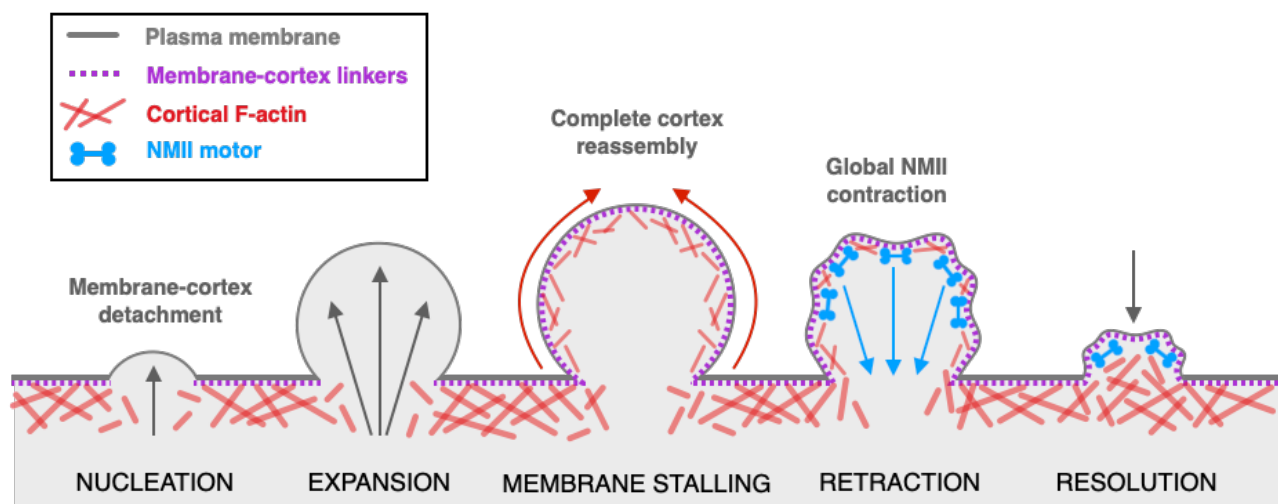


**Figure 3. Transient Bleb Life Cycle.**

Bleb formation is also enhanced by local weaknesses in the actin cortex and reduced interactions of the cortex with the plasma membrane (Paluch & Raz, 2013; Diz-Munos et al., 2012). However, reassembly of a homogenous cortical actin network at the bleb membrane, followed by the assembly and contraction of NMII motors drives bleb retraction (Figure 3; Charras et al., 2006; 2008). In some cases, when cortical reassembly is incomplete at the time of contraction, local NMII activity at the base of the bleb can generate retrograde flows of the partially formed actomyosin cortex, leading to bleb stabilization (Shih & Yamada et al., 2010; Paluch et al., 2016). In the case of leader



bleb-based (LBB) migration, high intracellular pressure drives the rapid transfer of cytoplasm and organelles into the bleb, generating a single elongated protrusion (Figure 2C; Berget et al., 2015; Liu et al., 2015; Maugis et al., 2010). Leader bleb formation requires the polarization of high NMII activity to generate a gradient of contractility in the bleb cortex, coupled to a flowing cortical network (Figure 4; Ruprecht et al., 2015; Liu et al., 2015; Bergert et al., 2015). Non-specific friction with the matrix and continuous peristaltic treadmilling of the polarized cortex power LBB motility (Ruprecht et al., 2015; Bergert et al., 2015; Cowan et al., 2022).

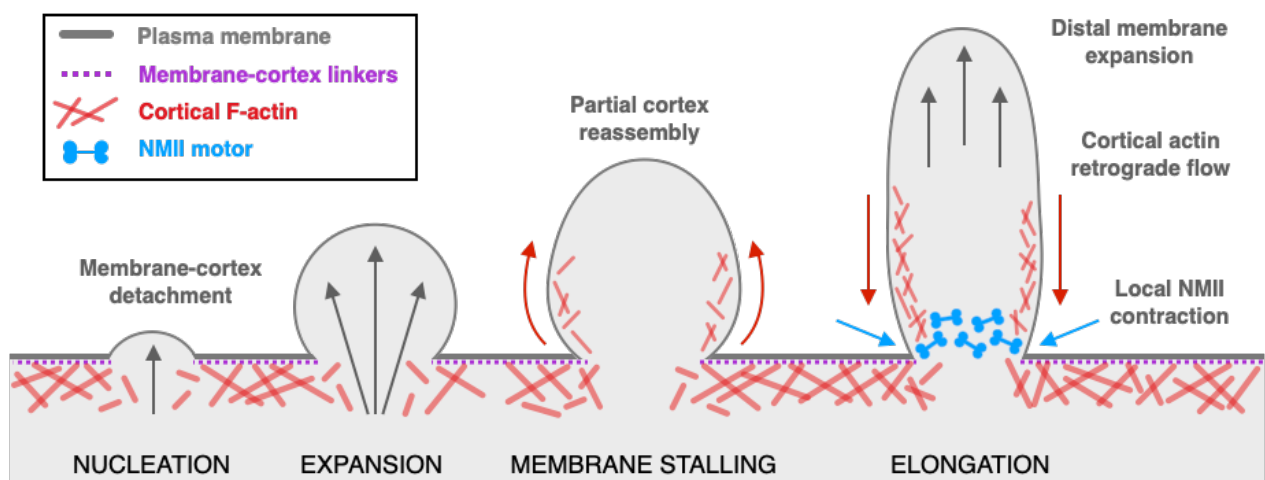


**Figure 4. Elongation of a Stable Bleb**

Clearly modes of mesenchymal and amoeboid migration are mechanistically distinct and involve significantly different types of forces: polymerization and traction for mesenchymal, or pressure and friction for amoeboid (Yamada and Sixt, 2019). Yet, all modes of migration require tight regulation of the actin cytoskeleton, making it a major determinant of cell shape and migration behavior, including the ability to transition between different modes of migration.

## Migration Mode as a Spectrum

Many highly motile cell types display strong morphological and behavioral plasticity and can switch between multiple modes of migration, allowing for optimal navigation through diverse tissue environments *in vivo*. This phenomenon has been well characterized in cancer cells, both *in vivo* within the tumor microenvironment as well as in 3D matrix models *in vitro* (Liu et al., 2015; Ruprecht et al., 2015; Logue et al., 2015; Tozluoglu et al., 2013; Sahai & Marshall, 2003; Wolf et al., 2003). Transformed cancer cells sustain significant genetic reprogramming and deregulation such that they take on less specialized phenotypes than their non-transformed counterparts, conferring greater phenotypic plasticity, including during cell migration (Pandya et al., 2017; Friedl & Alexander, 2011). Put simply, if more genes are accessible, it is easier and faster for cells to turn motility programs on and off as needed. However, these migration mode switches happen quite rapidly in response to environmental changes – on the scale of minutes or even seconds in some cases – suggesting that the shift from one motility program to another may be driven by mechanisms more immediate than genetic regulation (Venturini et al., 2020; Liu et al., 2015; Pankova et al., 2010). It is intriguing, the notion that cancer cells optimize their migration behavior in direct response to their environment – specifically, it calls to mind the question of whether or not this propensity for migration mode switching is unique to transformed cells or if all motile cell types maintain some degree of phenotypic plasticity.

Previous work has shown that by modulating the chemical and mechanical properties of the extracellular environment *in vitro*, cells can be induced to undergo significant changes in morphology and migration behavior even without any direct alteration to gene expression (Friedl & Wolf, 2010; Balzer et al., 2012). Liu et al. (2015) screened a wide range of cell types with diverse morphological and migratory profiles and found that for nearly all cell types, non-adhesive confinement rapidly induces the transition toward an amoeboid-like mode of migration, independent of their default motility program. Interestingly, spontaneously polarizing cells transition towards one of two distinct modes of amoeboid migration – pseudopodal or LBB migration (Liu et al., 2015). In agreement with similar studies, the authors found that LBB migration was consistently much faster than pseudopodal-amoeboid migration, yet both populations are still significantly faster than their non-confined counterparts (Sahai & Marshall, 2003; Ruprecht et al., 2015; Krummel et al., 2014). The field has postulated that the speed of migration is coupled with the rate of cortical flows (Liu et al., 2015; Ruprecht et al., 2015; Maiuri et al., 2015).

Many cell types display a preference for one or the other, with nearly all non-transformed cell types tending to take on the slower pseudopodal-amoeboid mode of migration, regardless of confinement level (Liu et al., 2015). In contrast, immune cells and transformed cells of both epithelial and mesenchymal origin utilize pseudopodal-amoeboid migration when weakly confined, but upon increasing the level of confinement and thereby the magnitude of compressive force being applied, they switch to the faster

LBB motility program (Liu et al., 2015; Lomakin et al., 2019; Venturini et al., 2020)

Surprisingly, even muscle cell precursors, which did not respond to low confinement, take on both modes of amoeboid migration under stronger mechanical compression (Liu et al., 2015). Thus, while some cell types appear to be more predisposed to strong migration plasticity, the evidence suggests that it is possible, perhaps, for all cells to transition across a spectrum of migration modes under the appropriate conditions.

### **Molecular Machines of Cell Migration**

Cell migration is a fundamental property of cells in nearly every physiological niche and involves complex mechanical interactions that range from tissue-level dynamics down to individual molecular-scale events (Lauffenbergen & Horwitz, 1996; Trepap et al., 2012). Cells can produce internal forces to power their own movement, critical during immune invasion or cancer metastasis (Shutova & Svitkina, 2018). Alternatively, cells can experience external forces and be pushed or pulled by other cells in the microenvironment, as happens during wound healing or bulk tissue growth (Simske et al., 2010; Gurtner et al., 2008). Because the organization and homeostatic maintenance of multicellular organisms largely depends on cell shape and movement, proper regulation of cell migration is essential (Pandya et al., 2017;).

Cell movement requires highly dynamic regulation of the cytoskeleton, a diverse group of filamentous scaffolds and molecular motors, as well as their associated nucleators, crosslinkers, and other modulators of cytoskeletal dynamics. The fundamental building blocks of the cytoskeleton are three (or four, *see The Cortical*

*Septin Cytoskeleton*) biopolymers: microtubules, intermediate filaments, and actin microfilaments (Alberts et al., 2007). The first, MTs, are strong, rigid polymeric tubes of tubulin monomers and are typically associated with intracellular transport, organelle positioning, and chromosomal segregation during cell division. Meanwhile, IFs are a highly heterogeneous class of polymers that form extensive filamentous networks and, broadly, contribute to cellular mechanics. Finally, actin microfilaments are the most dynamic cytoskeletal structures and appear in diverse higher-order arrays. Because actin filament networks can undergo rapid remodeling events and contribute to both protrusive and contractile force production, they are essential for cell migration and the control of cell shape (Pollard & Borisy, 2003; Alberts et al., 2007).

### **Actin: A Dynamic Cytoskeletal Polymer**

Actin is the one of the most abundant and highly-conserved proteins in eukaryotic cells and participates in more protein-protein interactions than any other known protein (Dominguez & Holmes, 2011). It comprises around 10% of total protein weight in muscle cells and between 1-5% in non-muscle cell. In cells, actin concentrations average approximately 1 mM in its filamentous form and a few tens of  $\mu\text{M}$  in its globular form (Abraham et. al., 1999). Vertebrates express many isoforms of actin, falling into one of three groups:  $\alpha$ -isoforms, found exclusively cardiac, skeletal, and smooth muscle fibers, and the more dynamic  $\beta$ - and  $\gamma$ -isoforms, found in both non-muscle and muscle cells as components of the cellular cytoskeleton (Lodish et. al., 2016). Actin can exist in either its soluble monomeric form as globular or G-actin or in its

polymerized form as filamentous or F-actin (Alberts et al., 2007).

One important characteristic of actin is its ability to assemble linear polymers called microfilaments, which play integral roles in many cellular processes, including structural support, intracellular trafficking, cell division, and migration. Three key properties of actin microfilaments underlie their multifaceted functionality: First, actin polymerization is highly dynamic and reversible, such that stable filaments often display steady state turnover, a mechanism called actin treadmilling. Second, actin filaments are polarized, with one pointed minus (–) end and one barbed plus (+) end, which display different binding affinities for ADP- versus ATP-bound monomers (Wegner & Isenberg, 1983; Carlier et al., 1990). Finally, the actin cytoskeleton has many interaction partners, some that comprise an entire family of actin-binding proteins (ABPs), which drive the modification and organization of microfilaments to support their diverse intracellular functions (Pollard, 2016). Ultimately, the higher arrays formed by actin filaments and their binding partners contribute to essential cellular functions, including migration, which specifically relies on the dynamic assembly and disassembly of complex actin networks (Pollard & Borisy, 2003; Abraham et al., 1999).

### **The Actomyosin Cortex**

Cell migration requires the cooperation of many functionally distinct higher-order actomyosin arrays, including actin stress fibers and the actomyosin cortex. Together these structures generate the protrusive and contractile forces, respectively, that are required for diverse modes of both mesenchymal and amoeboid migration. The cell

cortex is a principal component of the actin cytoskeleton and underlies the plasma membrane of nearly all eukaryotic cells. From the molecular to the tissue level, the actomyosin cortex provides the basis for many essential biological processes, including the regulation of cell division, migration, tissue morphogenesis, and more (Reymann et al., 2016; Bergert et al., 2012; Rauzi et al., 2008). Two of the most important functions of the cortex are to regulate cell shape and contractility, which in turn provides the foundation for many of these fundamental processes (Bergert et al., 2012; Salbreux et al., 2012; Callan-Jones et al., 2016).

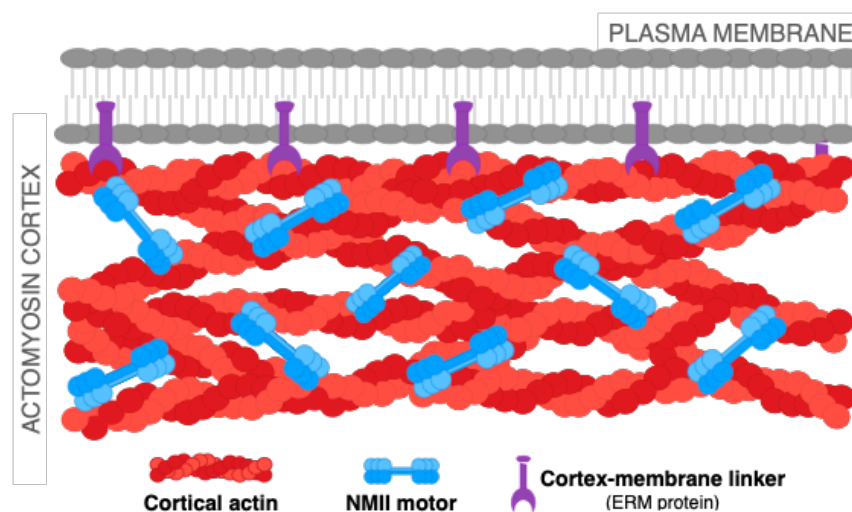


**Figure 5. Cytoskeletal Components of the Cell Cortex**

**Architecture and contractility.** At the cell periphery, cortical F-actin is arranged into a structurally dynamic meshwork and bound to the plasma membrane, a process involving various functionally distinct ABPs. In addition to F-actin, the main components of the cortex include cortex-membrane linkers, regulators of actin filament architecture, and motor proteins (Figure 5; Alberts et al., 2007). Cortex-membrane linkers, such as the ERM proteins – ezrin, radixin, and moesin – anchor cortical F-actin to the inner

surface of the membrane (Niggli & Rossy, 2008). Indeed, disrupting the function of ERM proteins increases the frequency of cortex-membrane detachment (Sliogyrte et al., 2014; Diz-Munos et al., 2010).

Some ABPs regulate the length and polymerization of actin filaments and, by extension, the thickness and density of the cortex. Meanwhile, actin bundling and crosslinking proteins link filaments to one another to form the cortical meshwork. These have indispensable roles in cell migration as the length, orientation, and connectivity of cortical actin filaments are key determinants of contractility (Ennomani et al., 2016; Krueger et al., 2018). Actin bundlers, such as fascin and fimbrin, align individual filaments into parallel or anti-parallel stacks, like in filopodia, while actin crosslinkers, such as filamin, contribute to the more disordered, mesh-like architecture of the cortical actin network (Svitkina et al., 2003; Logue et al., 2015; Adams et al., 2021). Other ABPs, like alpha-actinin, appear to generate both bundled and crosslinked arrays (Svitkina et al., 2003; Logue et al., 2015; Krueger et al., 2018). Therefore, actin crosslinking proteins are major determinants of cortical architecture and are thereby indispensable for both new cortex formation, as well as dynamic cortical remodeling.

Contractile properties of the cortex depend on both the architecture of the F-actin network, as determined by crosslinking ABPs, as well as the organization and activity of NMII motors (Ennomani et al., 2016; Krueger et al., 2018). When assembled within the cortical meshwork, NMII motors pull on actin filaments, often in response to tensile strain, which generates contractile stresses (Figure 6; Mayer et al., 2010; Chugh &



Paluch, 2018). Non-uniform transmission of these forces across the reticulated F-actin network produces gradients of cortical tension that can result in large-scale cellular contractions and cortical flows (Vogel et al., 2020; Yu et al., 2018; Mayer et al., 2010). During many cellular processes, regulation of cortical contractility is highly regulated in both space and time. For instance, at the beginning of cell division, cells undergo mitotic rounding, thought to be driven by progressive increases in cortical tension and F-actin reorganization into a uniform cortical layer (Reymann et al., 2016). However, during late mitosis, cortical actomyosin contraction at the equator of the cell generates global advective flows away from the poles, ultimately leading to furrow ingression and cytokinesis (Reymann et al., 2016). In short, local fluctuations in actomyosin contractility can lead to global cortex remodeling. Thus, the organization and assembly of new cortical networks depends, in part, on properties of the existing actomyosin network.

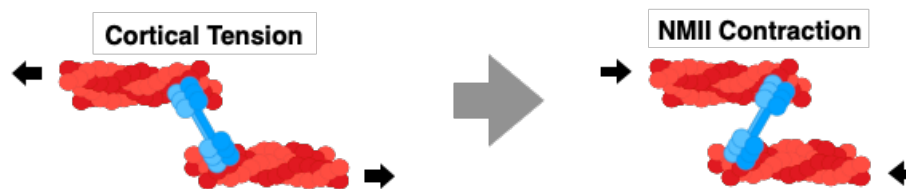


**Figure 6. NMIID-Dependent Contractile Force Generation**

### **The Cortical Septin Cytoskeleton**

The septin cytoskeleton is a family of highly conserved small GTP binding proteins of 30-65 kDa, recognized as the unique “fourth component” of the cytoskeleton (Mostowy & Cossart et al., 2012). Septins are ubiquitous molecular scaffolds, with key roles in cytoskeletal organization and stabilization, particularly at sites of mechanical strain (Kinoshita, 2006; Spiliotis & Gladfelter, 2012; Bridges & Gladfelter, 2015). Septins

localize to and bind both the plasma membrane and tensile actomyosin structures to reinforce architectural stability (Caudron & Barral, 2009; Gilden & Krummel, 2010; Bridges et al., 2016; Spiliotis, 2018). First identified in the budding yeast, *Saccharomyces cerevisiae*, septins were named for the observation that they localize to the septating bud neck in dividing cells, where they are essential for budding yeast cytokinesis (Hartwell, 1971; Hall & Russell, 2012; Gladfelter et al., 2001). During cytokinesis in budding yeast, septins assemble into rings at the bud neck, which serve as scaffolds for the recruitment of cytoskeletal proteins required for cytokinesis. Septins are also required for the assembly of the contractile actomyosin ring that drives cytokinesis in mammalian cells (Joo et al., 2007).

Outside of cell division, septins associate with the cell membrane at the base of specialized structures like cilia and flagella and have been shown to be indispensable for ciliogenesis and spermiogenesis in metazoans (Saarikangas & Barral, 2011). With respect to human health and disease, septins also play a roles in tumorigenesis, neurological disorders, and cellular host defense mechanisms during infections, to name a few (Peterson & Petty, 2010; Dolat et al., 2014). The following section outlines the mechanisms of septin filament assembly and the importance of the septin cytoskeleton in mammalian cell migration.

### **Filament Structure & Assembly**

Septins are expressed in all eukaryotes except plants, and the number of septin gene varies highly by species (Nishihama et al., 2011; Cao et al., 2009). To date, 13

functional genes have been identified, encoding tissue-specific and ubiquitously expressed members of the septin cytoskeleton (Kinoshita, 2003). Based on their sequence homology and C-terminal structure, the 13 septin genes can be subdivided into four groups, named according to their founding members: SEPT2, SEPT6, SEPT7, and SEPT3 (Figure 7A; Macara et al., 2002). All known septins share several common structural domains: an N-terminal polybasic region (PBR), a highly-conserved GTP-binding domain (GBD), and a septin-unique domain (SUD) near the C-terminus (Figure 7B; Trimble, 1999). However, members of the SEPT3 subgroup, including SEPT9, do not possess a C-terminal coiled-coil tail, while subgroup SEPT2 has two coiled-coil domains and subgroups SEPT6 and SEPT7 each have one (Figure 7A; Macara et al., 2002; Kinoshita, 2003). Functionally, the short PBR at the N-terminus has been found to directly bind PIP<sub>2</sub> and likely mediates interactions with the plasma membrane (Zhang et al., 1999). Meanwhile, the C-terminal coiled-coil tails of SEPT2/6/7 are thought to facilitate protein-protein interactions (Trimble, 1999).

In cells, septin subunits assemble into heteromeric oligomers, also referred to as protofilaments, that maintain a conserved rod-like shape (Sirajuddin et al., 2007). Individual subunits maintain two surfaces where they interact with one another in filaments: the G-face comprising the GBD and the NC-face where the PBR of the N-terminus and the C-terminal coiled-coiled tail are brought together during protein folding (Figure 7B-C; Sirajuddin et al., 2007). Mammalian cells exhibit both hexamers and octamers, in which septin subunits assemble into a non-polar palindromic organization

(Figure 7C; Sellin et al., 2011; Demay et al., 2011). Septin hexamers contain two subunits each from groups SEPT2/6/7, while octamers also contain two SEPT9 subunits (subgroup SEPT3). These rod-shaped complexes provide the basic monomers of filament assembly in cells.

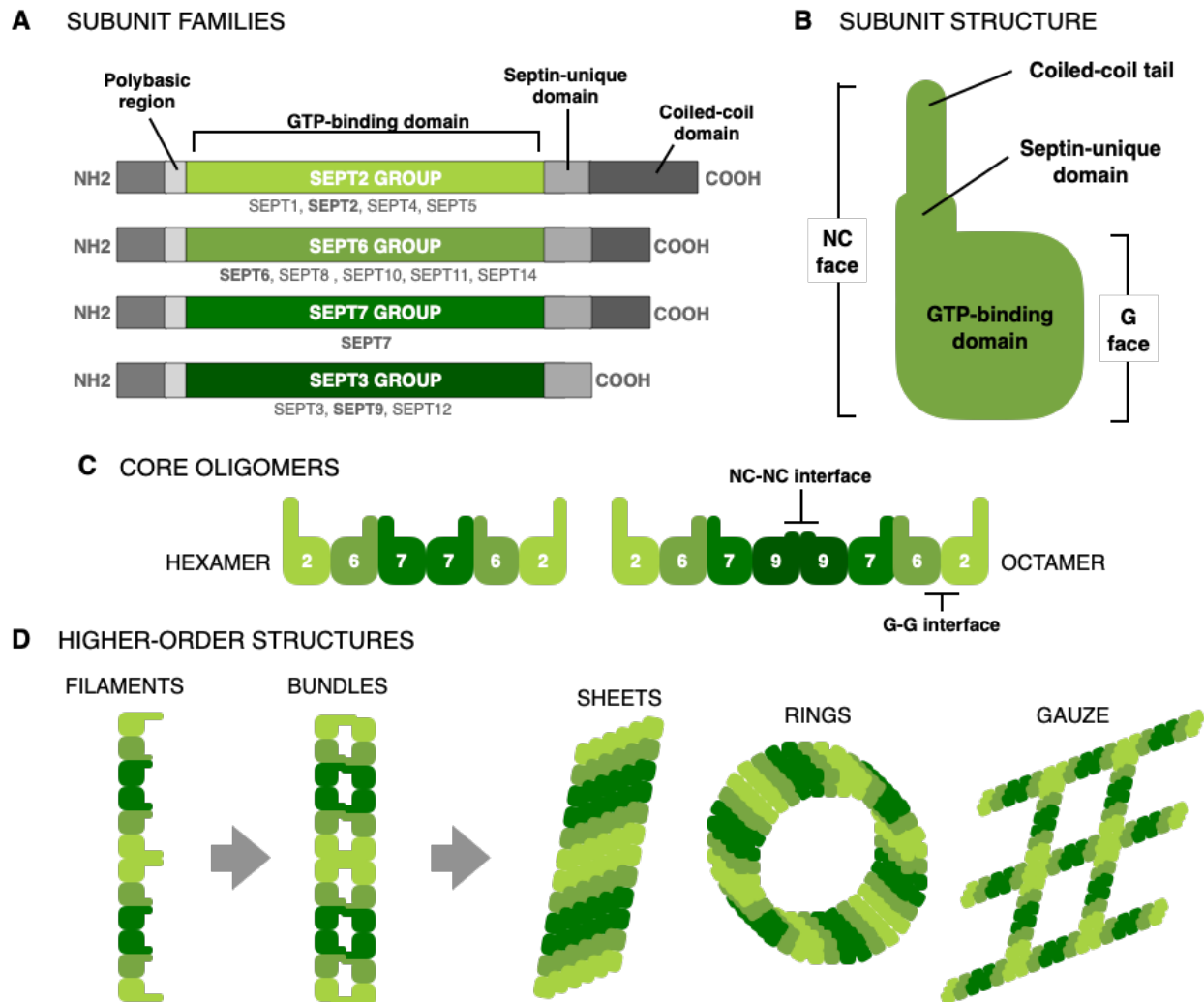


**Figure 7. Septin Domains and Filament Assembly.** **A)** The mammalian septin cytoskeleton includes 13 paralogs, comprising four families: SEPT2, SEPT6, SEPT7, and SEPT3. All groups share conserved proline-rich, polybasic, and guanine-nucleotide (GTP) binding domains and differ by their septin-unique domains and coiled-coil tail structure. **B)** Folded septin subunits maintain a G-face, comprised of the GTP-binding domain, and an NC-face, comprised of the N-terminal and the C-terminal coiled-coil tail. **C)** Septin subunits assemble into palindromic hexamers (*left*) or octamers (*right*) that form the basic units of septin filaments. Both hexamers and octamers contain members of the SEPT2, 6, and 7 groups. Members of the SEPT3 family, including SEPT9, are only found in octamers. **D)** Assembly of higher-order septin structures involves step-wise assembly of linear septin filaments, which form filament bundles, which form higher-order arrays such as sheets, rings, and gauze.

## Septin-Actomyosin Interactions at the Cortex

Septin monomers polymerize into filaments and bundles which can associate with the membrane and other cytoskeletal filaments like actin and microtubules (Kinoshita et al., 2002; Gildea & Krummel, 2010; Spiliotis, 2018). Unlike actin filaments, septin filaments are nonpolar and can thus polymerize at both ends. Septins can participate in microtubule- or actin-templated assembly, while membrane-binding has been found to enhance the autonomous assembly of septin filaments and higher-order structures, such as sheets, gauzes, and rings (Figure 7D; Spiliotis, 2018; Szuba et al., 2021). This can contribute to the organization of higher-order actin arrays if septin-actin association occurs concurrently with assembly (Weems et al., 2023). For instance, septins have been shown to be indispensable for the retraction of membrane blebs and appear to assemble at the cortex-free membrane concordant with the reassembly of cortical actomyosin (Gildea et al., 2012).

Cortical septins are also important regulators of cell shape and rigidity (Bridges & Gladfelter, 2015). Septins can recognize and localize to regions of micron-scale membrane curvature and have been shown to participate in the bending and bundling of cortical F-actin at sites of membrane or cortex deformation (Bridges et al., 2016; Cannon et al., 2019; Bridges & Gladfelter, 2015; Mavrikis et al., 2014) For example, during amoeboid migration of T-cells through a 3D collagen matrix, the assembly of cortical septin rings appears to template the condensation of circumferential, actin-rich bundles at regions of matrix-imposed steric hindrance (Zhovmer et al., 2022). During

cell division, mammalian SEPT2 has specifically been proposed to scaffold the activation and assembly of myosin motors during contractile ring formation at the cytokinetic cleavage furrow by directly binding NMIIA and its activating kinases (Joo et al., 2007).

Notably, many septin-associated actomyosin structures, e.g. ventral stress fibers and contractile rings, are physically associated with the cell cortex, such that the regulation of cortical mechanics often underlies the assembly of these higher-order structures (Mavrakis et al., 2014; Vignaud et al., 2020; Reymann et al., 2016). As the cell cortex represents a contractile actomyosin array that is, by definition, mechanically coupled to the plasma membrane, the septin cytoskeleton is often involved in the organization of cortical actomyosin networks, particularly at sites of mechanical strain (Zhovmer et al., 2022; Gilden et al., 2012). Additionally, septins are thought to play a role in mechanotransduction pathways originating at the plasma membrane through interactions with actin at adhesion sites, SFs, and the cortex (Lam & Calvo, 2019; Bridges & Gladfelter, 2015).

Overall, the septin cytoskeleton is critical for the assembly and maintenance of functional actomyosin networks at throughout the plasma membrane and in the cytoplasm (Spiliotis & McMurray, 2020; Spiliotis, 2018; Bridges & Gladfelter, 2015). However, the precise mechanisms by which mammalian septins contribute to the assembly and stabilization of cortical actomyosin networks remains an area under active investigation.

### **Project Aims**

1. Describe the factors regulating migration mode plasticity in fibroblasts.
2. Characterize the organization of septins, actin, and NMII motors during bleb retraction versus stabilization and persistent leader bleb-based motility.
3. Evaluate the impacts of global septin depletion on the assembly and stability of cortical actomyosin networks.

CHAPTER 3  
MATERIALS AND METHODS  
**Experimental Methods**

**Cell lines and culture**

Wildtype (M28) and zyxin-null (M27) mouse embryonic fibroblasts (MEFs) stably expressing zyxin-EGFP (Hoffman et al., 2003; 2012) were a gift of Mary Beckerle's laboratory (University of Utah, Salt Lake City, UT). The SEPT2-EGFP (*unpublished*, Shreya Chandrasekar, Loyola University Chicago) and NMIIA-EGFP (Beach lab, Loyola University Chicago) knock-in cell lines were generated from M28 and JR20 (Rotty et al., 2017) parental MEFs, respectively, using CRISPR/Cas9. HEK293FT cells were cultured to prepare lentivirus for stable cell line generation. All cells were cultured in Dulbecco's modified Eagle's Medium (DMEM; MT10013CV, Corning) supplemented with 10% FBEssence (10803034, Avantor Seradign) and 1X antibiotic-antimycotic (MT3004CI, Corning) at 37°C in 5% CO<sub>2</sub>. All cell lines were grown on uncoated tissue culture dishes and detached with TrypLE Express (12604039, Gibco) dissociation reagent prior to plating. For live imaging experiments, cells were seeded on glass bottom 6-well plates (P06G-1.5-20F, MatTek) or #1.5 glass coverslips in Leibovit's L-15 medium without phenol red (21083027, Gibco) supplemented with 10% FBEssence.



### **Lentiviral stable cell lines**

HEK293FT cells were transfected for lentivirus preparation using the LipoD293 system (SL100668, SignaGen) and the accompanying transfection protocol. Briefly, a dish of HEK293FT cells was grown to approximately 65-70% confluence. Approximately 1 hour prior to transfection, the media on the cells was changed, taking care to avoid disturbing the monolayer. At a 1:2:2 (w/w/w) ratio, envelope plasmid pMD2.G (Addgene Plasmid #12259), packaging plasmid psPAX2 (Addgene Plasmid #12260), and 1-4ug of lentiviral DNA were combined with the appropriate volume of LipoD293 transfection reagent in serum free DMEM. The transfection mixture was then added dropwise to the dish of HEK293FT cells. The media was changed after 24 hours and collected at 48 and 72 hours post-transfection. Viral media was centrifuged at 2000xg (full speed) for 10 minutes, and the supernatant was transferred to a fresh conical for immediate use or stored at -80°C. To generate stable cell lines, MEFs were grown in 6cm or 10cm dishes to approximately 60% confluence and infected with viral media for 24 hours. After a minimum of 3 media changes, or 3-5 days, stably transfected MEFs were selected by antibiotic selection or FACS sorting.

### **Plasmids**

For visualization of F-actin in live-cell imaging experiments, MEFs were transfected with either pLV-LifeAct-tdTomato (Addgene plasmid #64048) or pLV-3x-mScarlet-FTractin (gift from Dr. John A. Hammer, NHLBI/NIH, Bethesda, MD). pLV-3x-iRFP-SEPT2 was generated by removing FTractin from the pLV-3x-iRFP670-FTractin

plasmid (gift from Dr. John A. Hammer, NHLBI/NIH, Bethesda, MD) by digestion with Not1HF and Afe1. The sequence encoding SEPT2 isoform A was PCR amplified from a SEPT2-EGFP plasmid (*unpublished*, Shreya Chandrasekar, Loyola University Chicago) and introduced into the 3x-iRFP670 lentiviral backbone via Gibson cloning.

### **shRNA-Mediated Septin Knockdown Cell Lines**

In order to generate stable septin knockdown cell lines, wildtype (WT) MEFs were incubated with viral media from HEK293FT cells that had been transfected with lentiviral shRNA constructs against SEPT7 (shSEPT7). After 24 hours in viral media, infected MEFs were grown in complete DMEM for 3-5 days. To control for off target effects, a second population of MEFs were infected in parallel with viral media containing lentiviral particles for non-targeting shRNAs (shNT). All shRNA constructs contained a selection marker for puromycin resistance, so both the knockdown and NT control populations were screened for positive shRNA expression with 2ug/ml puromycin. A plate of non-transfected WT MEFs was treated in parallel. Antibiotic selection media was replaced every day until all cells in the WT control plate were dead. Five constructs were initially screened for highest knockdown efficiency and the best two were selected for subsequent experiments. Knockdown efficiencies were verified by western blot and normalized fluorescent intensity of SEPT7 in fixed and immunostained cells. All quantification of fold changes in protein expression were normalized to either WT or NT controls. All shRNAs were obtained from SigmaAldrich and construct information is listed in Table 1 below.

**Table 1. shRNA Construct Information**

Construct/Vector	Product Number	TRC Number	Target Region
shSEPT7-1	SHCLNG-NM_009859	TRCN000101845	CDS
shSEPT7-2	SHCLNG-NM_009859	TRCN000101846	CDS
shSEPT7-3	SHCLNG-NM_009859	TRCN000101847	CDS
shSEPT7-4	SHCLNG-NM_009859	TRCN000101848	CDS
shSEPT7-5	SHCLNG-NM_009859	TRCN000349183	3' UTR
shNT (pLKO.1)	SHC002	TRC1 Empty Vector	Non-targeting control

### **Fabrication of the Cell Confiner**

Two cell confiners, a 6-well glass bottom plate and a single-well confinement chamber, were used for confined migration and high resolution molecular imaging experiments, respectively. The design of these confiners was adapted from LeBerre et al., 2012, and the method is described in detail in LeBerre et al., 2014. Both systems consist of a large PDMS pillar and a structured micropillar confinement slide. The height of the large pillars varied between confiners: approximately 20mm for the multi-well plate or approximately 10mm for the single-well chamber. Briefly, the large pillars were made with a 20:1 (w/w) mixture of PDMS polymer A: crosslinker B, which was mixed thoroughly and cured in a custom mold. First, the mold was filled about  $\frac{3}{4}$  of the way to the top with the mixture and set in a vacuum chamber for 10-15 minutes to remove all air bubbles. The mold was filled the remainder of the way up, and pillars were baked overnight at 37°C. Before each use, debris was removed from the large PDMS pillars with tape, and they were rinsed well with isopropanol. Pillars were incubated in imaging media for a minimum of 1 hour prior to confinement.

To make the micropillar confinement slide, round 12x12mm coverslips were plasma-activated for 2 minutes. A mixture of 8:1 (w/w) PDMS polymer A: crosslinker B was mixed well and poured onto a custom silicone wafer modified via photolithography (gift of Mathew Piel's Lab, Institute de Curie, Paris, France). The wafer surface has a micropattern that serves as a mold to generate micropillars of 5 $\mu$ m height. The PDMS was allowed to spread into a thin layer across the surface of the wafer, while air bubbles were removed in the vacuum chamber for 5-10 minutes. The plasma-activated surface of the round coverslips was pressed into the PDMS layer, gently enough to avoid breaking the glass but hard enough to ensure the layer beneath was as thin as possible while removing all air bubbles. The PDMS was cured on a hot plate at 95°C for 10-15 minutes or until the consistency of a rubber eraser. After baking, the excess PDMS was peeled away, the wafer was flooded with isopropanol, and the confinement slides were lifted with a newly opened razor or scalpel. The surface of the micropillars was passivated with PLL-PEG or PMOXA for a minimum of 1 hour at room temperature or overnight at 4°C, following another plasma-activation step. Prior to use, the confinement slides were rinsed in isopropanol and allowed to air dry. Slides were incubated in imaging media for a minimum of 1 hour prior to confinement experiments.

To assemble the 6-well confiner plate, cells were plated and a thin sheet of PDMS was used to adhere the large pillars to the lid of the plate. The 6-well plate was gently, but quickly, closed while taking care to avoid shearing. While applying pressure, the lid was fixed to the plate using adhesive tape. Cells were imaged immediately

following confinement.

To assemble the single-well imaging chamber (Figure 8A), a 22x30mm glass coverslip was placed into the lower metal tray, which could be pre-treated with the appropriate surface coatings depending on the migration conditions required. The upper magnetic well piece was then snapped into place to seal the chamber, and cells were seeded. The large pillar was assembled onto the custom made confiner lid (Figure 8B; Pete Caron, Loyola University Chicago) and cells were confined by lowering the pillar into place while the magnetic posts in the lid retracted into place (Figure 8C). Again, cells were immediately imaged after confinement, or fixed after a minimum of 1 hour.

### **Confined Migration Experiments**

For live imaging experiments, cells were seeded on glass bottom 6-well plates (P06G-1.5-20F, MatTek) or #1.5 glass coverslips in Leibovitch's L-15 medium without phenol red (L15; 21083027, Gibco) supplemented with 10% FBEssence. For substrate-adhesion studies, coverslips were plasma cleaned for 1-2 minutes under a weak flow of clean, dry air. Wells and coverslips were treated with 25ug/mL fibronectin (FC01010MG, MilliporeSigma) or passivated with 0.5mg/mL PLL-PEG (JenKem) or 1mg/mL PMOXA (SuSos) for 1 hour at room temperature or overnight at 4°C. Wells and coverslips were rinsed three times with 1X PBS and once with MilliQ H<sub>2</sub>O to remove excess substrate and allowed to air dry. Cells were seeded at 100,000/mL in either 1mL L15 for the 22x30mm imaging chambers or in 1.5-2mL L15 for 6-well experiments. Cells were incubated for 15-30 minutes prior to confinement and imaged immediately.

### ***In Situ* Fixation under Confinement**

To fix cells under confinement for immunofluorescence, MEFs were plated and confined for at least one hour prior to fixation. While cells were confined, the media was aspirated, and cells were gently washed 3 times with warm 1X cytoskeleton buffer, incubating for 30 seconds during each wash. Cells were pre-fixed for 5 minutes and fixed for 15 minutes. After three 30 second washes with 1X PBS, cells were permeabilized for 15 minutes and blocked for 30 minutes. After blocking, the confiner was disassembled, and the fixed micropillar slide was incubated pillar-side-down with 8-10  $\mu$ L of primary antibody solution for 1 hour at room temperature or overnight at 4°C. After incubation, slides were rinsed with 1X PBS and washed three times with 0.1% PBS-tween (PBS-T), incubating for 5-10 minutes during each wash. Fixed micropillar slides were incubated for 1 hour with secondary antibodies and stains, while the mounting reagent, ProLong Glass (P36980, Invitrogen), was brought to room temperature. After staining, slides were washed three times with 1X PBS for 30 seconds each time, rinsed once with MilliQ H<sub>2</sub>O, and allowed to air dry. Fixed and stained micropillar slides were mounted pillar-side-down on 22x30mm glass coverslips with a small drop of ProLong Glass antifade mountant. Mounted slides were allowed to cure in the dark at room temperature for a minimum of 6-8 hours before imaging. For best results, the micropillar slide and coverslip were reassembled into the confinement chamber while curing to prevent excess space or air bubbles getting between the pillars and coverslip, which would impede imaging. All antibodies and staining solutions were

prepared in blocking buffer, and all incubations were performed at room temperature unless otherwise noted. Table 2 below lists recipes for all reagents.

**Table 2. Fixation Reagents and Buffers**

10X <b>Cytoskeletal buffer</b> (CB) <i>(Diluted 1:10 in PBS for 1X solution)</i>	0.1M MES monohydrate free acid 0.03M MgCl <sub>2</sub> 1.38M KCl 0.02M EGTA
<b>Pre-fixation buffer</b> <i>(in 1X CB)</i>	0.25% glutaraldehyde
<b>Fixation buffer</b> <i>(in 1X CB)</i>	0.25% glutaraldehyde 4% PFA
<b>Permeabilization buffer</b> <i>(in 1X PBS)</i>	0.2% Triton-X
<b>Blocking buffer</b> <i>(in 1X PBS)</i>	3% BSA 0.1% Triton-X

### **Drug Treatments, Antibodies, Molecular Stains,**

For live-cell imaging under confinement, cells were incubated in L15 media with 20nM Calyculin A (C5552, SigmaAldrich) for 15-30 minutes prior to being confined. Calyculin A was kept in the media throughout imaging.

For western blots, primary antibodies against SEPT7, SEPT2, MYHC (NMIIA) and NMIIB (MYH10) were used at a 1:2000 dilution. For immunofluorescence microscopy, primary antibodies against SEPT7, SEPT2, and NMIIA were used at a 1:200 dilution. Secondary antibodies and phalloidin were used at a 1:400 dilution. For both live-cell imaging experiments and immunofluorescence sample preparation, Hoechst 33342 nuclear stain was used at a 1:10000 dilution. For live-cell imaging, cells were incubated with Hoechst for 1 hour prior to plating in fresh L15 media.

**Table 3. Antibodies and Stains**

<b>Antibody/stain</b>	<b>Species</b>	<b>Source</b>
Anti-SEPT2	Rabbit	ProteinTech, 11397-1-AP
Anti-SEPT7	Rabbit	IBL, 18991
Anti-MYHC (NMIIA)	Mouse	BioLegend, 922701
Anti-MYH10 (NMIIB)	Mouse	GeneTex, GT246
AlexaFluor 555 Anti-Mouse	Goat	Invitrogen, A11004
AlexaFluor 647 Anti-Rabbit	Donkey	Invitrogen, A31571
AlexaFluor 488 Phalloidin	n/a	Invitrogen, A12379

### **Western blotting**

Cells were detached, pelleted, and resuspended well in cold PBS. Cells were spun again at 2000xg (full speed) for five minutes and lysed via pipet in ice cold 2X Laemmli sample buffer (1610737, BioRad). Lysates were sonicated until fluid and boiled for five minutes at 95°C, then either used immediately or stored at -20°C for future use. Samples were loaded per manufacturer's instructions and run on 4-15% Tris/glycine stain-free gels (Mini-PROTEAN TGX Stain-Free, BioRad) in Tris/Glycine/SDS running buffer (1610732, BioRad). Gels were rinsed with PBS and activated with UV light to quantify total protein loading. Prior to transfer, 0.22µm PVDF membranes (L00735, Genscript) were wet in isopropanol for several seconds then incubated in equilibration buffer (L00726, Genscript) for one minute. Bands were transferred using the standard protocol on the eBlot wet transfer system (Genscript) in Tris/glycine transfer buffer (L00726, Genscript). After transfer, membranes were rinsed once with PBS and blocked with 5% milk in 0.1% PBS-T for a minimum of 1 hour at



room temperature. Membranes were incubated with primary antibodies overnight at 4°C with constant agitation. After three 5 minute washes in 0.1% PBS-T, membranes were rinsed with PBS and incubated with secondary antibodies for 1 hour at room temperature with constant agitation. Membranes were again washed three times for 5 minutes each with 0.1% PBS-T and rinsed thoroughly with PBS.

Protein bands were visualized on a ChemiDoc illuminator system. For all quantification, band intensity was normalized first to total protein from gel activation and then to control samples (e.g. shNT), with correction for background signal.

## **Imaging**

All live imaging was performed on a 3i Marianas imaging system consisting of an Zeiss Axio Observer inverted microscope attached to a Yokogawa W1 Confocal Spinning Disk using 405, 488, 561, and 637nm lasers. For confined migration experiments a 20X/\_\_\_NA objective was used. For high resolution imaging of cortical dynamics 63X/1.4 NA and 100X/1.4 NA Plan-Apochromat objectives (Zeiss) were used. The microscope was controlled using 3i Slidebook 6 software.

Fixed imaging was done on a Zeiss LSM 880 Airyscan microscope using a 63X/1.4 NA Plan-Apochromat objective in the “SR” acquisition mode. Raw data was processed using ZEN software with automated processing strength.

## **Image and Data Analysis**

### **Migration Phenotype Counting**

To quantify migration phenotypes of NT controls or septin-depleted MEFs, time

lapse movies were taken over a period of 2 hours following CalA treatment and non-adhesive confinement. In two independent experiments, 30 fields were taken of each population. Phenotypes were counted by eye for each time point and classified as either round, unstable, or stable/leader. The phenotype counts were averaged across time points and then average counts from both experiments were compiled. Percentages were calculated from the compiled counts and plotted in Excel.

### **Cortical Dynamics**

**Density gradients.** To measure gradients of cortical density in transient, stable, and leader blebs, the linescan tool in ImageJ/FIJI was used to draw an ROI of 1 pixel width from base to tip through the center of the bleb. Using the plot profile tool, gray value versus distance measurements along the ROI were taken and corrected for average background intensity. The normalized fluorescent intensity measurements were plotted in Excel.

**Cortical flows.** The multi-kymograph tool in ImageJ/FIJI was used to measure rates of cortical actin or septin flow in stable and leader blebs. For non-motile stable blebs, the line tool was used to draw an ROI of 11-35 pixels wide from base to tip of the bleb. The line width varied based on the maximum size that could cover the greatest area of the bleb throughout the entire timelapse. For motile blebs, individual frames were aligned based on the position of the nucleus and concatenated into a time lapse stack. Kymographs were generated, and slopes were traced manually with the line drawing tool. The rate of flow was calculated from the width and height of the line, and

units were converted to distance and time based on the average frame interval and magnification used for acquisition.

For comparisons of actin-septin flow rates, each bleb was represented as one point on a scatter plot of actin versus septin flow rate ( $\mu\text{m}/\text{ms}$ ). Excel was used to generate a trendline and correlation coefficient for the scatterplot data.

### **Quantification of Protein Expression**

**Western Blot.** From the exported blot image, the fluorescent intensities of each band were measured in ImageJ/FIJI. A rectangular ROI of a fixed area was used to measure the mean gray value of each band, which was corrected against average background signal from the blot. Each band was normalized to total protein loading from the mean gray value of its corresponding lane in the gel activation image, and then each sample was normalized to the appropriate control (e.g. WT or NT samples). Plots of fold-change in expression were generated in Excel.

**Immunofluorescence.** The freeform selection tool in ImageJ/FIJI was used to draw an ROI around the perimeter of each cell. For each image, the area, mean gray value, integrated density, and average background signal were measured. The corrected total cell fluorescence (CTCF) was calculated for each cell as *integrated density - (ROI area \* average background)*. The average CTCF for septin-depleted and WT populations were used to calculate the fold-change in expression of SEPT7 by normalizing to the WT value, and data plotted in Excel.

## Statistics

Figure **20D**: Data represents retrograde flow measurements of N = 60 blebs from a total of 20 individual cells. Automated linear regression analysis was performed through Excel to generate a best of fit line. The value of correlation coefficient ( $R^2$ ) is displayed on the plot.

Figure **22C**: Data represents measurements from three independent populations of shSEPT7-treated MEFs (i.e. all made from different rounds of shRNA transfection). Each population was sampled in triplicate. The plot displays the average fold-change in expression across all 9 measurements for both SEPT7 and SEPT2.

Figure **22E**: SEPT7 expression data represents measurements from two independent populations, for both shSEPT7-1 and shSEPT7-3, each sampled in triplicate. Plot displays average fold-change in SEPT7 expression across all 6 replicates of each shRNA construct. SEPT2 expression data represents measurements from two independent populations, for both shSEPT7-1 and shSEPT7-3, each sampled in duplicate. Plot displays average fold-change in SEPT2 expression across all 4 replicates of each shRNA construct.

Figure **23B**: Data represents average CTCF measurements from N = 20 cells for WT or N = 25 cells from septin-depleted MEFs, both normalized to WT.

Figure **24B**: Data represents average percentages across two independent experiments with a minimum of N = 100 cells per population (NT or shSEPT7) per experiment.

Figure **25C**: Data represents measurements from two independent populations for both

shSEPT7-1 and shSEPT-3, each sampled in triplicate. Plot displays average fold-change in NMIIA expression across all 6 replicates.

Figure **25D**: Data represents measurements from one population expressing shSEPT-3, sampled in triplicate. Plot displays average fold-change in NMIIB expression across all 3 replicates.

## CHAPTER 4

### MAIN RESULTS

#### **Fibroblast Migration Behavior Depends on Adhesion & Contractility**

Most cell types are thought to maintain a “default” motility program. Fibroblasts, for instance, typically are described using mesenchymal migration modes – specifically, using actin-rich lamellipodial protrusions, extensive cell-matrix adhesions, and strong SFs of bundled actomyosin. Immune cells, in contrast, are thought to use amoeboid migration modes characterized actin driven expansion of the cell cortex and non-specific adhesion with the surrounding matrix (Paluch et al., 2016). Many cancer cells are thought to display strong migration plasticity both *in vivo* and *in vitro*, allowing them to navigate complex environments (Wolf et al., 2003; Petrie et al., 2012; Tozluoglu et al., 2013; Liu et al., 2015; Logue et al., 2015). It remains unclear the degree to which fibroblasts retain their default mesenchymal modes of migration within different environments.

Recent studies have suggested that under the optimal conditions it is possible for all cells to transition between migration modes. Cues that drive this transition include both cell-intrinsic factors, such as intracellular signaling and cytoskeletal dynamics, as well as extrinsic factors, such as cell-matrix interactions and ECM geometry, stiffness, etc. The current state of the field has proposed that the balance of protrusion, adhesion,

and contractility regulates the transition between motility modes (Liu et al., 2015; Lammermann & Sixt, 2009).

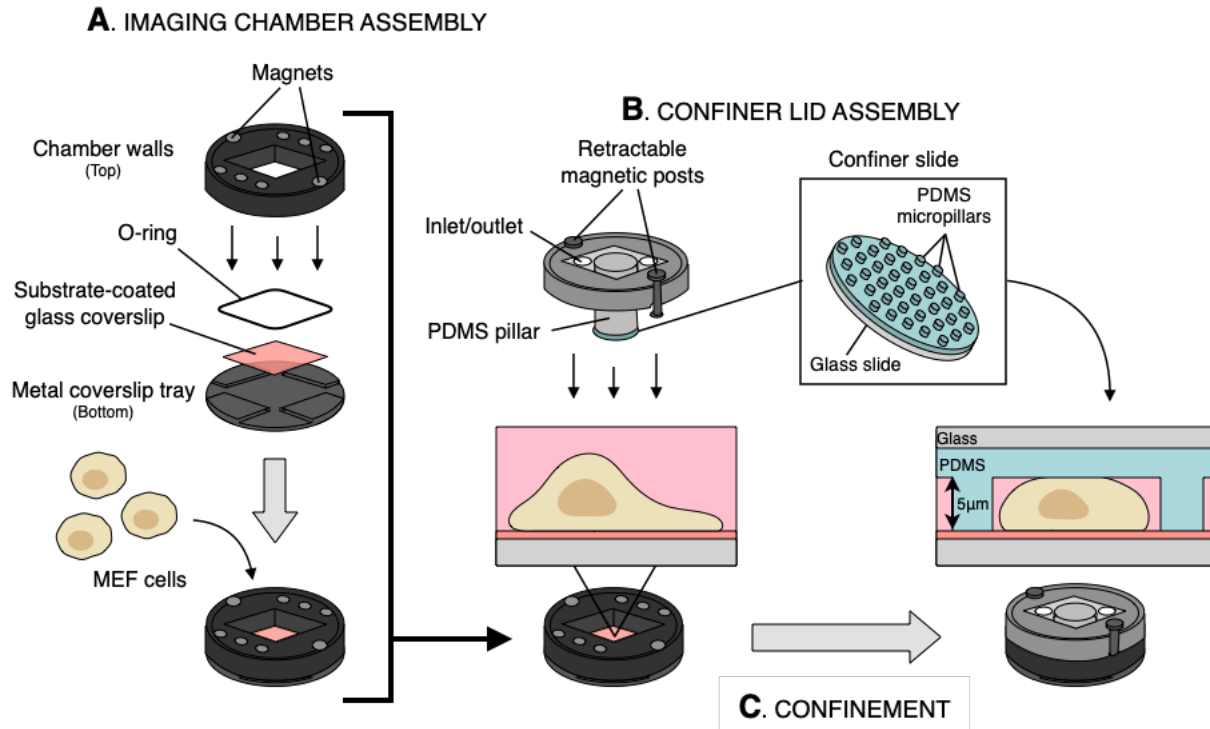


**Figure 8. Cell Confinement System Overview.** **A) Imaging chamber assembly:** the top of the imaging chamber, which forms the walls of the well once the chamber is fully assembled, is inlaid with strong magnets that run from its upper to lower surface. A rubber O-ring is inserted at the base of the chamber walls to create a sealed well that prevents fluid leakage during live imaging. After the glass coverslip is correctly positioned on the lower metal tray, the magnets tightly secure the top and bottom pieces of the chamber, locking the coverslip in place. **B) Confiner lid assembly:** a large PDMS pillar is first attached to the center of a custom-designed confiner lid. A small glass slide, modified with small PDMS micropillars of fixed height — 5 $\mu$ m in this case — is then attached to the bottom face of the large pillar (adapted from LeBerre et al., 2014). The lid itself has a transparent inset that contains two inlet/outlet holes for *in situ* drug treatments, fixation reagents, and/or media replacement. **C) Confinement:** to confine cells in the imaging chamber, retractable magnetic posts in the confiner lid are aligned with the magnets set into the top of the chamber well, locking the confiner lid into position. When pressure is applied from above, the posts retract, which lowers the micropillars into place, confining the cells beneath. (For details on fabrication of the cell confiner see methods)

Using a cell culture line derived from mouse embryonic fibroblasts (MEFs) as a model system for mesenchymal migration, I sought to investigate the conditions that promote a mesenchymal-to-amoeboid transition (MAT). In this section, I will describe the effects of mechanical confinement, cell-substrate adhesion, and cortical contractility on the morphology and migration behavior of MEFs *in vitro*.

## **Non-Adhesive Confinement Disrupts Mechanisms of Mesenchymal Motility**

To systematically evaluate how the chemical and mechanical properties of the extracellular environment affect fibroblast migration behavior, I used a specialized microfluidic system to confine cells between two flat coverslips (Figure 8, *adapted from* LeBerre et al, 2014). Briefly, to control the height of confinement, the upper coverslip was modified with PDMS micropillars of a fixed height (Figure 8B; Liu et al., 2015). To control the degree of cell-substrate adhesion, the lower coverslip was coated with different substrates of varied adhesiveness levels (Figure 8A). Following confinement (Figure 8C), I used live-cell confocal microscopy to image fluorescently-tagged proteins of interest and evaluated how cells responded to different environmental conditions.

**Confinement reduces MEF spread area and motility.** Mesenchymal migration is characterized by large, mostly flat cells, a cytoskeleton that has large stress fibers, and focal adhesions that anchor the cell to the ECM. Forces generated by NMII motors in the cytoskeleton are transmitted through these adhesions and onto their extracellular matrix (Schwarz & Gardel, 2012). Fibroblasts can also deposit their own matrix via secretion of compounds such as fibronectin (FN), further promoting strong substrate adhesion and promoting mesenchymal migration. Therefore, I first sought to determine how MEFs respond to confinement on highly adhesive substrates that facilitate integrin-mediated adhesion and most closely resemble their “native” microenvironment. MEF cells were plated onto FN-coated coverslips and allowed to migrate without confinement or confined to a vertical height of 5 $\mu$ m. This height was determined by empirically, as



cells confined at 5 $\mu$ m displayed deformation of both the cell body and the nucleus, indicating that the cells were compressed between the two surfaces (LeBerre et al., 2014; Lomakin et al., 2019).

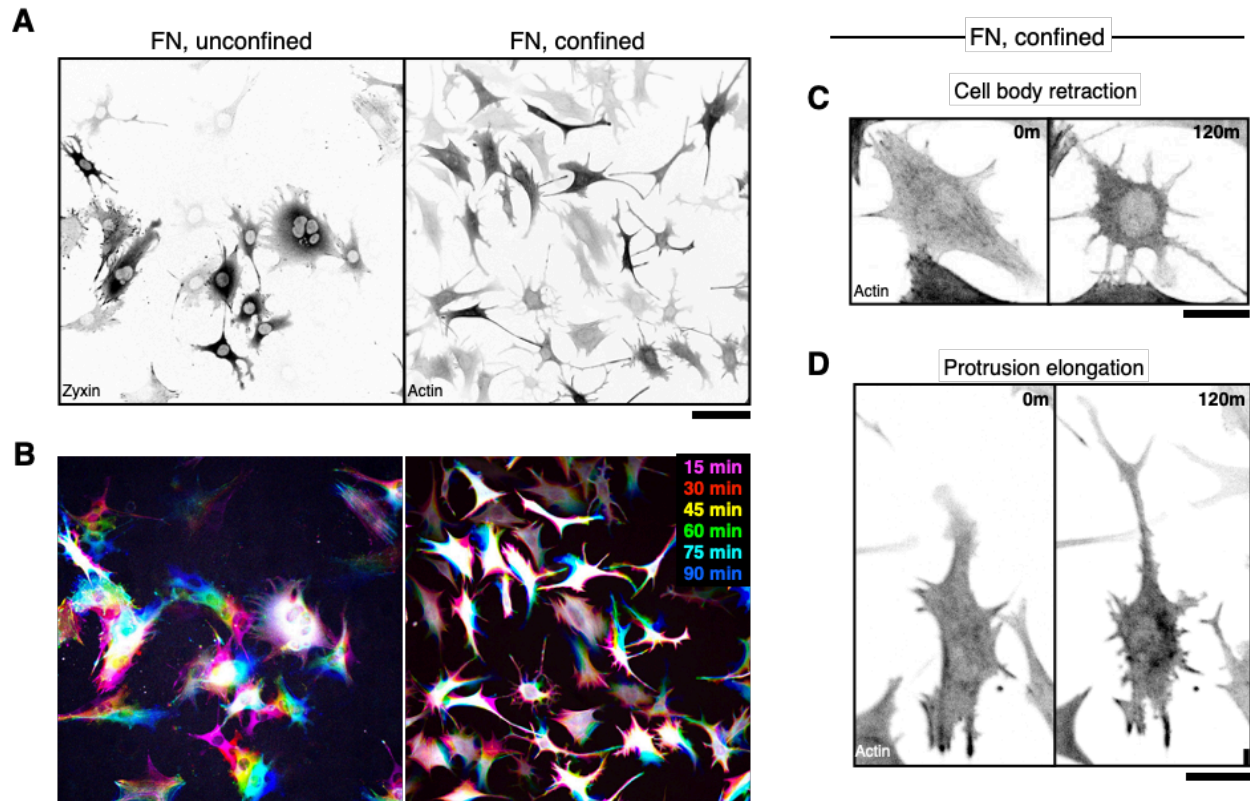


**Figure 9. Confinement Alters MEF Protrusion and Morphology.** **A)** MEFs expressing zyxin-EGFP and LifeAct-tdTomato, plated on fibronectin (FN) and allowed to migrate unconfined (*left*) or under 5 $\mu$ m confinement (*right*). Scale bar = 100 $\mu$ m. **B)** Time lapse composite of cells in (A). Color-coded by elapsed time post-confinement. **C, D)** MEFs expressing LifeAct-tdTomato, confined on FN, immediately (*left*) or after 2 hours (*right*) post-confinement displaying changes in cell body margin (C) and protrusion morphology (D). Scale bars = 50 $\mu$ m.

When left unconfined, MEFs spread normally and formed broad, actin-rich lamellipodia as well as numerous FAs with the FN substrate (Figure 9A, *left*). When confined at 5  $\mu$ m in the high-adhesion environment, MEFs tended to retract, forming fewer lamellipodia and more thin pseudopod-like structures that resembled the morphology of naïve neurites seen at early stages of neuronal development (Reese & Drapeau, 1998). (Figure 9A, *right*, 9C). This retraction of the cell body has been

correlated with increased contractility, which favors a more compact morphology (Sahai & Marshall, 2003). Most motile cells, however, still displayed a narrow, ruffled lamellipodia-like protrusion at the proximal tip of some projections, typically indicating the direction of migration (Figure 9D). This suggests that these cells are still using adhesion mediated mechanisms to interact with the substrate. While dynamic, these protrusions typically did not result in cell motility, as most cells showed little translocation over the 2 hours under confinement (Figure 9B, D).

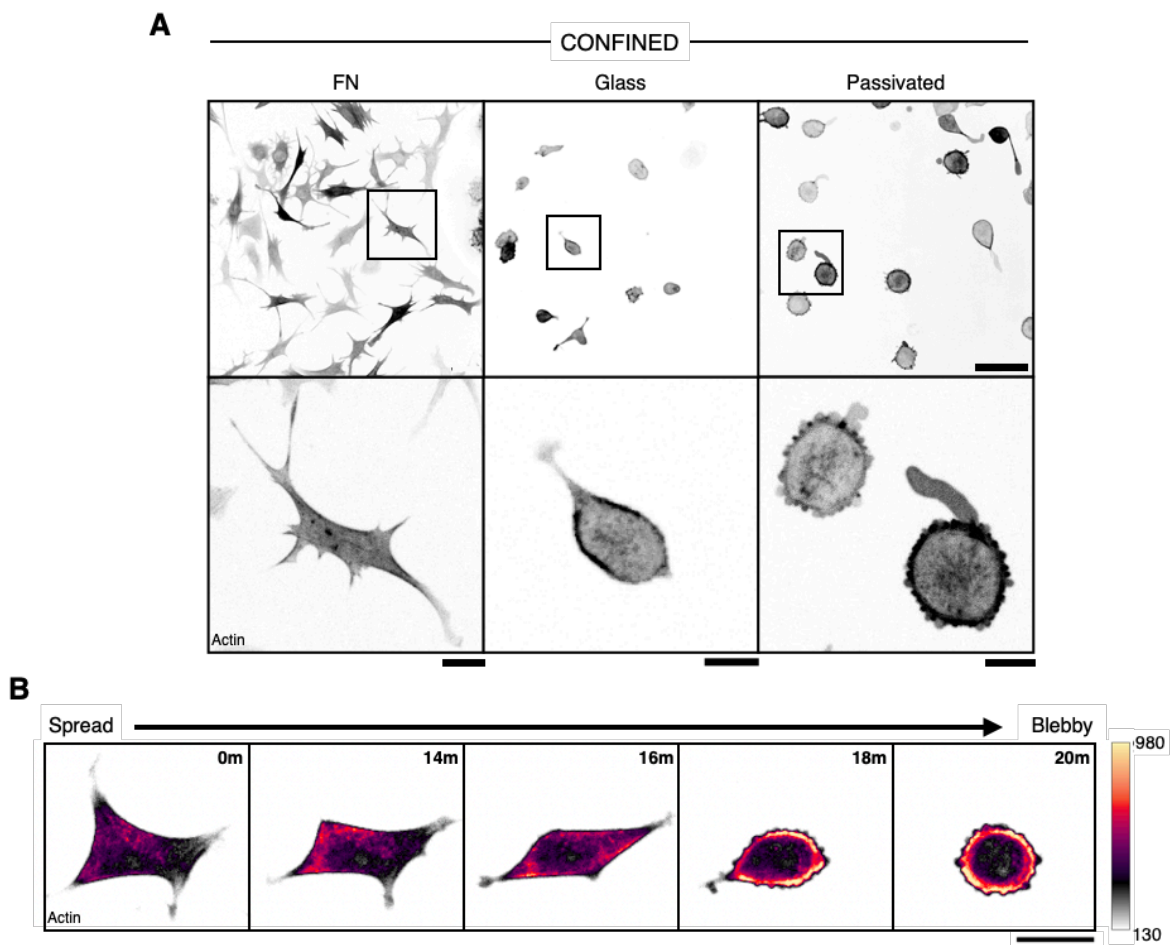


**Figure 10. Adhesion Inhibition Drives Rounding and Transient Blebbing under Confinement.** **A)** *Top:* Representative images of MEFs confined to 5 $\mu$ m on FN (*left*), untreated glass (*center*), or passivated glass (*right*). Scale bar = 100 $\mu$ m. *Bottom:* enlarged view of regions indicated by black boxes in panels above. Scale bars = 20 $\mu$ m **B)** Time lapse series of a confined MEF on untreated glass during a transition from spread/mesenchymal to rounded/blebby morphology. Calibration bar displays range of normalized fluorescent intensities. Scale bar = 10 $\mu$ m. All cells shown express LifeAct-tdTomato.

**Inhibition of adhesions drives cell rounding and dynamic blebbing.** Next, I tested how the degree of substrate adhesion affects the morphology and migration behavior of confined MEFs. In addition to plating cells on FN, MEFs also were seeded onto either uncoated or passivated glass surfaces. While uncoated glass represents an intermediate level of adhesion in comparison to the other two conditions, passivation of the coverslip surface with polymers such as PLL-PEG and PMOXA almost completely impairs the ability of cells to form adhesions.

MEFs confined on uncoated glass exhibited similarly retracted cell margins as those plated on FN but displayed greater morphological diversity. The most common phenotype observed was a rounded cell body with a dense cortex and a short actin-rich protrusion at the anterior edge (Figure 10A, *center*). This is consistent with previous work showing that mesenchymal cells, and specifically MEFs, tend to take on a pseudopodal-amoeboid mode of motility upon confinement with low adhesion (Liu et al., 2015). This morphology was most frequent seen shortly after confinement and typically led to a fully rounded shape that exhibited transient blebbing (Figure 10B).

Similarly, practically all cells confined on the passivated surface immediately became rounded and began blebbing, forming both smaller round blebs, as well as larger elongated blebs (Figure 10A, *right*). Blebs form when the plasma membrane detaches from the underlying cortex, often due to high intracellular pressure that promotes cortical rupture and cytoplasmic flow into the budding protrusion. High cortical contractility can elevate intracellular pressure and thus the frequency of cortical rupture,

leading to increased membrane blebs (Sahai & Yamada, 2003; Shih & Yamada, 2010).

This data further supports that confinement increases cortical contractility.

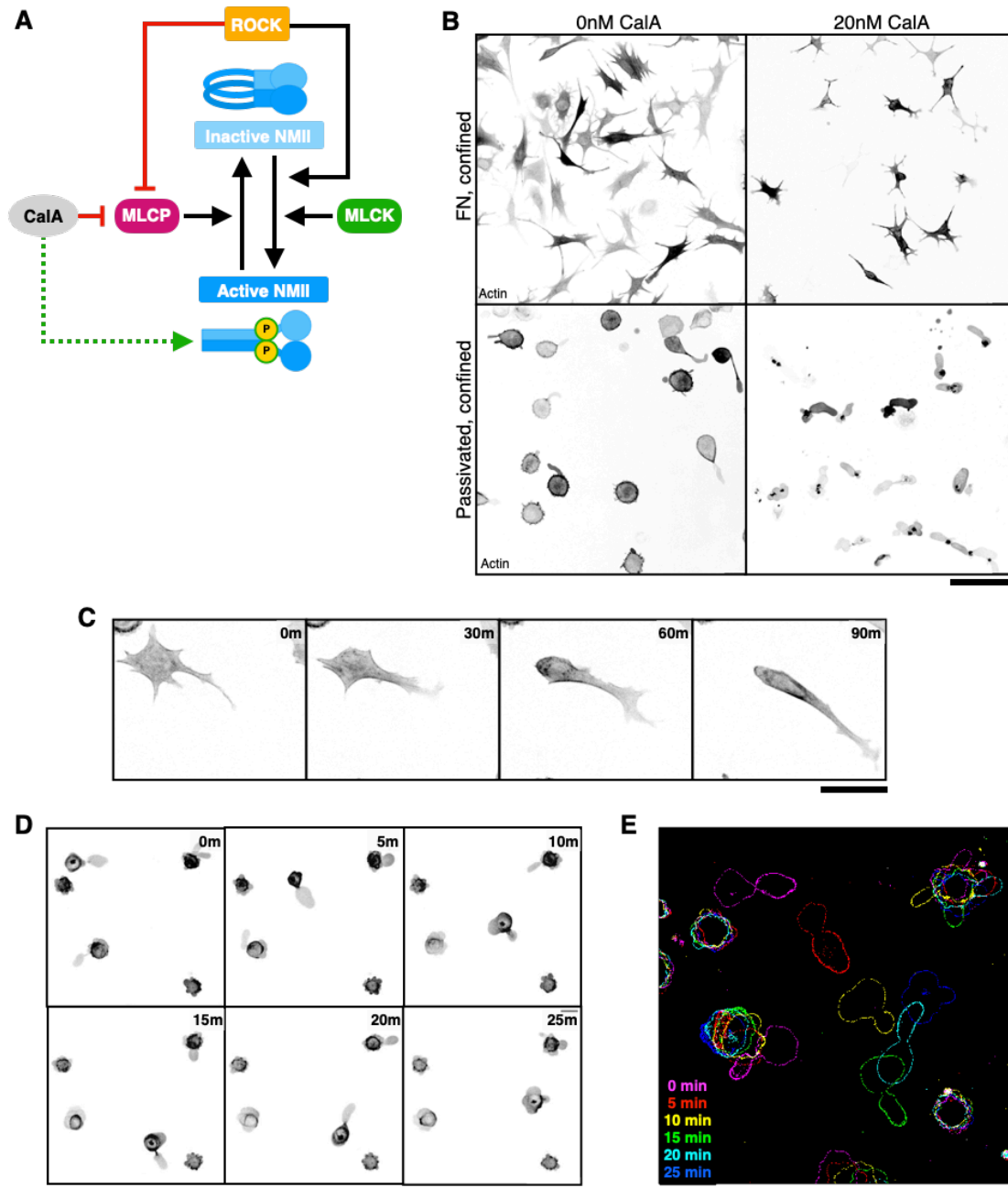


**Figure 11. High NMI Activity Drives Migration Mode Switching.** **A)** Calyculin A is a protein phosphatase inhibitor that prolongs NMI activation by preventing dephosphorylation of myosin regulatory light chain. **B)** MEFs confined to  $5\mu\text{m}$  on either FN (*top*) or passivated glass (*bottom*) and either with (*right*) or without (*left*) CaIA treatment. Scale bar =  $100\mu\text{m}$ . **C)** Confined MEF migrating with elongated morphology on FN with 20nM CaIA treatment. Scale bar =  $50\mu\text{m}$ . **D)** Time lapse series of confined MEFs migration on passivated glass with 20nM CaIA treatment. Scale bar =  $50\mu\text{m}$ . **E)** Time lapse composite of cells in (D). Color coded by time-point. Scale bar =  $50\mu\text{m}$ . All cells shown express LifeAct-tdTomato.

## High Contractility Drives Fast Amoeboid Migration

To confirm that the effects of confinement leading to retraction of the cell margin were indeed due to increased cortical contractility, I treated cells with Calyculin A (CalA), a general protein phosphatase inhibitor, concurrently with confinement. In this case, preventing the removal of the phosphate group from the regulatory light chain of active NMII will prolong the activity of the motors and lead to a global increase in contractility (Figure 11A).

**Enrichment of NMII activity promotes migration mode switching.** When treated with CalA and confined on FN, MEFs displayed even further retraction of the cell margin, confirming that the neurite-like morphology observed earlier for MEFs confined on FN was likely caused by increased cortical contractility (Figure 11B, top panels). Cells that maintained their motility migrated more slowly than even cells confined on FN without CalA. However, a small subpopulation of CalA-treated MEFs took on an elongated shape, such that both the cell body and leading protrusion appeared to be roughly the same width (Figure 11C). This morphology resembled what has been described as a nuclear piston, or lobopodial, motility program.

Importantly, this mode of migration has been observed in fibroblasts that maintain robust cell-substrate adhesion following the increase in actomyosin contractility that occurs upon inhibition of MMP-mediated matrix degradation (Petrie et al., 2017). As the name suggests, during this type of migration, cells use their nuclei like a piston to generate a high-pressure compartment at the front of the cell, which promotes the

formation of narrow, pressurized lobopodial protrusions (Petrie et al., 2012). This mode of migration requires high actomyosin contractility both at the rear, where cortical contraction pushes the nucleus forward, and in front of the nucleus, where contractile SFs physically couple FAs at the anterior margin to the vimentin IF network that encapsulate the nucleus at the rear of the cell. Contraction of SFs pulls the nucleus forward along the path generated by the protruding lobopodia, repeating the cycle of pressurization, protrusion, and translocation (Petrie et al., 2012). Due to the increased intracellular pressure, lobopodial cells often form small, round blebs along their lateral edges, similar to those seen in MEFs confined on passivated surfaces. This result indicates that the modulation of actomyosin contractility can drive migration mode transitions, even in highly-adhesive conditions.

**High contractility without adhesion drives fast amoeboid motility.** Previous work on migration plasticity has shown that the fast, leader bleb-based (LBB) mode of amoeboid migration depends on both the absence of adhesions and strong cortical flows (Paluch et al., 2016; Bergert et al., 2015; Ruprecht et al., 2015). However, studies suggested that non-transformed mesenchymal cells rarely, if ever, use LBB migration, instead preferring the slower pseudopodal-amoeboid motility program (Liu et al., 2015).

To determine if MEFs could be induced to undergo MAT to take on the LBB mode of migration, I again treated MEFs with 20nM CalA and confined them on passivated surfaces. Surprisingly, nearly all cells formed large, stable leader blebs immediately following confinement (Figure 11B, *bottom panels*). Meanwhile, a smaller

subpopulation of polarized cells displayed rapid translocation, at the scale of 5-10um per minute (Figure 11D-E). In comparison to all other conditions evaluated, CalA-treated cells migrating under non-adhesive confinement moved with the highest velocity, consistent with the LBB motility phenotype (Figures 9B, 11E).

It is important to note the distinction between the elongated, stable blebs seen in MEFs under non-adhesive confinement without CalA and a true leader bleb. While the former can form independent of motility status, the latter constitutes a locomotive structure that facilitates fast amoeboid migration (Garcia-Arcos et al., 2022). Elongated stable blebs are also typically smaller than leader blebs, containing a significantly lower proportion of total cell volume. While elongated stable blebs can become leader blebs upon cytoplasmic transfer and onset of locomotion, they remain functionally distinct.

In this section, I have described the effects of mechanical confinement, substrate-adhesion, and cortical contractility on the morphology and migration behavior of MEFs. Confinement under conditions promoting strong cell-substrate adhesion results in significantly decreased cell spreading and retraction of lamellipodia into elongated neurite-like protrusions (Figure 9C). The presence of ECM, however, allows cells to maintain adhesion to the environment, thereby limiting the increase in cortical contractility (Figure 10A). In contrast, when FA assembly is blocked by passivation of the confining surfaces, cells become fully rounded upon compression and form many transient blebs across the cell margin, indicative of increased intracellular pressure (Figure 10A). Further enrichment of cortical contractility via prolonged activation of NMII

motors ultimately drives the transition from an immotile, dynamic blebbing morphology to a fast LBB mode of migration, following spontaneous polarization (Figure 11B, *bottom panels*). Together, these findings confirm that, under the appropriate conditions, MEFs display migration plasticity and can transition to a fast amoeboid mode of migration.

Figure 12 graphically summarizes the effects of contractility and adhesion on MEF morphology.

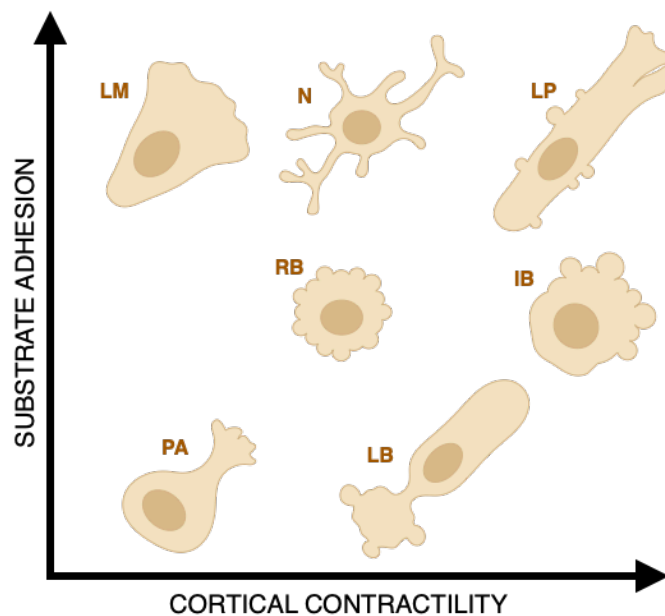


**Figure 12. Effects of Contractility and Substrate Adhesion on MEF Migration Behavior.** Graphical summary of observed MEF morphologies as a function of cell-substrate adhesion and cortical contractility. Substrate adhesion level increases along the vertical axis from none to weak adhesion to strong integrin-mediated adhesion, corresponding to surfaces of passivated glass, untreated glass, and FN, respectively. Cortical contractility level increases along the horizontal axis from low to intermediate to high contractility, corresponding to conditions of no confinement,  $5\mu\text{m}$  confinement, and  $5\mu\text{m}$  confinement with NMII enrichment (+ CalA), respectively. From left to right, top to bottom: (LM) lamellipodial, (N) neurite-like, (LP) lobopodial, (RB) immotile, rounded blebbing, (IB) intermittent blebbing, (PA) pseudopodal-amoeboid, (LB) leader bleb-amoeboid. *Modified from Liu et. al., 2015.*

### Cortical Dynamics Mediate Migration Mode Switching

In the previous section, I reported that modulation of extracellular conditions and cortical contractility can induce MEFs to take on a fast, LBB mode of migration. This agrees with previous studies, which have shown that, in contrast to lamellipodial or



lobopodial modes of fibroblast motility, LBB migration requires the absence of cell-matrix adhesions and, further, relies on cortical contractility to generate long-range flows that power locomotion (Paluch et al., 2016, Liu et al., 2015, Ruprecht et al., 2015). While this type of motility has been observed in cells from diverse tissues of origin *in vitro*, including immune cells, muscle precursors, and many transformed cancer cell types (Liu et al., 2015, Ruprecht et al., 2015, Logue et al., 2015, Bergert et al., 2015), the specific molecular mechanisms governing LBB in MEFs have not yet been described in detail.

Using high resolution confocal microscopy, in combination with our micropillar confinement system, I imaged actin, NMII, and associated proteins in live MEFs to delineate the discrete molecular events occurring at the cortex during the transition to LBB migration. In this section, I will describe how the dynamic assembly and reticulation of actomyosin networks drives coordinated changes in cortical organization and contractile activity.

### **Loss of Adhesions Drives Cortical Actomyosin Remodeling**

The transition from normally spread, mesenchymal morphology to a rounded, transiently blebbing states requires increased cortical contractility and the inhibition of FA formation (Figure 10A). In transformed cancer cells, the absence of FAs is often accompanied by a corresponding loss of thick actomyosin SFs, which are major hallmarks of mesenchymal migration. While inhibition of integrin-based adhesions has been shown to disrupt SF assembly and promote amoeboid migration, cells that form

nascent adhesions without corresponding SF formation may still employ mechanisms of amoeboid migration (Liu et al., 2015; Poincloux et al., 2011). Therefore, it follows that FA-dependent SF polymerization, rather than the presence of FAs themselves, may be a key limiting factor for MAT. Thus, I first sought to delineate the how key structures of the actin cytoskeleton, including SFs, are affected by the loss of FAs during the transition from lamellipodial to LBB motility.

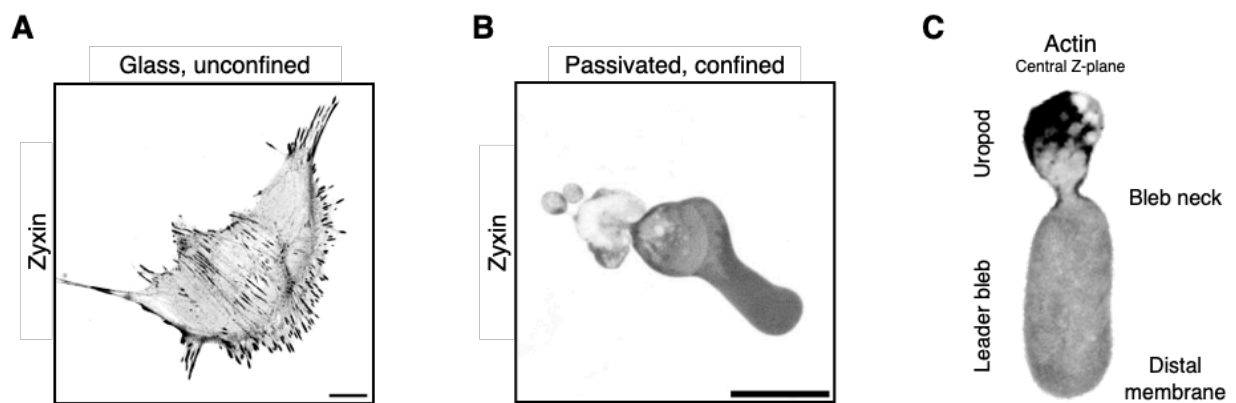


**Figure 13. Leader Bleb-Based Migration Does Not Require Focal Adhesions or Stress Fibers.** **A-B)** Zyxin-EGFP localization in MEFs migrating in 2D on glass (A)\* or under non-adhesive confinement (B). \*Data courtesy of Dr. Lee Troughton, Loyola University Chicago. Scale bars = 20 $\mu$ m. **C)** Central z-plane of a confined MEF expressing 3x-mScarlet-Ftractin using LBB migration. Highlights key regions of leader bleb cells and lack of internal actin structures.

I first evaluated how the localization of FA components is altered in MEFs using the LBB motility program, in comparison to those using their typical mode of lamellipodial migration. As introduced previously, zyxin is a mechanosensitive adhesion plaque protein that fortifies the linkage between integrin-bound adaptors at the plasma membrane and the internal actomyosin cytoskeleton, helping to mediate adhesion-dependent force transmission. Because zyxin plays a crucial role in the mechanical regulation of SF assembly and is only present in mature complexes, I specifically chose to evaluate zyxin localization as a marker for mature FA assembly in confined MEFs.

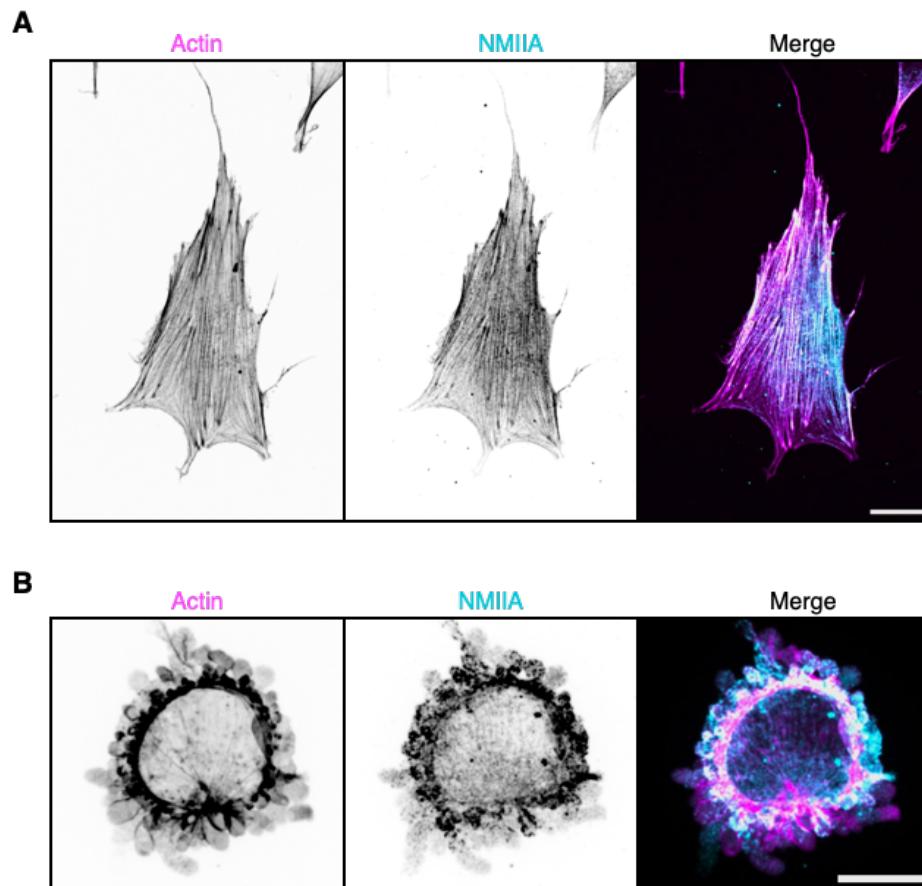


**Figure 14. Loss of Stress Fibers Coincides with Cortical Actomyosin Enrichment.** Fixed MEFs stained for F-actin (phalloidin) or immunostained for NMIIA **A**) Co-localization of F-actin and NMIIA to stress fibers in fixed unconfined MEFs on untreated glass. Scale bar = 20 $\mu$ m. **B**) Cortical co-localization of F-actin and NMIIA in MEFs under non-adhesive confinement with CalA treatment. Scale bar = 10 $\mu$ m.

In contrast to the punctate localization of zyxin in unconfined MEFs (Figure 13B), upon non-adhesive confinement and NMII activation, zyxin appeared diffuse in both the cytoplasm of the leader bleb and the posterior uropod (Figure 13A). This also further confirmed that MEFs using LBB migration do not require specific adhesion to the ECM and, instead, appear to rely on alternative adhesion-independent mechanisms of migration. In agreement with previous studies of cancer motility, I also found that when FA assembly was inhibited by surface passivation, MEFs displayed a corresponding loss of SFs (Figure 14A-B). Instead, F-actin and NMII assembly in blebs was almost

exclusively restricted to the cortex, while the interior was consistently devoid of internal actomyosin structures (Figure 13C, 14B). Meanwhile, the increase in cortical density observed when cells transition from a spread to a rounded morphology suggests that the disassembly of SFs may be coordinated with the redistribution of F-actin and NMII to the cortex (Figure 14A-B). This further confirms that LBB migration does not involve FA-mediated traction and, instead, indicates that the requirement for high NMII activity involves another contractility-dependent motility mechanism, mediated by the cortex.

### **Distal Cortex Depletion Enables Bleb Stabilization**

Clearly, the loss of adhesions and SFs drives extensive reorganization of the actin cytoskeleton leading to increased cortical density and, hypothetically, increased cortical contractility as a result. I have shown that non-adhesive confinement drives cellular rounding and transient bleb formation, presumably due to the contractility-dependent rise in intracellular pressure (Figure 10A). Without further enhancement of NMII activity, however, round blebby MEFs remain largely immotile, suggesting that high NMII-mediated cortical contractility is required to establish polarity ahead of leader bleb formation (Figure 10A). Because F-actin and NMII localization is restricted to the cortex of leader blebs, I next focused on delineating the changes in cortical network organization that trigger the switch from an immotile, blebby phenotype to fast, polarized LBB migration. To distinguish between the mechanisms of actomyosin assembly that lead to bleb stabilization, as opposed to retraction, I investigated differences between F-actin dynamics in the cortex of round transient blebs versus elongated stable blebs.

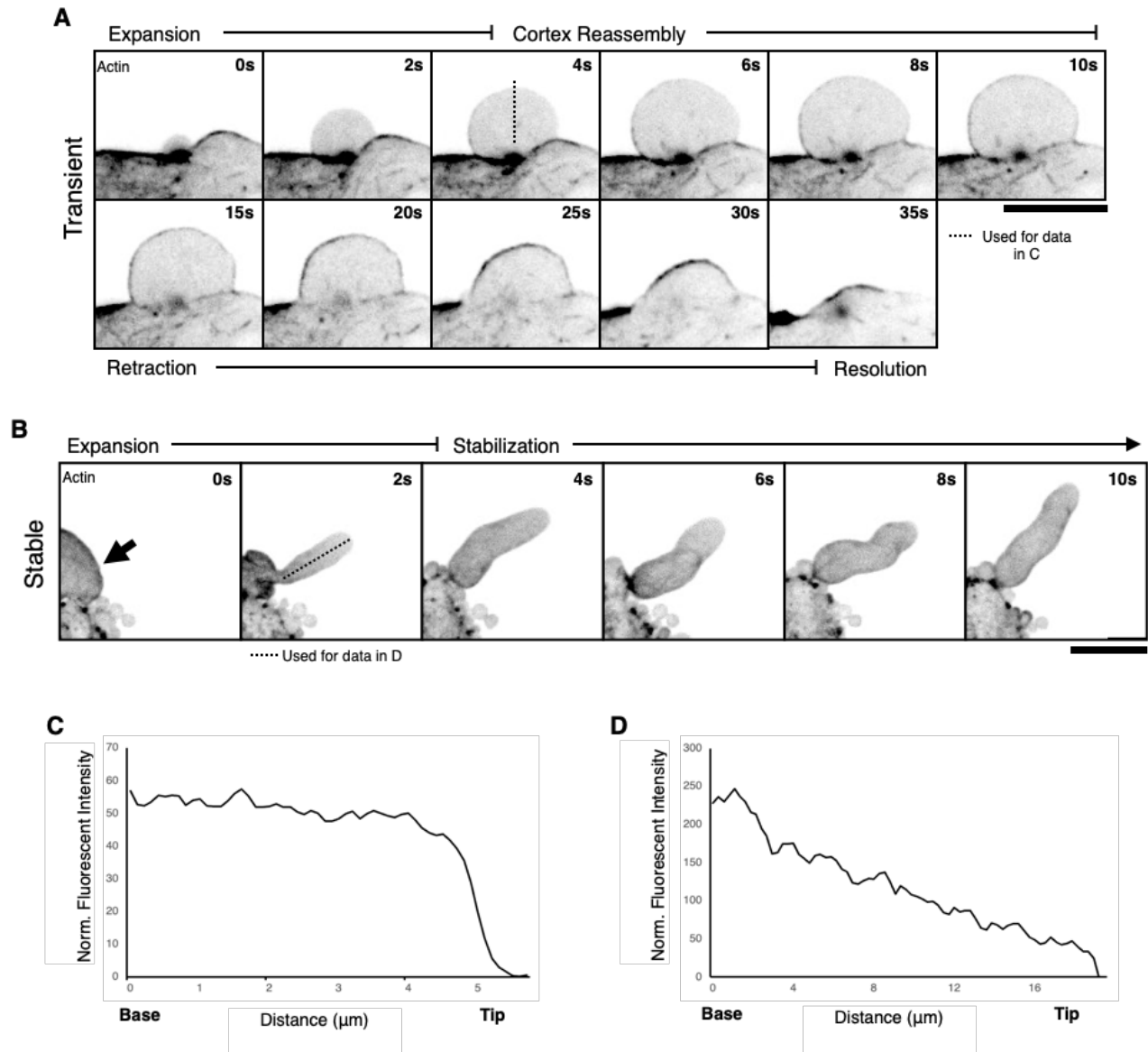


**Figure 15. Non-Adhesive Confinement Generates Two Types of Blebs.** **A)** Time lapse series of the expansion-retraction cycle of a transient, rounded bleb. Scale bar =  $10\mu\text{m}$ . **B)** Time lapse series of the expansion and stabilization of an elongated stable bleb. Red arrow indicates the site of cortical rupture and bleb nucleation. Scale bar =  $20\mu\text{m}$ . All cells shown express LifeAct-tdTomato. **C-D)** Actin distribution along region indicated by black dotted lines in (A, 4s) and (B, 2s), respectively.

In transient blebs, cortical actomyosin assembly at the distal membrane stalls expansion and retracts the bleb (Charras et al., 2006; 2008). Elongating stable blebs, however, appear to resist actomyosin accumulation and subsequent retraction (Figure 15A-B). While retractile bleb dynamics have been well characterized, under closer

examination of F-actin and NMIIA assembly in the stable bleb cortex, I found that these two types of pressurized protrusions have distinct actin distributions. While transient blebs maintain a fairly uniform density of actin throughout the expansion stage, stable blebs rapidly generate an actin gradient along their length as they elongate (Figure 15BC-D). This gradient forms almost immediately upon nucleation and appears to be maintained throughout stable bleb persistence (Figure 15D). This is similar to the gradient of cortical actin seen in motile leader bleb cells (Figure 16; Liu et al., 2015).

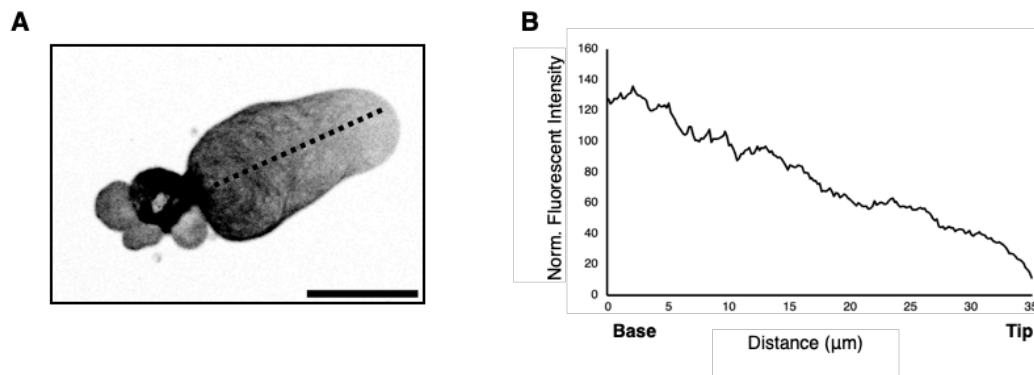


**Figure 16. MEFs Using Leader Bleb-Based Motility Display a Cortical Actin Density Gradient. A)** MEF using LBB migration under non-adhesive confinement with 20nM CalA treatment. Scale bar = 20μm. **B)** Gradient of fluorescent intensity of LifeAct-tdTomato in the cortex of the MEF in (A). Black dotted line indicates ROI of fluorescent intensity measurement from base to tip.

Without homogenous reassembly of cortical actin at the distal membrane, as in transient blebs, stable blebs resist retraction and persist in their elongated steady-state (Figure 15B). In motile amoeboid cells using LBB migration, the gradient of actin is generated and maintained by retrograde cortical flows that maintains a cortex-depleted distal membrane (Ruprecht et al., 2015; Liu et al., 2015; Bergert et al., 2015). To determine if bleb elongation and stabilization requires a similar mechanism in confined MEFs, I investigated the distribution and dynamics of cortical actin during stable bleb formation and persistence.

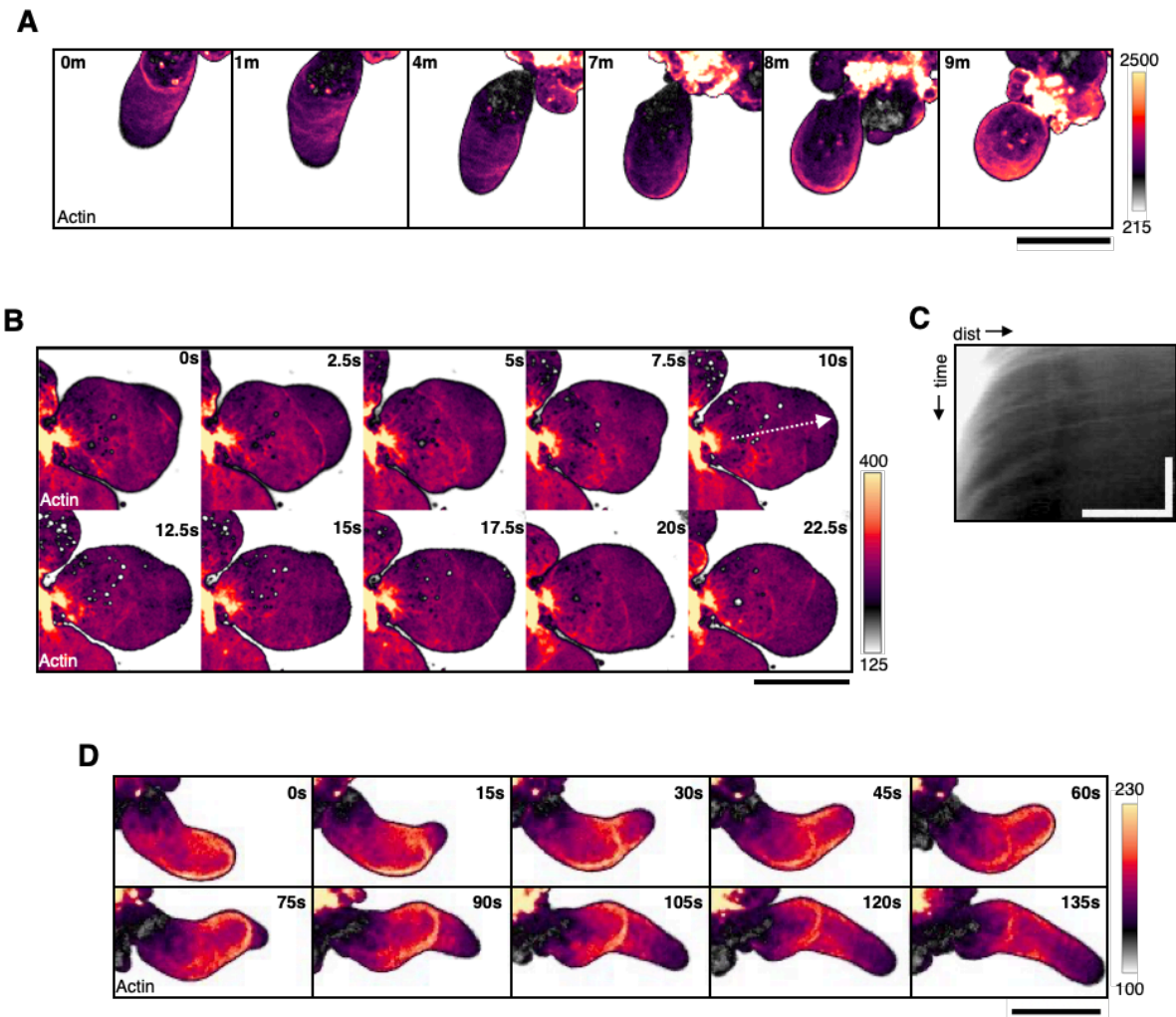


**Figure 17. Retrograde Flow Maintains a Cortex-Depleted Distal Membrane in Stable Blebs.** **A)** Time lapse series of actin accumulation at the distal membrane of a stable bleb. Scale bar = 20 $\mu$ m. **B)** Time lapse series of actin retrograde flow in the stable bleb cortex. White dotted arrow indicates ROI for kymograph in (C). Scale bar = 20 $\mu$ m. **C)** Kymograph of cortical actin flow in (B). Vertical scale bar = 20s, horizontal scale bar = 5 $\mu$ m. **D)** Time lapse series of consecutive compound blebbing events in a stable bleb. Scale bar = 20 $\mu$ m.

As in transient blebs, stable blebs were retracted upon the eventual accumulation of cortical actin at the distal membrane (Figure 17A). Notably, this occurred at a much more extended time scale than during the retraction of rounded, transient blebs and also corresponded to the collapse of the stable bleb's cortical actin gradient (Figure 15A-B, 17A). Together with previous characterizations of bleb dynamics, this result indicates that cortex-depletion at the distal membrane is a requirement for bleb

stabilization and persistence (Charras et al., 2008; Tooley et al., 2009; Logue et al., 2015). Unlike transient blebs, stable blebs that maintained persistence exhibited rear-directed waves of actin (Figure 17B). Under closer examination, it became evident that these unidirectional waves were the result of pulsatile cortical retrograde flows (Figure 17B-C). Interestingly, these actin flows increased in velocity with closer proximity to the base of the stable bleb, suggesting a feedback mechanism in which of network advection may be coupled to the rate of cortical flow (Figure 17C).

The most important function of these flows appeared to be related to the depletion of cortical actin from the distal membrane of the bleb. Indeed, upon closer examination, I found that compound blebbing events at the distal membrane could trigger re-emergence of cortical retrograde flows even once cortex reassembly had been initiated (Figure 17D). Here, “compound blebbing” refers to a phenomenon that occurs when the cortex has not yet been assembled into a full homogenous layer at the distal membrane, such that the newly formed network still maintains sites of network instability. Thus, the high-pressure conditions within the cytosol of the bleb can rupture the fragile network at the distal membrane to prolong stability (Figure 17D).

Furthermore, consecutive compound blebbing are likely to generate prolonged cortical flows that, if occurring over a long-range, can contribute to LBB motility. This has been observed in both embryonic progenitors and cancer cells, where repeated compound blebbing events can generate waves that are eventually amplified into steady-state retrograde flows to sustain motility (Ruprecht et al., 2015; Bergert et al., 2015).



## Contractility Gradients Generate Cortical Flows for Bleb Stabilization

In motile leader bleb cells, retrograde cortical flows are generated and sustained by polarized contractility activity of NMII at the base of the bleb coupled with steady network turnover (Liu et al., 2015; Logue et al., 2015). To investigate if the flows generated in the stable bleb cortex of confined MEFs are mechanistically similar to those involved in LBB migration, I examined the localization of NMII motors during bleb elongation and stabilization.

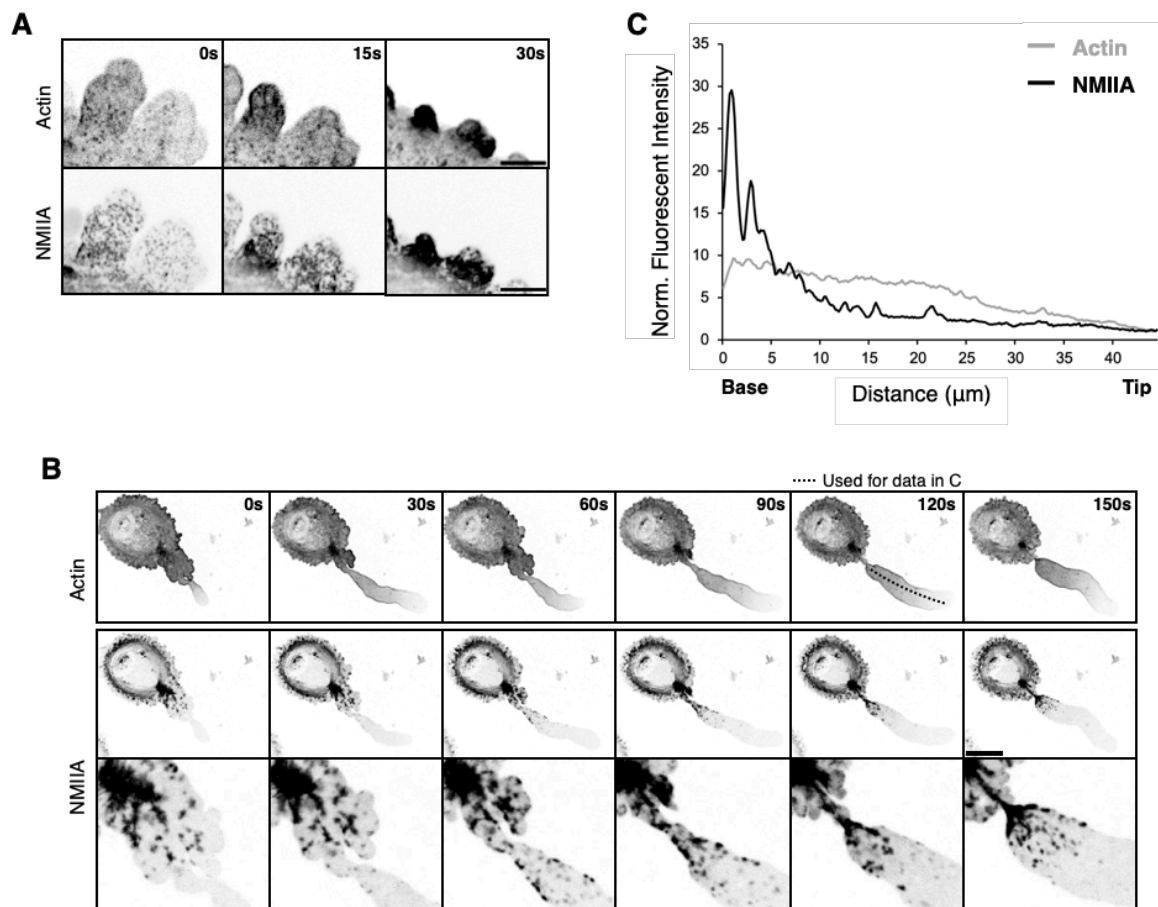


**Figure 18. Stable and Transient Bleb Display Distinct NMII Profiles.** MEFs treated with CalA under non-adhesive confinement, expressing Ftractin and NMIIA-EGFP. **A)** Time lapse series of the membrane localization and global contraction of cortical actin and NMII during retraction of a round, transient bleb. Scale bar = 10µm. **B)** Time lapse series of cortical actin and NMIIA during stable bleb elongation. NMIIA accumulation at the base of the bleb correlates with closure of the bleb neck and simultaneous stabilization of the cortical actin gradient. Scale bar = 20µm. **C)** Base-to-tip distribution of cortical actin and NMIIA in the stable bleb, from panel B at 120s.

While NMIIA contraction at the transient bleb membrane follows complete cortical actin assembly (Figure 15A, 18A), NMIIA localization in the stable bleb cortex is restricted to the proximal region, closest to the base (Figure 18B-C). Interestingly, during elongation of the stable bleb, the time scale of NMII clustering at the base corresponds to closure of the bleb neck (Figure 18B). NMIIA accumulation also appears to follow an initial stage of diffusion into the bleb, followed by retrograde flow back to the base (Figure 18B). In leader blebs, this has been attributed to the capture of NMII motors by flowing actin and translocation of motors to the rears (Liu et al., 2015). Meanwhile, a gradient of cortical actin forms almost immediately after nucleation, which persists unless the bleb is eventually retracted (Figure 15B, 17A). Compared to the gradient of cortical actin, which declines steadily from base to tip, the majority of cortical NMIIA distribution was localized to the proximal third of the bleb following stabilization (Figure 18C). Because this region also corresponds to the highest rate of retrograde flow (Figure 17C), it is likely that the accumulation of NMIIA motors at the base of the bleb facilitates stabilization, as seen in the initiation of LBB migration (Liu et al., 2015; Ruprecht et al., 2015; Bergert et al., 2015).

Overall, these results indicate an important role for NMII contractility in 1) generating high intracellular tension required for bleb formation and 2) facilitating gradients in cortical tension that can produce cortical flows required for bleb stabilization. However, it is likely still that additional ABPs cooperate with actomyosin to organize the cortical network during retrograde flow and facilitate network turnover to sustain bleb stability.

## **Septins Associate with Actomyosin in the Stable Bleb Cortex**

Many ABPs have been found to cooperate with cortical F-actin and NMII motors during LBB migration. These include actin bundlers and crosslinkers like fascin and filamin that contribute to network architecture as well as regulators of cortex turnover, such as cofilin, ADF, and profilin (Logue et al., 2015; Adams et al., 2021). Importantly, stable bleb persistence and LBB motility rely on a strong gradient of contractility to sustain retrograde flows that deplete the distal membrane of cortical actin (Liu et al., 2015; Berget et al., 2015; Ruprecht et al., 2015). This means that the base of the bleb represents an actomyosin network experiencing high tension due to an increased density of NMII motors (Figure 18B-C).

Through their ability to interact with F-actin and NMII motors, septins have been found to play roles in modulating cortex rigidity in response to tensile strain, particularly during amoeboid migration (Gilden et al., 2012; Tooley et al., 2009). Because the cortex as a whole represents a contractile actomyosin array that is, by definition, mechanically coupled to the plasma membrane, I hypothesized that septins may play a role in the organization and stability of the cortical actomyosin network in the stable bleb. Thus, I investigated how non-adhesive confinement of MEFs would alter septin localization and coordination of septin-actomyosin dynamics.

### **Non-Adhesive Confinement Promotes Septin Localization to the Cortex**

Septins localize to and bind both the plasma membrane and tensile actomyosin structures to reinforce architectural stability (Bridges & Gladfelter, 2015; Gilden &

Krummel, 2010). In non-confined MEFs, septins localize with actin to the plasma membrane and decorate ventral SFs (Figure 19A). Upon non-adhesive confinement, however, septin filaments become enriched at the cortex, mirroring the redistribution of actomyosin (Figure 19B, *left*, 14A-B). They were frequently observed in higher densities at the base of blebs, similar to cortical actin (Figure 19B; 15A).

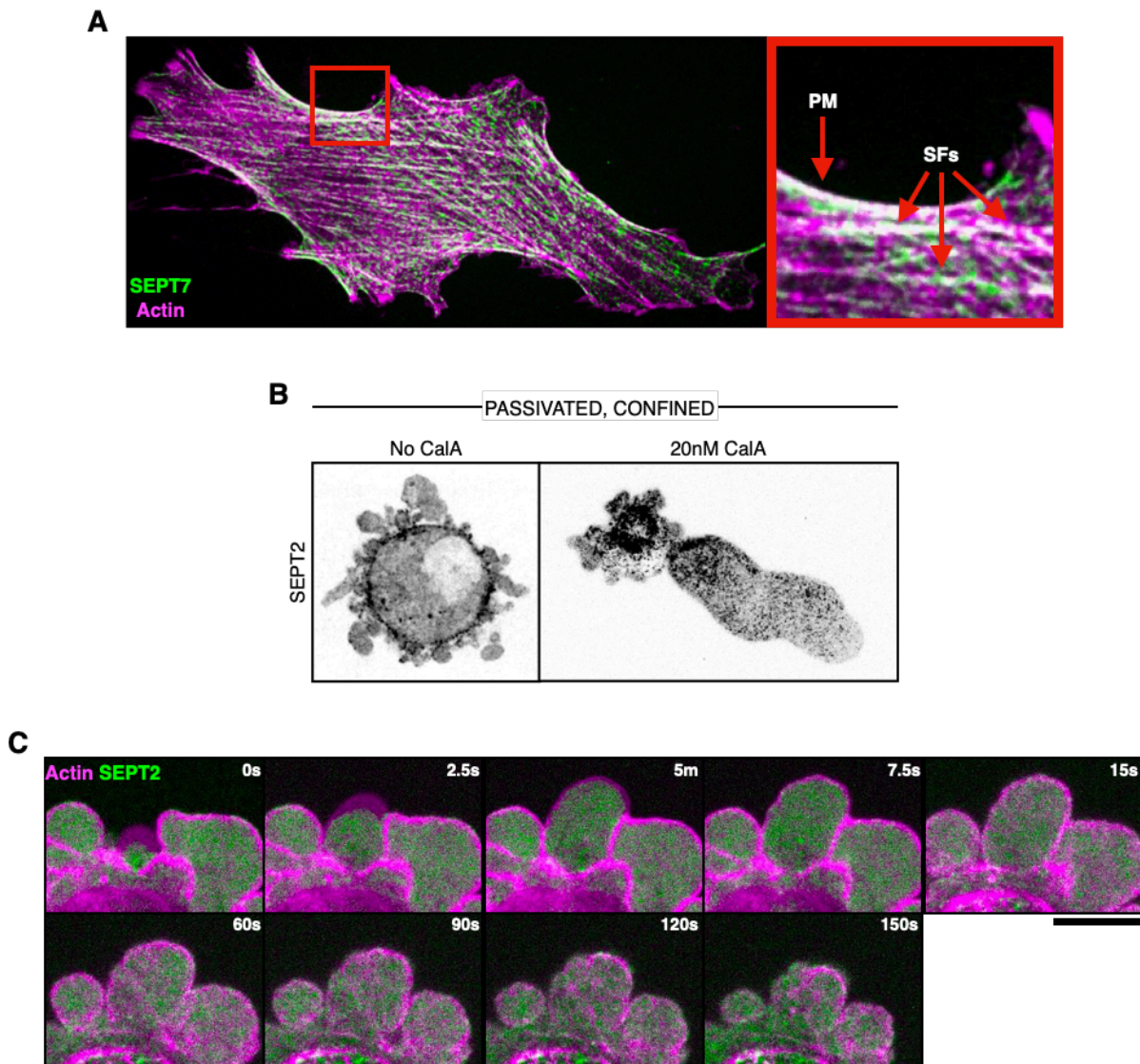


**Figure 19. Non-Adhesive Confinement Alters Cortical Septin Dynamics.** **A)** Immunostained MEF displaying colocalization of actin and SEPT7 at stress fibers (SFs) and the plasma membrane (PM). **B)** Localization of SEPT2 in MEFs under non-adhesive confinement, without (*left*) or with (*right*) CalA-induced enrichment of NMII activity. **C)** Time lapse series of coordinated enrichment of SEPT2 and actin at the distal membrane of transient blebs during retraction. Scale bar = 10 $\mu$ m.

During retraction of transient blebs, septins localized to the distal membrane following cortical actin reassembly (Figure 19C). Septin enrichment at the bleb membrane appeared to coincide with the onset of bleb retraction, and septins remained at the membrane throughout the end of retraction and resolution. This result agrees with previous reports that septins are required for membrane retraction in amoeboid migrating T-cells (Tooley et al., 2009; Gilden et al., 2012). Indeed, these studies have further shown that depletion of septins correlates to an increase in non-productive blebbing that can disrupt cell polarity and halt migration (Gilden et al., 2012).

### **Septins and Actin Display Coordinated Dynamics in the Bleb Cortex**

When MEFs were treated with CalA prior to non-adhesive confinement, septin localization again mirrored that of actin, forming a distinct cortical density gradient from base to tip (Figure 19B, *right*, 20B). It has recently been proposed that septins share a mutually interdependent relationship with contractile SFs, such that the disassembly of SFs leads to septin-actin dissociation while, in turn, the inhibition of septins can lead to a disruption in SF assembly (Zhovmer et al., 2022; Spiliotis & Nakos, 2021; Fuchtbacher et al., 2011). Thus, this translocation of septins to the cortex may be a result of SF disassembly in the cytoplasm in combination with increased cortical tension due to confinement. Likewise, there is an apparent increase in septin enrichment at the proximal regions of the stable bleb, correlating to higher NMII density and, thus, cortical tension (Figure 18B-C; 19B, *right*). This could also be attributed to the tendency of septin filaments to bind regions of membrane curvature. Because of the similarities in

septin and actin localization in both transient and stable blebs, I next investigated the coordination of septin-actin dynamics at the cortex of elongated blebs.

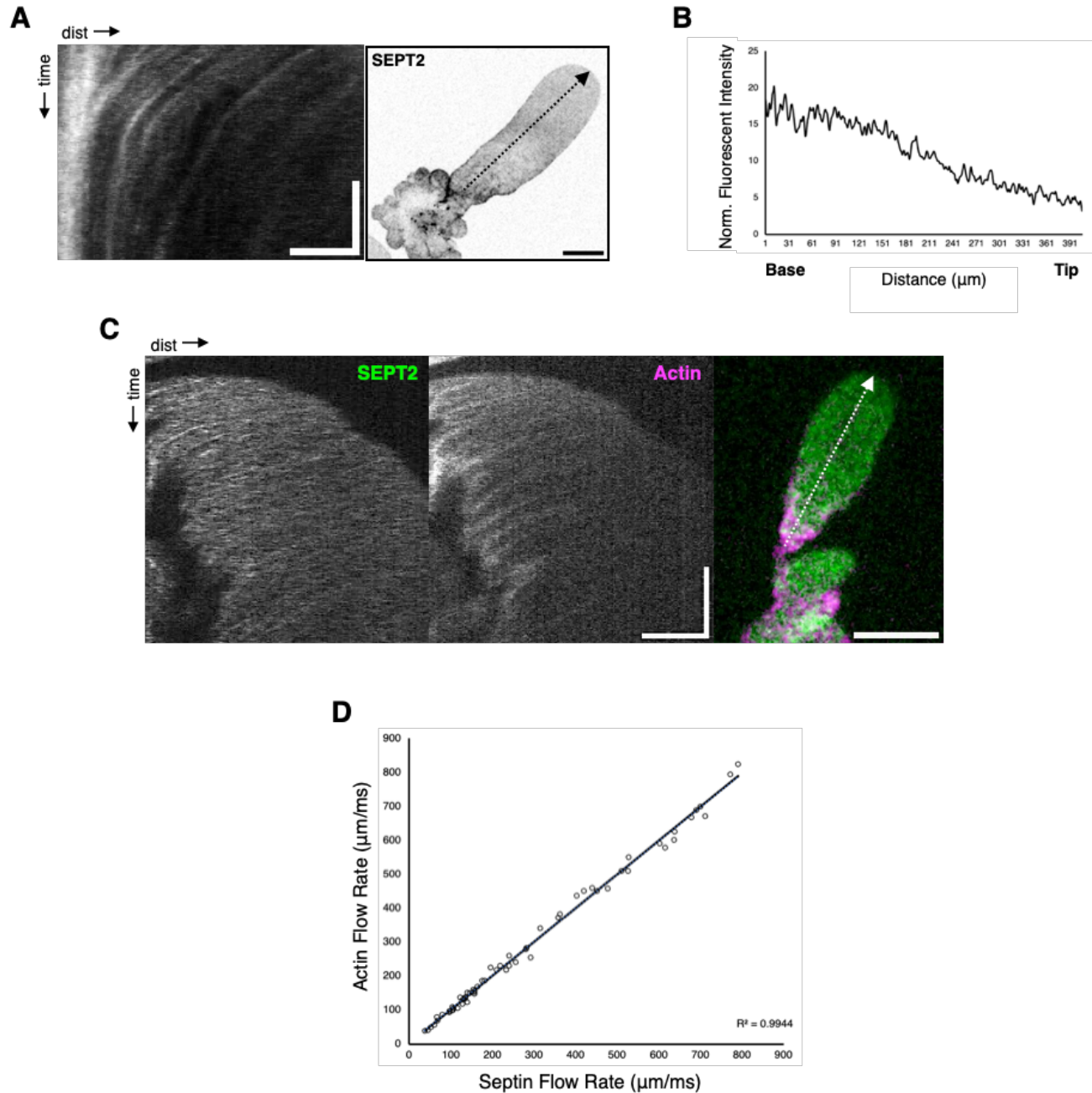


**Figure 20. Septins and Actin Undergo Coordinated Flows in the Bleb Cortex.** **A)** Cortical retrograde flow of SEPT2 in the leader bleb cortex. The kymograph ROI is indicated by the black dotted arrow. Kymograph: vertical scale bar = 5s, horizontal scale bar = 5μm. Image: scale bar = 10μm. **B)** Distribution of SEPT2 along the region indicated by the arrow in (A). **C)** Cortical retrograde flow of SEPT2 and actin in the stable bleb cortex, indicated by the white dotted arrow. Kymographs: vertical scale bar = 5s, horizontal scale bar = 5μm. Image: scale bar = 10μm. **D)** Plot of retrograde flow rates of actin (y-axis) or SEPT2 (x-axis). N = 60 blebs from 20 individual cells.

In the cortex of stable and leader blebs, septins undergo retrograde flow (Figure 20A). Similar to actin, the velocity of cortical flow appears highest at the base of bleb where septin density is also at its maximum (Figure 20A-B). To further assess the significance of these similarities, I compared the rates of SEPT2 and actin retrograde flows in cells expressing fluorescent tags for both proteins (Figure 20C). It appeared that, regardless of overall velocity, the rates of septin and actin flow were highly correlated. Indeed, when compared in a linear model, the relationship between septin-actin retrograde flow exhibited direct correlation, indicated by an R value of 0.9944 (Figure 20D).

While it is clear that septins and actomyosin interact in the bleb cortex and display highly correlated dynamics, the functional consequences of these interactions remained unclear. Because septins have been found to promote cortex rigidity and stability in response to deformation stress, it is plausible that the septin cytoskeleton regulates confinement-induced architectural reorganization of the cortical actin network in MEFs (Gilden et al., 2012; Zhovmer et al., 2022). Still, the contributions of this functional relationship have not yet been delineated.

### **Global Septin Depletion Alters Cortical Dynamics**

I have shown that septins interact with the cortical F-actin network in both dynamic and stable blebs, but the functional relationship between cortical septins and actomyosin during bleb stabilization and the switch to LBB migration remains unclear. Therefore, to evaluate how septins affect cortical actomyosin organization and

contractility, I generated a stable septin-depleted MEF cell line. I selected SEPT7 as the target protein for shRNA-mediated knock down for two key reasons: 1) it is an essential subunit of both septin hexamers and octamers, and 2) unlike SEPT2 or SEPT6, it is the only member of its group (Figure 21A; Spiliotis, 2018; Woods & Gladfelter et al., 2021). Thus, SEPT7 depletion cannot be rescued by upregulating the expression of another subunit in the same group.

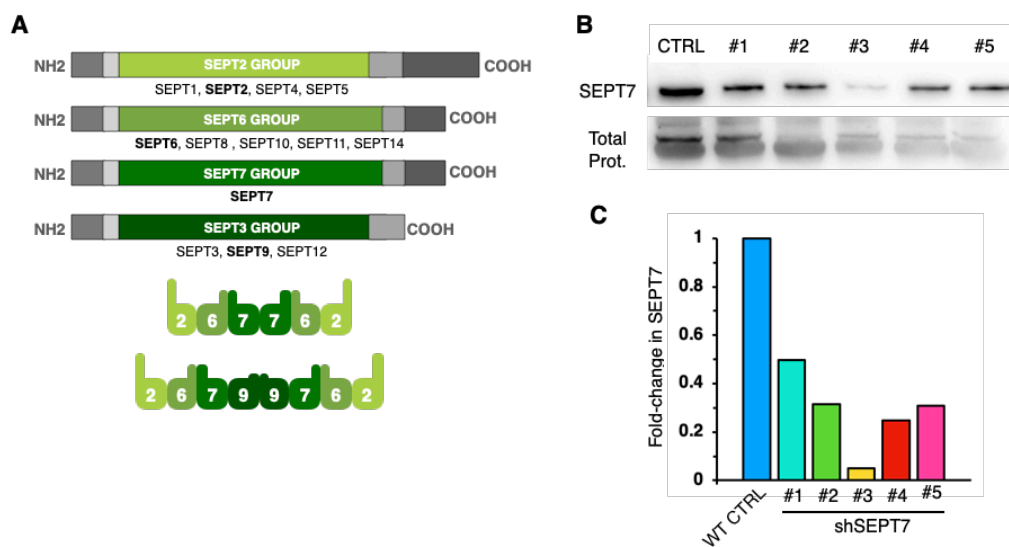


**Figure 21. Overview of shRNA-Mediated Septin Knockdown Experiments.** **A)** SEPT7 is the only member of its subgroup and is essential for both hexamer and octamer protofilament assembly. **B)** Five shSEPT7 constructs were initially tested \*Data courtesy of Maggie Utgaard, Loyola University Chicago. **C)** Quantification of SEPT7 expression from blot in (B). Normalized to total protein loading.

### SEPT7 knockdown disrupts septin filament assembly.

First, five different shRNA constructs were tested and their effects on SEPT7 expression quantified (Figure 21B-C). Because it displayed the best knock down efficiency in preliminary screenings, I transfected MEFs with construct #3 (shSEPT7-3) to generate the stable septin-depleted cell line. To evaluate knock down efficiency, I quantified the expression levels of SEPT7, the target protein, as well as SEPT2, another



essential subunit of both septin hexamers and octamers, via western blot. Compared to MEFs treated with non-targeting control shRNAs (shNT), all three independent MEF populations transfected with shSEPT7-3 generated displayed, on average, over a 60% reduction in SEPT7 expression and over a 40% reduction in SEPT2 expression (Figure 22A-C). This result indicates that knocking down one septin subunit impacts the expression of the target protein's interaction partners, suggesting a potential feedback mechanism for septin subunit expression and assembly.

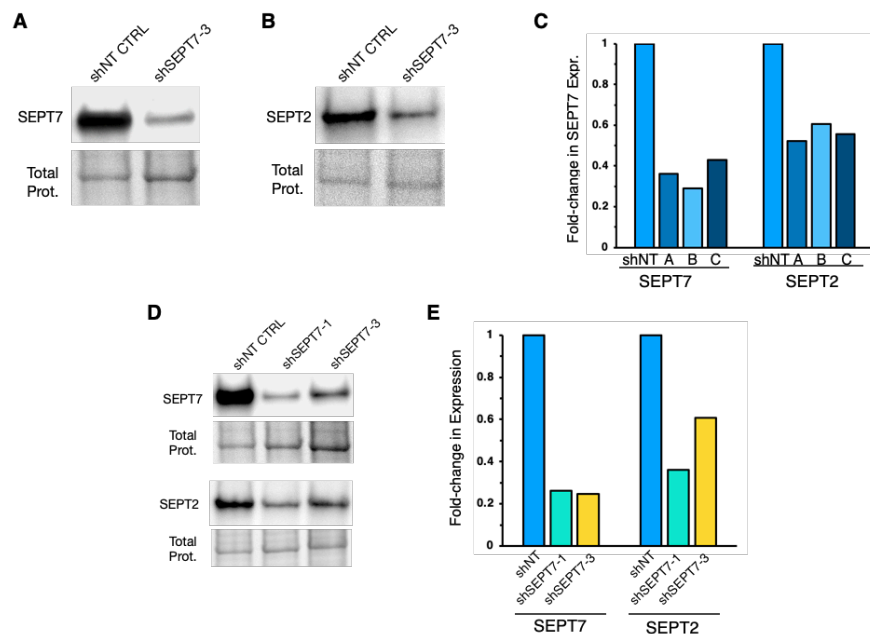


**Figure 22. SEPT7 Depletion Reduces Septin Filament Assembly.** **A-B)** Western blots of samples from MEFs expressing shNT or shSEPT7-3 blotted against SEPT7 (A) or SEPT2 (B). **C)** Quantification of western blot data in (A, B): three independent populations, each run in triplicate for both SEPT7 and SEPT2. **D)** Western blot of samples from MEFs expressing shNT, shSEPT7-1, or shSEPT7-3. **E)** Quantification of western blot data in (C). SEPT7: Average of two independent populations each run in triplicate for both constructs. SEPT2: Average of two independent populations, each run in duplicate for both constructs.

To verify that these results were due to shRNA-targeting, I expressed a second shSEPT7 construct, shSEPT7-1 in MEFs and quantified the differences in both SEPT7 and SEPT2 expression relative to cells expressing shSEPT7-3. Indeed, both shRNAs disrupted septin expression and had a similar effect on SEPT7 levels – an average

reduction of over 70% across 3 independent populations (Figure 22D-E). However, shSEPT7-1 expression appeared to deplete SEPT2 more than SEPT7 (Figure 22E).

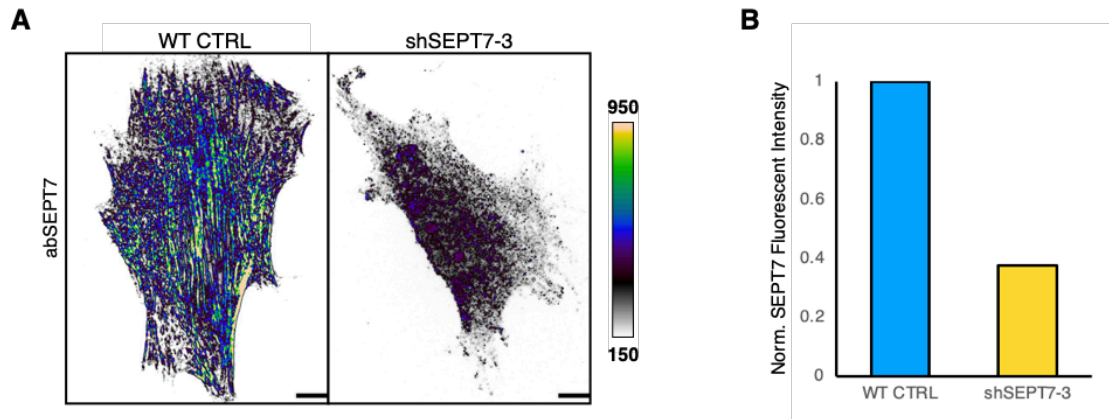


**Figure 22. SEPT7 Depletion Disrupts Septin Filament Assembly.** **A)** Representative images of fixed WT and SEPT7-knockdown MEFs, immunostained against SEPT7. **B)** Relative fluorescent intensity fold-change of SEPT7, normalized to background and WT controls. N = 20 cells for WT; N = 25 cells for septin knockdowns.

To confirm that shRNA-mediated knockdown of SEPT7 disrupts septin filament assembly, I looked at changes in the quantity and localization of SEPT7 in non-confined fixed and immunostained cells (Figure 23A). Compared to the WT control population, MEFs expressing shSEPT7-3 displayed an approximately 60% reduction, on average, in septin filament assembly, indicated by the decrease in SEPT7 expression (Figure 23B). While cells maintained a low level of SEPT7 expression, the distribution of septin filaments was diffuse in the cytoplasm of septin knockdown cells, in contrast to the strong association of septin filaments with the membrane and actomyosin SFs seen in the WT controls (Figure 23A).

### Septin Depletion Increases NMII Motor Expression

To assess the effect of septin depletion on MEF migration behavior, I confined cells expressing either shNT or shSEPT7-3 on passivated surfaces with CalA to

stimulate high NMI activity. These conditions mirrored that of earlier experiments performed with WT cells. I categorized bleb morphology into three groups: round, unstable, or stable/leader (Figure 24A). Cells categorized as “round” displayed a spheroid cell body with a dense cortex and small, transient blebs around their margins. Cells categorized as “unstable” exhibited intermediate characteristics between fully rounded and fully stabilized, typically representing a pre-polarization stage such as circus or compound blebbing. Finally, cells categorized as “stable” exhibited either a stable, elongated bleb or were fully polarized with a motile leader bleb morphology.

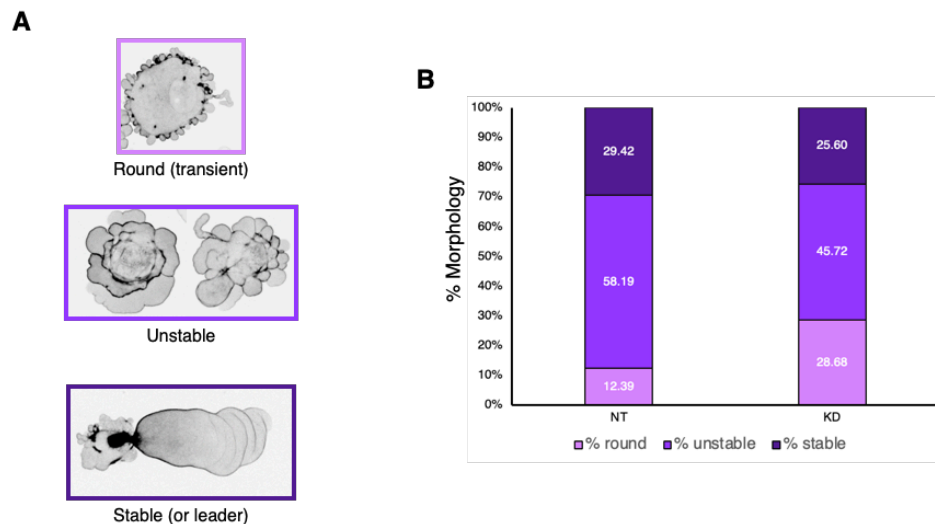


**Figure 23. Septin Depletion Increases Cell Rounding and Transient Blebbing.** **A)** Representative images of MEF morphology categories. **B)** Quantification of bleb morphologies. All cells were treated with 20nM CalA and confined on passivated surfaces. Plot displays average morphology percentages from two independent experiments. Minimum of N = 100 cells per condition per experiment.

Compared to NT controls, septin-depleted cells had a higher frequency of cell rounding and transient blebbing, with a corresponding decrease in unstable blebbing (Figure 24B). Notably, the septin knockdown cells did not appear to display a significant change in the frequency of stable or leader bleb formation, despite a lower frequency of cells displaying the more dynamic intermediate phenotypes (Figure 24B). This suggests

that disruption of septin filament assembly may impact cells' ability to polarize following initial confinement. Transient blebbing can occur due to cells not maintaining a high enough level of contractility to promote polarization but can also be the result of hypercontractility (Cowan et al., 2022). Due to the unexpected response of the septin-depleted MEFs to confinement and CaIA treatment, I investigated how septin depletion may impact cortical dynamics by quantifying changes in NMII motor expression.

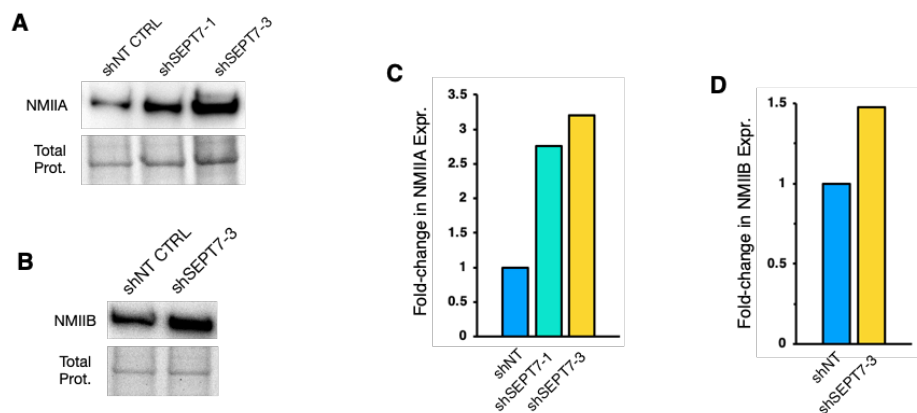


**Figure 24. Septin Depletion Correlates to Increased NMIIA/B Expression.** All bands were initially corrected for background signal and normalized to total protein loading. **A,C)** Average of three independent populations expressing shSEPT7-3, each run in triplicate; average of two independent populations expressing shSEPT7-1, each run in triplicate. Both normalized to shNT-expressing controls. **B,D)** Average from triplicates of one population expressing shSEPT7-3. Normalized to shNT-expressing controls.

In comparison to shNT-expressing controls, septin-depleted MEFs displayed a significant increase in NMIIA expression (Figure 25C). Cells expressing shSEPT7-1 exhibited over a 2.5-fold increase, while those expressing shSEPT7-3 had over a 3-fold increase in NMIIA expression (Figure 25C). Similarly, MEFs expressing shSEPT7-3 displayed a nearly 1.5-fold increase, on average, in NMIIIB expression (Figure 25D). Together, these results may indicate and explain why septin-depleted MEFs were more sensitive than NT controls to NMII enrichment under non-adhesive confinement.

## CHAPTER 5

### DISCUSSION

Blebs in mammalian cells have been studied for nearly 20 years in many different cellular contexts (Charras et al., 2008; Tinevez et al., 2009). Studies in cell migration have shown that the formation of a single polarized bleb can facilitate fast amoeboid-like migration in the absence of cellular adhesions to the matrix (Charras & Paluch, 2008; Liu et al., 2015). Researchers have recently discovered that these large blebs are sustained by persistent cortical flows, coupled to an NMII-dependent contractility gradient that powers motility (Bergert et al., 2012; 2015; Liu et al., 2015; Ruprecht et al., 2015; Maiuri et al., 2015). Such motility can be observed in breast cancer cells *in vivo* within tumor microenvironments (Tozluoglu et al., 2013; Wolf et al., 2003; Freidl & Alexander, 2011).

In this thesis, I have identified three types of functionally distinct blebs that form during MAT in MEFs: round transient blebs, elongated stable blebs, and large leader blebs that confer fast amoeboid motility (Figure 26). While the dynamics of transient blebs and the mechanisms of bleb-based motility have been well characterized, only the steady-state pictures have been described. It remains unclear how cells transition from a non-polarized state to a polarized state with only large, elongated blebs. Further, the field has yet to clearly define the properties distinguishing stable blebs that form on

contractile spheroid cells and the larger leader blebs that confer fast amoeboid motility.

To appreciate the functional differences between these types of blebs, we must first evaluate the molecular mechanisms of bleb stabilization and initiation of motility and how cortical dynamics contribute to these processes.

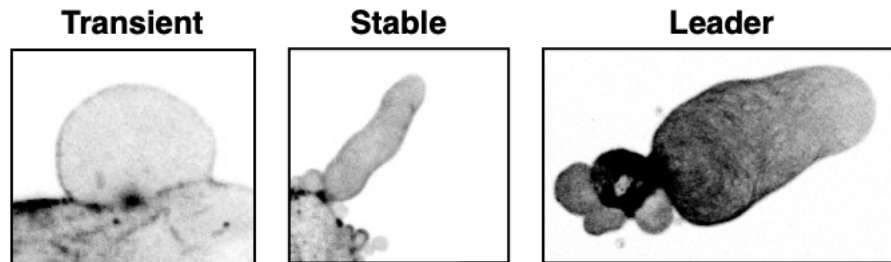


**Figure 25. Different Types of Blebs in Confined MEFs.**

### **Bleb Formation: Balancing Polymerization, Adhesion, and Contractility**

Under confinement, cells are subject to compressive stress and must resist deformation, typically by increasing the density and rigidity of their cortex (Venturini et al., 2020; Bergert et al., 2012; 2015). The rigidity of the cortex can be controlled by modulating the composition, organization, and abundance of the cortical network (Cartegena-Rivera et al., 2016; Ennomani et al., 2016; Gilden & Krummel, 2010; Chugh et al., 2017). When MEFs are confined, regardless of substrate adhesion, they become less spread and display higher cortical densities in comparison to unconfined controls (Figure 10A-B). It is important to note that cortical tension and intracellular pressure are not necessarily correlated to cortical density (Tinevez et al., 2009; Bergert et al., 2012; 2015). In this case, however, when cells are confined to a level sufficient to deform the nucleus, mechanotransduction pathways directly trigger NMII activation (Venturini et al., 2020; Lomakin et al., 2019). Rising NMII contractile activity increases the tension of the

cell's cortex and, thus, its internal pressure (Venturini et al., 2020; Tinevez et al., 2009; Bergert et al., 2012). Thus, in the context of confinement, this reduction of spread area can likely be attributed to a global increase in cortical contractility (Sahai & Marshall, 2003)

When MEFs cannot form strong adhesions with the substrate this increase in basal NMII contractility is enough to trigger the transition from a spread morphology to a rounded cell body. This change in shape coincides with increased blebbing, yet is typically not enough to trigger the switch to LBB migration (Figure 10A). This suggests that focal adhesions connected to the substrate maintain enough anchorage to limit excessive cortical contractility, thereby preventing cell rounding and the consequent increase in cortical density required for polarization. Indeed, when cells are confined on fibronectin, which supports strong adhesion, no blebs are observed (Figure 9A, 10A). Instead, the cell maintains its anchoring points at the periphery but reduces its cell body, resulting in thin neurite-like protrusions that prevent the cell from fully rounding (Figure 9C-D, 10A). While this retraction can be enhanced by CalA-induced enrichment of NMII activation (Figure 11B-C), these sites of cell-substrate adhesion still limit the ability of the contractile cortex to fully round up the cell.

The loss of integrins has been previously reported to drive cells to amoeboid migration modes (Liu et al., 2015; Barnhart et al., 2011; Carragher et al., 2006). Similarly, exogenous expression of integrins has been shown to inhibit amoeboid migration, indicating that the ability to form adhesions with the extracellular environment

is a key determinant of migration mode (Carragher et al., 2006). The notion that cell-matrix adhesion may be a limiting factor for MAT is likely due to the adhesion-dependent nature of SF assembly (Tojkander et al., 2015; Hirata et al., 2007). Previous work has shown that even when cells do form adhesions with the ECM, if there is no associated SF formation, these cells can still utilize mechanisms of amoeboid motility (Poincloux et al., 2011). Because contractile SFs can compete with the cortex for the recruitment of F-actin and NMII (Liu et al., 2015; Lomakin et al., 2015), it follows that the reduction of adhesion-dependent SF assembly has a strong correlation to increased cortical density and contractility (Figure 14A-B).

When MEFs are plated in low-adhesive environments (e.g. uncoated glass), I saw an apparent increase in intracellular pressure from confinement as evidenced by a higher frequency of membrane-cortex detachment and bleb formation (Figure 10). While some cells confined on weakly adhesive surfaces became fully rounded, most exhibited a pseudopodal-amoeboid phenotype with an actin-rich protrusion at their leading edge and only displayed round, transient blebs along their lateral and rear margins (Figure 10A). Because MEFs, by nature, favor mesenchymal migration mechanisms that do not rely on high cortical contractility and can deposit their own matrix, it is likely that cells still form weak nascent adhesions even on untreated glass.

On passivated surfaces, MEFs were unable to form adhesions and instead began to form elongated stable blebs in addition to transient blebs. These were most often seen on spherical cells displaying high densities of cortical actomyosin (Figure



10A, 14B). These stable blebs were distinct from the pseudopodal-amoeboid protrusions in that they were not driven by actin polymerization at the leading membrane (Figure 15A). Prior work has shown that decreasing the height of confinement, and therefore increasing cortical contractility, can increase the frequency of stable bleb elongation relative to the formation of pseudopodal protrusions and transient blebs (Liu et al., 2015, Garcia-Arcos et al., 2022). Together, these results suggest a correlative link between the reduction of polymerization-driven protrusions and actomyosin based stress fibers, which both favor mesenchymal-like motility, and increased NMII-driven contractile forces in the cortex that power bleb formation and stabilization, which favor amoeboid motility (Bergert et al., 2012; Paluch et al., 2016; Liu et al., 2015).

### **Bleb Shape and Stabilization: When Contractility Breaks Symmetry**

Two key material properties of the cortical actin network are 1) connectivity, regulated by crosslinkers and bundles, and 2) contractility. The contractile properties of the cortical actin network depend on the generation of active stresses by molecular motors, such as NMII (Vogel et al., 2020; Ennommani et al., 2016; Alvarado et al., 2013). Cells can modify the material properties of their cortex in response to many cues, including cell cycle, extracellular signals, or confinement (Reymann et al., 2016; Venturini et al., 2020; Lomakin et al., 2019). Notably, many cellular processes are orchestrated by actomyosin contractility gradients, such as symmetry breaking during early *C. elegans* development. Asymmetric NMII distribution in the anterior and

posterior sides of the embryo produces anisotropic stresses that generate cortical flows (Mayer et al., 2010; Munro & Bowerman, 2009). Adhesion-independent cell migration, too, can rely on stochastic cortex fluctuations and contractility to break symmetry (Bergert et al., 2015; Ruprecht et al., 2015; Graziano et al., 2019). This is an important principle for bleb stabilization and the initiation of LBB motility.

Several distinctions can be made between the stable blebs that MEFs exhibit under non-adhesive confinement and the transient blebs observed in mitosis or apoptosis: 1) shape – stable blebs are elongated rather than spherical, 2) lifetime – as their name suggests, stable blebs resist retraction and persist longer than smaller dynamic blebs, and 3) actomyosin organization – while both transient and stable blebs are initially devoid of a cortex, stable blebs exhibit a distinct cortical gradient that forms shortly after their nucleation and collapses if they are retracted (Figure 15B, D, 17A). This cortical density gradient is also observed in motile leader blebs, indicating that these two structures share a mechanistic origin (Figure 16A-B, 26).

### **Determinants of Bleb Shape**

It is important to note that dendritic actin networks, such as the cortex, are inherently non-homogenous – i.e. the architecture and orientation of cortical actin filaments is not uniform across the entire cell (Salbreux et al., 2012). Recent models of cortical mechanics show that at low contractility, stochastic fluctuations are tempered by the cortex, but can be amplified by high contractility (Garcia-Arcos et al., 2022; Xu et al., 2019). High contractility can, in turn, generate local instabilities in the network that are

necessary to break symmetry, including blebbing (Xu et al., 2019; Salbreux et al., 2012). This property of cortical networks contributes to cell shape and polarity and is especially important during amoeboid migration, which often relies on cortical flows (Liu et al., 2015, Ruprecht et al., 2015, Bergert et al., 2015).

Under non-adhesive confinement, the contractility-dependent increase in intracellular pressure promotes blebbing, which generates sites of local network failure (Figure 10A, 14B, 15A). This leads to a rear-directed gradient of contractility that promotes bleb expansion (Figure 18B-C). At nucleation, both transient and stable blebs have the same shape, but transient bleb expansion quickly stalls once the pressures inside the bleb and the cell's cytoplasm reach an equilibrium or when actin reassembles into a homogenous cortex beneath the bleb membrane (Figure 15A-B, 17A; Charras et al., 2006). If the actin in the bleb is not homogeneously distributed and maintains regions of cortical instability, however, NMII-mediated retraction of the initial protrusion can generate a second bleb at regions where the cortex is fragile (Figure 17D). Repeated compound blebbing events can promote polarization, leading to a steady-state in which sustained cortical retrograde flow prevents retraction (Figure 17B-D).

Stable blebs can also form without compound blebbing and may acquire their elongated shape prior to NMII accumulation and contraction at their base (Figure 18B-C). This may be attributed to the rate of cytoplasm flow into the bleb, such that when high contractility elevates intracellular pressure, the rate of expansion exceeds the rate of cortex assembly (Tinevez et al., 2009; Bergert et al., 2012; Ruprecht et al., 2015).

Indeed, the frequencies of stable and leader bleb elongation are much lower without additional stimulation of NMII activity (Figure 11B). Therefore, high global contractility may be an early determinant of bleb shape. Likewise, when contractility is diminished by cell-matrix adhesion or actin-rich protrusions, blebs do not stabilize and are rapidly retracted if they form at all (Figure 10A, 11B). Furthermore, because actin polymerization in the bleb follows a gradient starting from the base, expansion may be limited to the distal membrane by the growing cortical network (Figure 17A). Because cortex assembly appears to stall transient bleb expansion in MEFs, it is likely that this is also the mechanism for restricting the width of elongating stable blebs.

Another possible mechanism for stable bleb elongation was proposed by a recent model studying the stress-strain relationship at the bleb membrane, which involves the unfolding of membrane invaginations to increase the available surface area for expansion (Lavi et al., 2019; Gouzdari et al., 2017). Because cortex reassembly in the bleb follows a gradient (Figure 15A-B, 17A), this membrane flattening could only occur at the actin-depleted distal tip, producing the elongated shape (Gouzdari et al., 2017). In agreement with this model, my results show that stable blebs form their elongated shape prior to closure of the neck (Figure 15B, 18B). Meanwhile subsequent NMII contraction at the base of the bleb corresponds to the stabilization of the cortical actin gradient, indicating that the neck of the stable bleb may represent a diffusion barrier that, when closed, stabilizes the steady-state (Figure 15B, 18B). If neck closure also restricts the flow of membrane lipids into the bleb, we expect that when the bleb

expands to a size where all membrane invaginations have been flattened, any further elongation would result in increased membrane tension at the distal margin. To investigate if neck closure indeed obstructs lipid flow, we could measure the difference in membrane tension between the base and tip of the bleb while increasing membrane-cortex attachment at the neck to inhibit membrane flows (Diz-Munos et al., 2010; Gouzdari et al., 2017).

### **Mechanisms of Bleb Stabilization**

While initial confinement produces high contractility, the intracellular pressure generated by confinement alone is not enough to drive polarization and motility (Figure 10A, 11B). Increasing NMII activity in combination with surface passivation leads to more stable blebbing and increases the frequency of MEFs transitioning to LBB motility (Figure 11D-E). This suggests that the bleb stabilization and motility may require some threshold of NMII-dependent cortical tension to trigger polarization (Tinevez et al., 2009). Yet, unconfined MEFs that were plated on non-adhesive substrates did not exhibit bleb stabilization nor polarity, even with drug-induced enrichment of NMII activity. Thus, external confinement appears to be necessary condition for the generation of contractility gradients that enable bleb stabilization and polarized migration.

Without external stimuli, such as chemokines or contact guidance cues, symmetry breaking requires stochastic fluctuations and non-homogenous force propagation across the cortical network (Bergert et al., 2015, Ruprecht et al., 2015,

Vogel et al., 2020; Yu et al., 2018). We may postulate then that confinement serves two purposes in this process: 1) providing a mechanical cue to increase contractility and 2) generating active stress in the contractile network. Confinement can directly stimulate contractility through a pathway in which nuclear deformation initiates cPLA2 signaling and increases intracellular  $\text{Ca}^{2+}$  concentration, which activates ROCK to promote NMII activation (Lomakin et al., 2019; Venturini et al., 2020).

Because  $5\mu\text{m}$  confinement results in nuclear deformation in MEFs, it is reasonable to assume that this confinement level activates pathways leading to high contractility. However, when the leader bleb detaches from the trailing uropod during LBB migration, these bleb fragments remain motile even when the nucleus is excluded from the fragment (Garcia-Arcos et al., 2022), which I have also observed anecdotally (Figure 27). Thus, while deformation of the nucleus is required for the initial activation of NMII contractility, it may not be a necessary condition to sustain bleb-based motility. Still, the question remains – why does bleb stabilization require confinement in addition to high contractility?

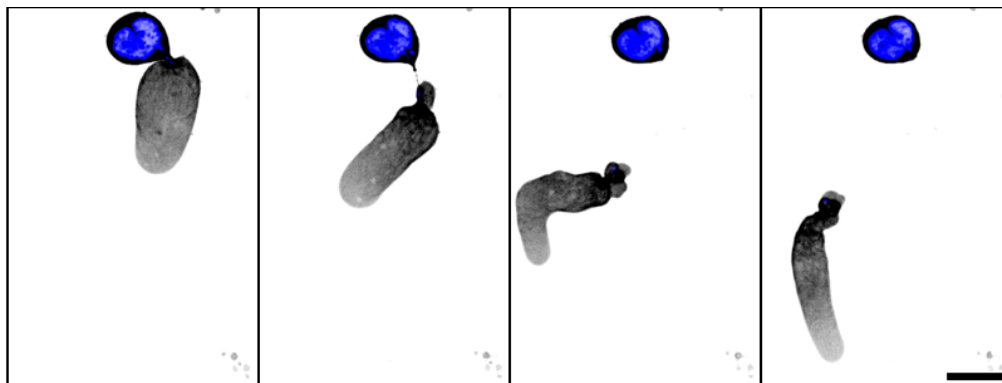


**Figure 26. Detachment of Motile Bleb Fragments from the Uropod**

Compressive forces produced by confinement generate stress in the active contractile network, enhancing the effects of random cortex perturbations (Yu et al., 2018). For instance, local contraction of NMII motors in a non-homogenous actin network generates anisotropic cortical tension (Vogel et al., 2020; Alvarado et al., 2017). Together with the pulsatile nature of actomyosin networks, these gradients in cortical tension can lead to advective flows (Mayer et al., 2010; Yu et al., 2018). This has most famously been observed during assembly of the contractile actomyosin ring at the cytokinetic cleavage furrow: equatorial contraction of NMII motors initiates bidirectional cortical flows away from the poles, creating a positive feedback loop where the accumulation of cortical actomyosin at the furrow progressively increases contractility and, thus, the velocity of cortical flows (Reymann et al., 2016). Meanwhile, blebs can be thought of as individual herniation events, where sudden local relaxation of the network creates a steep, rear-directed contractility gradient as the bleb expands (Cattin et al., 2015). When global contractility is high, rapid elongation followed by local NMII contraction at the base of the bleb generates retrograde cortical flows (Figure 17B-D, 18B). Like in mitosis, condensation of actomyosin generates a region of high network density and contractility (Figure 16A-B, 18B-C). Yet unlike in mitosis, cortical flow in the stable bleb is unidirectional, creating a strong gradient that promotes bleb stabilization (Figure 17B-D) and, if strong enough, can provide the force asymmetry required for locomotion.

Overall, the role of confinement in bleb stabilization involves the activation of high

contractility to enhance coupling between stochastic cortex perturbations and symmetry breaking. In short, confinement provides the mechanical stimulus required to transform an initially homogenous cortex into a polarized steady-state through the NMII-driven generation of advective cortical flows.

### Leader Bleb Polarity

Studies of bleb-based motility have shown us that polarized blebbing requires positive feedback between NMII accumulation and convergent cortical flows (Liu et al., 2015; Ruprecht et al., 2015; Logue et al., 2015; Bergert et al., 2015; Ullo & Logue, 2018). Notably, these are the same mechanisms required for bleb stabilization. Yet, it remains unclear how stable blebs observed on blebby spheroid cells differ from the larger leader blebs that confer fast amoeboid motility. One consideration may be that while stable blebs are polarized on a local level, leader blebs exhibit cell-wide polarization and much longer-range cortical flows.

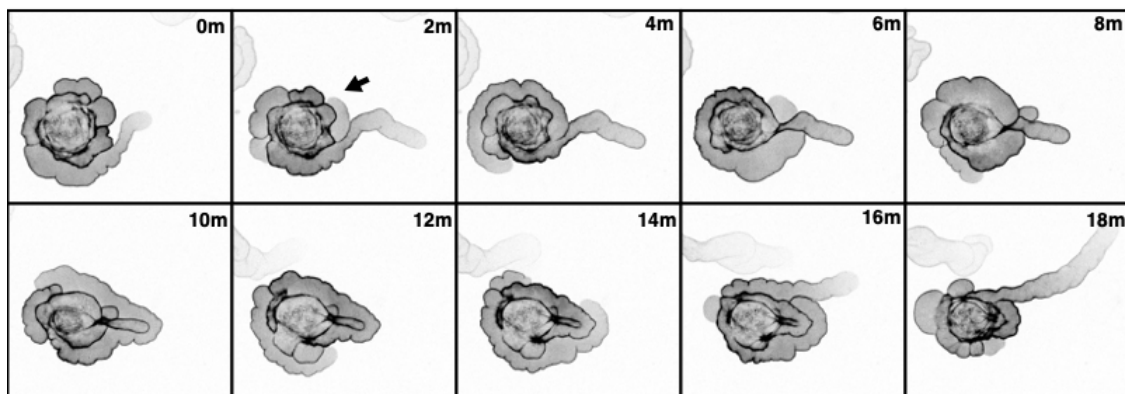


**Figure 27. Circus Blebbing Often Precedes Leader Bleb Elongation.**

For instance, MEF under non-adhesive confinement can form multiple stable blebs, oriented in opposing directions. Cells that exhibit more than one large stable bleb



are very rarely motile, indicating that to polarize ahead of migration, they must “choose” a leader bleb (Figure 11B, D-E). One mechanism that may contribute to polarization is circus blebbing, a phenomenon that often occurs in between short bursts of translocation in which one large, elongated bleb relentlessly travels around the cells’ periphery (Figure 28; Charras et al., 2008). Circus blebbing has previously been described by several groups but the function of circus blebs in LBB motility remains unclear (Fujinami, 1976; Johnson, 1976; Fujinami & Kageyama, 1975).

I propose that circus blebs may function in establishing whole-cell polarity to enable directional LBB migration. As the circus bleb travels, it eventually becomes one large structure encircling what will become the uropod. When the circus bleb establishes symmetry, by mechanisms not yet described in literature, it stops its circumferential motion and launches outward, similar to a lasso, transforming into a large leader bleb (Figure 28, 18m). Unlike leader blebs that exhibit distinct retrograde flow patterns, the rear cortex of circus blebs collapses into the cell body, forcing the cytosol to the leading edge. As circus blebs rapidly travel around the cell body through asymmetric compound blebbing events, they appear to “collect” the membrane and cytosol of smaller blebs (Figure 18; Charras et al., 2008). This may serve several purposes with respect to leader bleb polarity: 1) collating a membrane reservoir for leader bleb elongation, 2) aligning the direction of cytosolic flow towards one common distal membrane, 3) aligning the direction of cortical retrograde flow towards one common base. It is likely, still, that circus blebs are multifunctional and/or work in

concert with other mechanisms to promote leader bleb polarization – an important focus for future studies on MAT and bleb-based motility.

### **Consequences of Septin Depletion on Bleb Dynamics**

When septin filaments were depleted by expression of shRNAs against SEPT7, confined MEFs displayed a higher frequency of transient blebbing in coordination with increased cellular rounding (Figure 24). Several studies have shown that septins are required for rapid contraction of the cortex in cooperation with actomyosin (Tooley et al., 2009; Gilden et al., 2012). During interphase, septins are enriched at regions of cortex instability and are recruited to sites of actin depolymerization, including at the base of blebs (Gilden et al., 2012). However, amoeboid T-cells that express shRNAs against SEPT7 exhibit profound morphological defects including cortical instability, forming excessive blebs along the cell body that disrupt processive migration (Tooley et al., 2009). My observation of enhanced transient blebbing in confined MEFs appears to recapitulate these results, suggesting that cortical instability may be a conserved consequence of septin depletion (Figure 24).

During mitosis, persistent transient blebbing events serve to relieve high intracellular pressure caused by cellular rounding (Cattin et al., 2015). Following membrane-cortex detachment, rapid cytoplasm flow into the bleb drives expansion, triggered by the difference in pressure between inside of the cell and the external environment (Tinevez et al., 2009). Thus, stable bleb elongation and LBB motility likely rely on a balance between transient blebbing events and sustained high intracellular

pressure. During transient blebbing in confined MEFs, septins accumulate at the distal membrane following cortical actin reassembly and remain there until NMII-mediated retraction is complete (Figure 19C). This agrees with previous reports that septins interact with newly polymerized actin during bleb retraction are indispensable for membrane recapture during resolution of the bleb with the intact cell cortex (Gilden et al., 2012). Thus, the depletion of septins is likely to have direct impacts on bleb retraction. Impaired retraction may then reduce the cortical tension required for bleb stabilization. However, additional signaling pathways that influence cortical tension and bleb formation may also be impacted by septin depletion.

During bleb retraction, ezrin is rapidly recruited to the cortex-free membrane followed closely by Eps8, which together promote cortical actin polymerization through a pathway that requires RhoA-dependent ROCK activation at the bleb membrane (Charras et al., 2006; Logue et al., 2015; Aoki et al., 2016). Logue et al. (2015) showed that Eps8 bundling is required for bleb stability and network turnover, such that Eps8-KO or inhibition of Eps8 bundling activity prevents leader bleb formation. Eps8 is an actin-capping protein that also has bundling abilities and the balance between capping/bundling is regulated by Erk: phosphorylation of Eps8s promote bundling which, in turn, reduces capping (Logue et al., 2015). In melanoma, Eps8 capping activity is suppressed by Erk in the cortex of leader blebs, promoting high bundling activity to maintain cortex rigidity and tension-dependent hydrostatic pressure (Logue et al., 2015; Tinevez et al., 2009). Interestingly, the effects of Eps8-KO are phenocopied

by NMIIA inhibition: decreased cortical tension and intracellular pressure, but neither appears to effect any significant change in cell size or cortex thickness. This may indicate that an Erk-dependent loss of Eps8 bundling capacity would disrupt the contractility gradient required for bleb elongation and stabilization, in addition to impeding bleb retraction.

In a study on breast cancer metastasis, Zhang et al., (2016) showed that depletion of SEPT7 or SEPT2 can reduce Erk activity, which leads to enhanced invasiveness. Together with the effects of Erk signaling on promoting Eps8-mediated bleb retraction and cortical tension, this could indicate a two-fold impact of SEPT7 KD on bleb retraction. Overall, septin depletion appears to reduce cells' ability to retract blebs, which can relax intracellular pressure to a degree that prevents stable bleb formation (Tinevez et al., 2009; Charras and Paluch, 2008). Also, because ERK signaling can regulate pathways leading to NMII phosphorylation, a septin-dependent reduction of Erk activity could impair NMII activity even with elevated expression levels (Zhou et al., 2008). Likewise, in amoeboid T-cells the hyperactivation of NMIIA drives cells to collapse into non-motile spheroids that display non-productive and excessive blebbing (Zhovmer et al., 2022). This has been attributed to excess NMII activity generating a hypercontractile "locked" cortex that is less sensitive to stochastic fluctuations that would typically enable stable or leader bleb elongation (Lomakin et al., 2015). This could further explain why septin-depleted MEFs appear to have an altered

response to non-adhesive confinement and favor rapid transient blebbing over the formation of more stable bleb structures (Figure 24).

### **Conclusions & Future Directions**

I have shown that under the appropriate conditions, confined fibroblasts can display migration plasticity and, further, will transition from a lamellipodial to leader bleb-based migration mode upon the inhibition of cell-substrate adhesion and enrichment of NMII-dependent contractility. This study additionally proposes that the septin cytoskeleton may play a role in facilitating the stabilization of blebs and may contribute to cortical actomyosin-dependent mechanisms of fast amoeboid motility. Septins, further, appear to influence the expression of NMII motors, which suggests a significant role for septins in the regulation of cortical contractility. In conclusion of this thesis, two key questions stand out as further avenues for investigation.

#### *1. Is cortex flow coupled to the movement of membrane lipids?*

In this study, I investigated the dynamics of septins in coordination with actin in the bleb cortex but did not examine the potential roles for septins as diffusion barriers for the movement of membrane lipids and transmembrane proteins. Because septins can directly interact with PIP lipids in the plasma membrane, further examination of lipid flow through the neck of the stable or leader bleb, following its closure, could identify additional roles for septins in establishing polarity. This could also provide insight into mechanisms of creating the elongated shape of stable blebs if lipid flows are not restricted by the bleb neck.

*2. How does septin depletion alter NMII motor activity, independent of expression level, in different migration environments?*

While I have shown that septin depletion correlates with increased expression of both NMIIA and NMIIB, this study does not investigate how SEPT7 knockdown impacts the level of NMII motor activity, which is dependent on regulatory light chain (RLC) phosphorylation. Because increase RhoA-ROCK signaling has been linked to increased invasiveness of MEFs and CAFs, probing for changes in RLC phosphorylation, relative to total protein expression, could provide insight about how cortical septin-NMII crosstalk may influence cancer metastasis.

Overall, further investigation is required to delineate the precise contributions of the septin cytoskeleton in conferring migration plasticity, specifically in association with NMII motors. The functional relationship between the cortical septin and actomyosin cytoskeletons may ultimately provide valuable insight into the mechanisms governing cancer metastasis, immune dysregulation, and other detrimental outcomes of disrupted motility regulation.

## REFERENCE LIST

- Abraham, V. C., Krishnamurthi, V., Taylor, D. L., Lanni, F. (1999). The actin-based nanomachine at the leading edge of migrating cells. *Biophysical Journal*, 77(3), 1721–1732.
- Adams, G., Jr, López, M. P., Cartagena-Rivera, A. X., Waterman, C. M. (2021). Survey of cancer cell anatomy in nonadhesive confinement reveals a role for filamin-A and fascin-1 in leader bleb-based migration. *MBoC*, 32(18), 1772–1791.
- Alberts, B., Johnson, A., Walter, P., Lewis, J., Raff, M., Roberts, K. (2007). *Molecular Biology of the Cell*. (5<sup>th</sup> ed). New York: Garland Science.
- Alvarado, J., Sheinman, M., Sharma, A., MacKintosh, F.C., & Koenderink, G.H. (2017). Force percolation of contractile active gels. *Soft Matter*, 13, 5624–5644.
- Alvarado, J., Sheinman, M., Sharma, A., MacKintosh, F.C., & Koenderink, G.H. (2013). Molecular motors robustly drive active gels to a critically connected state. *Nature Phys*, 9, 591–597.
- Amann, K. J. & Pollard, T. D. (2001). Direct real-time observation of actin filament branching mediated by Arp2/3 complex using total internal reflection fluorescence microscopy. *PNAS USA*, 98(26), 15009–15013.
- Aoki, K., Maeda, F., Nagasako, T., Mochizuki, Y., Uchida, S., Ikenouchi, J. (2016). A RhoA and Rnd3 cycle regulates actin reassembly during membrane blebbing. *PNAS USA*, 113(13), e1863–1871.
- Balzer, E. M., Tong, Z., Paul, C. D., Hung, W. C., Stroka, K. M., Boggs, A. E., Martin, S. S., Konstantopoulos, K. (2012). Physical confinement alters tumor cell adhesion and migration phenotypes. *FASEB Journal*, 26(10), 4045–4056.
- Barnhart, E. L., Lee, K. C., Keren, K., Mogilner, A., Theriot, J. A. (2011). An adhesion-dependent switch between mechanisms that determine motile cell shape. *PLoS Biology*, 9(5), e1001059.
- Bear, J. E. & Haugh, J. M. (2014). Directed migration of mesenchymal cells: where signaling and the cytoskeleton meet. *Current opinion in cell biology*, 30, 74–82.
- Beningo, K.A., Dembo, M., Kaverina, I., Small, J.V., Wang, Y.L. (2001). Nascent focal adhesions are responsible for the generation of strong propulsive forces in migrating fibroblasts. *JCB*, 153(4), 881–888.
- Bergert, M., Chandradoss, S. D., Desai, R.A, Paluch, E. (2012). Cell mechanics control rapid transitions between blebs and lamellipodia during migration. *PNAS USA*, 109, 14434–14439.
- Bergert, M., Erzberger, A., Desai, R. (2015). Force transmission during adhesion-independent migration. *Nature Cell Biology*, 17, 524–529.
- Breitsprecher, D., Kiesewetter, A. K., Linkner, J., Vinzenz, M., Stradal, T. E., Small, J. V., Curth, U., Dickinson, R. B., Faix, J. (2011). Molecular mechanism of Ena/VASP-mediated actin-filament elongation. *The EMBO journal*, 30(3), 456–467.
- Bridges, A. A., Jentzsch, M. S., Oakes, P. W., Occhipinti, P., Gladfelter, A. (2016). Micron-scale plasma membrane curvature is recognized by the septin cytoskeleton. *JCB*. 213(1), 23-32.
- Bridges, A.A. & Gladfelter, A.S. (2015). Septin Form and Function at the Cell Cortex. *Journal of Biological Chemistry*. 290, 17173-80.
- Burridge, K. & Wittchen, E. S. (2013). The tension mounts: stress fibers as force-generating mechanotransducers. *JCB*, 200(1), 9–19.
- Callan-Jones, A.C., Ruprecht, V., Wieser, S., Heisenberg, C.P., Voituriez, R. (2016). Cortical Flow-Driven Shapes of Nonadherent Cells. *Phys. Rev. Lett.* 117, 028102.
- Cannon, K. S., Woods, B. L., Crutchley, J. M., & Gladfelter, A. S. (2019). An amphipathic helix enables septins to sense micrometer-scale membrane curvature. *JCB*, 218(4),

- Cao, L., Yonis, A., Vaghela, M., Barriga, E.H., Chugh, P., Smith, M.B., Maufront, J., Lavoie, G., Méant, A., Ferber, E., Bovellan, M., Alberts, A., Bertin, A., Mayor, R., Paluch, E.K., Roux, P.P., Jégou, A., Romet-Lemonne, G., Charras, G. (2020). SPIN90 associates with mDia1 and the Arp2/3 complex to regulate cortical actin organization. *Nature Cell Biology*, 22, 803–814.
- Carlier, M. F. (1990). Actin polymerization and ATP hydrolysis. *Advanced Biophysics*, 26, 51-73.
- Carragher, N.O., Walker, S.M., Scott Carragher, L.A., Harris, F., Sawyer, T.K., Brunton, V.G., Ozanne, B.W., and Frame, M.C. (2006). Calpain 2 and Src dependence distinguishes mesenchymal and amoeboid modes of tumour cell invasion: a link to integrin function. *Oncogene*, 25, 5726–5740.
- Cartagena-Rivera, A. X., Logue, J. S., Waterman, C. M., Chadwick, R. S. (2016). Actomyosin Cortical Mechanical Properties in Nonadherent Cells Determined by Atomic Force Microscopy. *Biophysical journal*, 110(11), 2528–2539.
- Cattin, C.J., Düggelin, M., Martinez-Martin, D., Gerber, C., Müller, D.J., Stewart, M.P. (2015). Mechanical control of mitotic progression in single animal cells. *PNAS USA*, 112, 11258–11263.
- Caudron, F. & Barral, Y. (2009). Septins and the lateral compartmentalization of eukaryotic membranes. *Developmental Cell*, 16, 493–506.
- Charras, G. & Paluch, E. (2008). Blebs lead the way: how to migrate without lamellipodia. *Nature Reviews Molecular Cell Biology*, 9, 730–736.
- Charras, G.T. (2008). A short history of blebbing. *Journal of Microscopy*, 231, 466–478.
- Charras, G.T., Coughlin, M., and Mitchison, T.J. (2008). Life and times of a cellular bleb. *Biophys*, 94:1836-1853.
- Charras, G.T., Hu, C.K., Coughlin, M., Mitchison, T.J. (2006). Reassembly of contractile actin cortex in cell blebs. *JCB*, 175, 477-90.
- Charras, G.T., Yarrow, J.C., Horton, M.A., Mahadevan, L., Mitchison, T.J. (2005). Non-equilibration of hydrostatic pressure in blebbing cells. *Nature*, 435, 365–369.
- Chugh, P. & Paluch, E. K. (2018). The actin cortex at a glance. *JCS*, 131(14).
- Chugh, P., A.G. Clark, M.B. Smith, D.A.D. Cassani, K. Dierkes, A. Ragab, P.P. Roux, G. Charras, G. Salbreux, and E.K. Paluch. (2017). Actin cortex architecture regulates cell surface tension. *Nature Cell Biology*, 19, 689–697.
- Colombelli, J., Besser, A., Kress, H., Reynaud, E. G., Girard, P., Caussin, E., Haselmann, U., Small, J. V., Schwarz, U. S., Stelzer, E. H. (2009). Mechanosensing in actin stress fibers revealed by a close correlation between force and protein localization. *JCS*, 122(10), 1665–1679.
- Cowan, J. M., Duggan, J. J., Hewitt, B. R., Petrie, R. J. (2022). Non-muscle myosin II and the plasticity of 3D cell migration. *Frontiers in cell and developmental biology*, 10, 1047256.
- Demay, B. S., Bai, X., Howard, L., Occhipinti, P., Meseroll, R. A., Spiliotis, E. T., Oldenbourg, R., Gladfelter, A. S. (2011). Septin filaments exhibit a dynamic, paired organization that is conserved from yeast to mammals. *JCB*, 193, 1065–1081.
- Diz-Muñoz, A., Krieg, M., Bergert, M., Ibarlucea-Benitez, I., Muller, D.J., Paluch, E., Heisenberg, C.-P. (2010). Control of Directed Cell Migration In Vivo by Membrane-to-Cortex Attachment. *PLOS Biology*, 8, e1000544.
- Dolat, L., Hu, Q., & Spiliotis, E. T. (2014). Septin functions in organ system physiology and pathology. *Biological chemistry*, 395(2), 123–141. <https://doi.org/10.1515/hsz-2013-0233>
- Dominguez, R. (2009). Actin filament nucleation and elongation factors-structure-function relationships. *Critical reviews in biochemistry and molecular biology*, 44(6), 351–366.
- Dominguez, R. & Holmes, K. C. (2011). Actin structure and function. *Annual review of biophysics*, 40, 169–186.
- Dupont, S., Morsut, L., Aragona, M., Enzo, E., Giulitti, S., Cordenonsi, M., Zanconato, F., Le Digabel, J., Forcato, M., Bicciato, S., Elvassore, N., Piccolo, S. (2011). Role of YAP/TAZ in mechanotransduction. *Nature*, 474(7350), 179–183.
- Ennomani, H., Letort, G., Guérin, C., Martiel, J. L., Cao, W., Nédélec, F., De La Cruz, E. M., Théry, M. Blanchoin, L. (2016). Architecture and connectivity govern actin network contractility. *Current Biology*, 26(5), 616-626.



- Friedl, P. & Alexander, S. (2011). Cancer invasion and the microenvironment: plasticity and reciprocity. *Cell*, 147(5), 992–1009.
- Friedl, P. & Wolf, K. (2003). Tumour-cell invasion and migration: diversity and escape mechanisms. *Nature Reviews Cancer*, 3(5), 362–374.
- Friedl, P. & Wolf, K. (2009). Proteolytic interstitial cell migration: a five-step process. *Cancer metastasis reviews*, 28(1-2), 129–135.
- Friedl, P. & Wolf, K. (2010). Plasticity of cell migration: a multiscale tuning model. *JCB*, 188(1), 11–19.
- Friedl, P., Borgmann, S., & Bröcker, E. B. (2001). Amoeboid leukocyte crawling through extracellular matrix: lessons from the Dictyostelium paradigm of cell movement. *Journal of leukocyte biology*, 70(4), 491–509.
- Fritz-Laylin, L. K., Lord, S. J., Mullins, R. D. (2017a). Our evolving view of cell motility. *Cell Cycle*, 16, 1735–1736.
- Fritz-Laylin, L. K., Lord, S. J., Mullins, R. D. (2017b). WASP and SCAR are evolutionarily conserved in actin-filled pseudopod-based motility. *JCB*, 216, 1673–1688.
- Füchtbauer, A., Lassen, L. B., Jensen, A. B., Howard, J., Quiroga, A.deS., Warming, S., Sørensen, A. B., Pedersen, F. S., Füchtbauer, E. M. (2011). Septin9 is involved in septin filament formation and cellular stability. *Biological chemistry*, 392(8-9), 769–777.
- Garcia-Arcos, J. M., Ziegler, J., Grigolon, S., Reymond, L., Shajepal, G., Cattin, C. J., Lomakin, A., Muller, D., Ruprecht, V., Wieser, S., Voituriez, R., Piel, M. (2022). Advection percolation in the actomyosin cortex drives amoeboid cell motility. bioRxiv.
- Gilden, J. & Krummel, M. F. (2010). Control of cortical rigidity by the cytoskeleton: emerging roles for septins. *Cytoskeleton*. 67(8), 477–486.
- Gilden J. K., Peck S., Chen Y. C., Krummel M. F. (2012). The septin cytoskeleton facilitates membrane retraction during motility and blebbing. *JCB*, 196, 103–114.
- Gladfelter, A. S., Pringle, J. R., Lew, D. J. (2001). The septin cortex at the yeast mother-bud neck. *Current opinion in microbiology*, 4(6), 681–689.
- Goudarzi, M., Tarbashevich, K., Mildner, K., Begemann, I., Garcia, J., Paksa, A., Reichman-Fried, M., Mahabaleshwar, H., Blaser, H., Hartwig, J., Zeuschner, D., Galic, M., Bagnat, M., Betz, T., Raz, E. (2017). Bleb Expansion in Migrating Cells Depends on Supply of Membrane from Cell Surface Invaginations. *Developmental Cell*, 43, 577-587.e5.
- Graziano, B.R., Town, J.P., Sitarska, E., Nagy, T.L., Fošnarč, M., Penič, S., Igljč, A., Kralj-Igljč, V., Gov, N.S., Diz-Muñoz, A., Weiner, O.D. (2019). Cell confinement reveals a branched-actin independent circuit for neutrophil polarity. *PLoS Biology*, 17, e3000457.
- Gurtner, G. C., Werner, S., Barrandon, Y., Longaker, M. T. (2008). Wound repair and regeneration. *Nature*, 453, 314–321
- Hall, P. A. & Russell, S. E. (2012). Mammalian septins: dynamic heteromers with roles in cellular morphogenesis and compartmentalization. *Journal of pathology*, 226(2), 287–299.
- Hartwell J. L. (1971). Plants used against cancer. A survey. *Lloydia*, 34(2), 204–255.
- Hirata, N., Takahashi, M., Yazawa, M. (2009). Diphosphorylation of regulatory light chain of myosin IIA is responsible for proper cell spreading. *BBRC*, 381(4), 682–687.
- Hotulainen, P. & Lappalainen, P. (2006). Stress fibers are generated by two distinct actin assembly mechanisms in motile cells. *JCB*, 173(3), 383–394.
- Joo E., Surka M. C., Trimble W. S. (2007). Mammalian SEPT2 is required for scaffolding nonmuscle myosin II and its kinases. *Developmental Cell*. 13, 677–690
- Khatau, S. B., Hale, C. M., Stewart-Hutchinson, P. J., Patel, M. S., Stewart, C. L., Searson, P. C., Hodzic, D., Wirtz, D. (2009). A perinuclear actin cap regulates nuclear shape. *PNAS USA*, 106(45), 19017–19022.
- Kinoshita, M. (2006). Diversity of septin scaffolds. *Current opinion in cell biology*, 18(1), 54–60.
- Kinoshita, M., Field, C. M., Coughlin, M. L., Straight, A. F., Mitchison, T. J. (2002). Self- and actin-templated assembly of mammalian septins. *Dev. Cell*. 3(6), 791-802.
- Krueger, D., Quinkler, T., Mortensen, S.A., Sachse, C., DeRenzis, S. (2019). Cross-linker-mediated

- regulation of actin network organization controls tissue morphogenesis. *JCB*, 218, 2743–2761.
- Krummel, M. F., Friedman, R. S., Jacobelli, J. (2014). Modes and mechanisms of T cell motility: roles for confinement and Myosin-IIA. *Current opinion in cell biology*, 30, 9–16.
- Lam, M. & Calvo, F. (2019). Regulation of mechanotransduction: Emerging roles for septins. *Cytoskeleton*, 76(1), 115–122.
- Lämmermann, T., Bader, B.L., Monkley, S.J., Worbs, T., Wedlich-Söldner, R., Hirsch, K., Keller, M., Förster, R., Critchley, D.R., Fässler, R., Sixt, M. (2008). Rapid leukocyte migration by integrin-independent flowing and squeezing. *Nature*, 453, 51–55.
- Lämmermann, T. & Sixt, M. (2009). Mechanical modes of ‘amoeboid’ cell migration. *Current Opinion in Cell Biology*, 21, 636–644.
- Lauffenburger, D. A. & Horwitz, A. F. (1996). Cell migration: a physically integrated molecular process. *Cell*, 84:359–369.
- Lavi, I., Goudarzi, M., Raz, E., Gov, N.S., Voituriez, R., Sens, P. (2019). Cellular Blebs and Membrane Invaginations Are Coupled through Membrane Tension Buffering. *Biophysical Journal*, 117, 1485–1495.
- Le Berre, M., Aubertin, J., & Piel, M. (2012). Fine control of nuclear confinement identifies a threshold deformation leading to lamina rupture and induction of specific genes. *Integrative biology : quantitative biosciences from nano to macro*, 4(11), 1406–1414.
- Le Berre, M., Zlotek-Zlotkiewicz, E., Bonazzi, D., Lautenschlaeger, F., Piel, M. (2014). Methods for Two-Dimensional Cell Confinement, in: *Methods in Cell Biology*. Elsevier, pp. 213–229.
- Liu, Y.J., LeBerre, M., Lautenschlaeger, F., Maiuri, P., Callan-Jones, A., Heuze, M., Takaki, T., Voituriz, R., and Piel, M. (2015). Confinement and low adhesion induce fast amoeboid migration of slow mesenchymal cells. *Cell*. 160, 659-672.
- Livne, A. & Geiger, B. (2016). The inner workings of stress fibers -from contractile machinery to focal adhesions and back. *JCS*, 129(7), 1293–1304.
- Lodish, H. F., Berk, A., Kaiser, C., Krieger, M., Bretscher, A., Ploegh, H., et al. (2016). "Cell Organization and Movement I: Microfilaments". In: *Molecular Cell Biology* (8th ed). New York: W.H. Freeman.
- Logue, J. S., Cartagena-Rivera, A. X., Baird, M. A., Davidson, M. W., Chadwick, R. S., Waterman, C. M. (2015). Erk regulation of actin capping and bundling by Eps8 promotes cortex tension and leader bleb-based migration. *eLife*, 4, e08314.
- Lomakin, A.J., Cattin, C.J., Cuvelier, D., Alraies, Z., Molina, M., Nader, G., Srivastava, N., Garcia-Arcos, J.M., Zhitnyak, I.Y., Bhargava, A., Driscoll, M.K., Welf, E.S., Fiolka, R., Petrie, R.J., Manel, N., Lennon-Duménil, A.M., Müller, D.J., Piel, M. (2019). The nucleus acts as a ruler tailoring cell responses to spatial constraints. *bioRxiv* 863514.
- Lomakin, A.J., Lee, K.-C., Han, S.J., Bui, D.A., Davidson, M., Mogilner, A., Danuser, G. (2015). Competition for actin between two distinct F-actin networks defines a bistable switch for cell polarization. *Nature Cell Biology*, 17, 1435–1445.
- Macara, I. G., Baldarelli, R., Field, C. M., Glotzer, M., Hayashi, Y., Hsu, S. C., Kennedy, M. B., Kinoshita, M., Longtine, M., Low, C., Maltais, L. J., McKenzie, L., Mitchison, T. J., Nishikawa, T., Noda, M., Petty, E. M., Peifer, M., Pringle, J. R., Robinson, P. J., Roth, D., ... Zieger, B. (2002). Mammalian septins nomenclature. *MBoC*, 13(12), 4111–4113.
- Maiuri, P., Rupprecht, J.-F., Wieser, S., Rupprecht, V., Bénichou, O., Carpi, N., Coppey, M., De Beco, S., Gov, N., Heisenberg, C.-P., Lage Crespo, C., Lautenschlaeger, F., Le Berre, M., Lennon-Dumenil, A.-M., Raab, M., Thiam, H.-R., Piel, M., Sixt, M., Voituriez, R. (2015). Actin Flows Mediate a Universal Coupling between Cell Speed and Cell Persistence. *Cell*, 161, 374–386.
- Maugis, B., Brugués, J., Nassoy, P., Guillen, N., Sens, P., Amblard, F. (2010). Dynamic instability of the intracellular pressure drives bleb-based motility. *JCS*, 123(22), 3884–3892.
- Mavrakakis, M., Azou-Gros, Y., Tsai, F. C., Alvarado, J., Bertin, A., Iv, F., Kress, A., Brasselet, S., Koenderink G. H., Lecuit T. (2014). Septins promote F-actin ring formation by crosslinking actin filaments into curved bundles. *Nature Cell Biology*, 16, 322–334
- Mayer, M., Depken, M., Bois, J.S., Jülicher, F., Grill, S.W., (2010). Anisotropies in cortical tension reveal

- the physical basis of polarizing cortical flows. *Nature*, 467, 617–621.
- Mejillano, M. R., Kojima, S., Applewhite, D. A., Gertler, F. B., Svitkina, T. M., Borisy, G. G. (2004). Lamellipodial versus filopodial mode of the actin nanomachinery: pivotal role of the filament barbed end. *Cell*, 118(3), 363–373.
- Mogilner, A. & Oster, G. (1996). Cell motility driven by actin polymerization. *Biophysical journal*, 71(6), 3030–3045.
- Mostowy, S. & Cossart, P. (2012) Septins: the fourth component of the cytoskeleton. *Nature Reviews Molecular Cell Biology*. 13,183–194.
- Munro, E. & Bowerman, B. (2009). Cellular symmetry breaking during *Caenorhabditis elegans* development. *CSH Perspectives in Biology*, 1, a003400.
- Niggli, V. & Rossy, J. (2008). Ezrin/radixin/moesin: versatile controllers of signaling molecules and of the cortical cytoskeleton. *IJBCB*, 40(3), 344–349.
- Nishihama, R., Onishi, M., Pringle, J. R. (2011). New insights into the phylogenetic distribution and evolutionary origins of the septins. *Biological chemistry*, 392(8-9), 681–687.
- Paluch, E.K., Aspalter, I.M., Sixt, M., (2016). Focal Adhesion–Independent Cell Migration. *Annual Reviews Cell Developmental Biology*, 32, 469–490.
- Paluch, E.K. & Raz, E., (2013). The role and regulation of blebs in cell migration. *Current Opinion in Cell Biology*, 25, 582–590.
- Pandya, P., Orgaz, J. L., Sanz-Moreno, V. (2017). Modes of invasion during tumour dissemination. *Molecular oncology*, 11(1), 5–27.
- Panková, K., Rösel, D., Novotný, M., Brábek, J. (2010). The molecular mechanisms of transition between mesenchymal and amoeboid invasiveness in tumor cells. *CMLS*, 67(1), 63–71.
- Peterson, E. A., & Petty, E. M. (2010). Conquering the complex world of human septins: implications for health and disease. *Clinical genetics*, 77(6), 511–524.
- Petrie, R. J. & Yamada, K. M. (2012). At the leading edge of three-dimensional cell migration. *JCS*, 125(24), 5917–5926.
- Petrie, R. J., Harlin, H. M., Korsak, L. I., Yamada, K. M. (2017). Activating the nuclear piston mechanism of 3D migration in tumor cells. *JCB*, 216(1), 93–100.
- Plastino, J. & Blanchoin, L. (2018). Dynamic stability of the actin ecosystem. *JCS*, 132(4), jcs219832.
- Poincloux, R., Collin, O., Lizárraga, F., Romao, M., Debray, M., Piel, M., Chavrier, P. (2011). Contractility of the cell rear drives invasion of breast tumor cells in 3D Matrigel. *PNAS USA*, 108(5), 1943–1948.
- Pollard T. D. (2016). Actin and Actin-Binding Proteins. *CSH Perspectives*, 8(8), a018226.
- Pollard, T. D. & Borisy, G. G. (2003). Cellular motility driven by assembly and disassembly of actin filaments. *Cell*, 112, 453–465.
- Rauzi, M., Verant, P., Lecuit, T., Lenne, P. F. (2008). Nature and anisotropy of cortical forces orienting *Drosophila* tissue morphogenesis. *Nature Cell Biology*, 10(12), 1401–1410.
- Reese, D. & Drapeau, P. (1998) Neurite growth patterns leading to functional synapses in an identified embryonic neuron. *Journal of Neuroscience*. 18(15), 5652-62.
- Reymann, A. C., Staniscia, F., Erzberger, A., Salbreux, G., Grill, S. W. (2016). Cortical flow aligns actin filaments to form a furrow. *eLife*, 5, e17807.
- Ruprecht, V., Wieser, S., Callan-Jones, A., Smutny, M., Morita, H., Sako, K., Barone, V., Ritsch-Marte, M., Sixt, M., Voituriez, R., Heisenberg, C. P. (2015). Cortical contractility triggers a stochastic switch to fast amoeboid cell motility. *Cell*, 160(4), 673–685.
- Saarikangas, J. & Barral, Y. (2011). The emerging functions of septins in metazoans. *EMBO reports*, 12(11), 1118–1126. <https://doi.org/10.1038/embor.2011.193>
- Sahai, E., & Marshall, C.J. (2003). Differing modes of tumour cell invasion have distinct requirements for Rho/ROCK signalling and extracellular proteolysis. *Nat. Cell Biol.* 5, 711–719.

- Salbreux, G., Charras, G., Paluch, E. (2012). Actin cortex mechanics and cellular morphogenesis. *Trends in Cell Biology*, 22, 536–545.
- Schwarz, U. S., & Gardel, M. L. (2012). United we stand: integrating the actin cytoskeleton and cell-matrix adhesions in cellular mechanotransduction. *JCS*, 125(13), 3051–3060.
- Sellin, M. E., Sandblad, L., Stenmark, S., Gullberg, M. (2011). Deciphering the rules governing assembly order of mammalian septin complexes. *MBoC*, 22(17), 3152–3164.
- Shih, W., & Yamada, S. (2010). Myosin IIA dependent retrograde flow drives 3D cell migration. *Biophysical journal*, 98(8), L29–L31. <https://doi.org/10.1016/j.bpj.2010.02.028>
- Shutova, M. S., & Svitkina, T. M. (2018). Mammalian nonmuscle myosin II comes in three flavors. *BBRC*, 506(2), 394–402.
- Simske, J.S. & Hardin, J. (2001). Getting into shape: Epidermal morphogenesis in *Caenorhabditis elegans* embryos. *Bioessays*, 23, 12–23.
- Sirajuddin M., Farkasovsky M., Hauer F., Kühlmann D., Macara I. G., Weyand M., Stark H., Wittinghofer A. (2007). Structural insight into filament formation by mammalian septins. *Nature*, 449, 311–315.
- Sliogeryte, K., Thorpe, S. D., Lee, D. A., Botto, L., Knight, M. M. (2014). Stem cell differentiation increases membrane-actin adhesion regulating cell blebability, migration and mechanics. *Scientific reports*, 4, 7307.
- Spiliotis, E. T. (2018). Spatial effects - site-specific regulation of actin and microtubule organization by septin GTPases. *JCS*, 131(1), jcs207555. <https://doi.org/10.1242/jcs.207555>
- Spiliotis, E. T. & Gladfelter, A. S. (2012). Spatial guidance of cell asymmetry: septin GTPases show the way. *Traffic (Copenhagen, Denmark)*, 13(2), 195–203.
- Spiliotis, E. T. & McMurray, M. A. (2020). Masters of asymmetry - lessons and perspectives from 50 years of septins. *MBoC*, 31(21), 2289–2297.
- Svitkina, T. (2018). The Actin Cytoskeleton and Actin-Based Motility. *CSH Perspectives in Biology*, 10(1), a018267. <https://doi.org/10.1101/cshperspect.a018267>
- Svitkina, TM, Bulanova, EA, Chaga, O. Y., Vignjevic, D. M., Kojima, S., Vasiliev, J. M., Borisy, G. G. (2003). Mechanism of filopodia initiation by reorganization of a dendritic network. *JCB*, 160(3), 409–421. <https://doi.org/10.1083/jcb.200210174>
- Szuba, A., Bano, F., Castro-Linares, G., Iv, F., Mavrakis, M., Richter, R. P., Bertin, A., Koenderink, G. H. (2021). Membrane binding controls ordered self-assembly of animal septins. *eLife*, 10, e63349.
- Tinevez, J.Y., Schulze, U., Salbreux, G., Roensch, J., Joanny, J.-F., Paluch, E. (2009). Role of cortical tension in bleb growth. *PNAS USA*, 106, 18581–18586.
- Tojkander, S., Gateva, G., Lappalainen, P. (2012). Actin stress fibers--assembly, dynamics and biological roles. *JCS*, 125(8), 1855–1864. <https://doi.org/10.1242/jcs.098087>
- Tojkander, S., Gateva, G., Husain, A., Krishnan, R., Lappalainen, P. (2015). Generation of contractile actomyosin bundles depends on mechanosensitive actin filament assembly and disassembly. *eLife*, 4, e06126. <https://doi.org/10.7554/eLife.06126>
- Tooley A. J., Gilden J., Jacobelli J., Beemiller P., Trimble W. S., Kinoshita M., Krummel M. F. (2009). Amoeboid T lymphocytes require the septin cytoskeleton for cortical integrity and persistent motility. *Nature Cell Biology*, 11, 17–26
- Tozluoğlu, M., Tournier, A. L., Jenkins, R. P., Hooper, S., Bates, P. A., Sahai, E. (2013). Matrix geometry determines optimal cancer cell migration strategy and modulates response to interventions. *Nature Cell Biology*, 15(7), 751–762. <https://doi.org/10.1038/ncb2775>
- Trepap, X., Chen, Z., Jacobson, K. (2012). Cell migration. *Comprehensive Physiology*, 2(4), 2369–2392.
- Ullo, M. F., & Logue, J. S. (2021). ADF and cofilin-1 collaborate to promote cortical actin flow and the leader bleb-based migration of confined cells. *eLife*, 10, e67856.
- Venturini, V., Pezzano, F., Castro, F.C., Häkkinen, H.-M., Jiménez-Delgado, S., Colomer-Rosell, M., Marro, M., Tolosa-Ramon, Q., Paz-López, S., Valverde, M.A., Weghuber, J., Loza-Alvarez, P., Krieg, M., Wieser, S., Ruprecht, V. (2020). The nucleus measures shape changes for cellular proprioception to control dynamic cell behavior. *Science (New York, N.Y.)*, 370(6514), eaba2644.
- Vicente-Manzanares, M., Zareno, J., Whitmore, L., Choi, C. K., Horwitz, A. F. (2007). Regulation of

- protrusion, adhesion dynamics, and polarity by myosins IIA and IIB in migrating cells. *JCB*, 176(5), 573–580. <https://doi.org/10.1083/jcb.200612043>
- Vignjevic, D., Kojima, S., Aratyn, Y., Danciu, O., Svitkina, T., Borisy, G. G. (2006). Role of fascin in filopodial protrusion. *JCB*, 174(6), 863–875. <https://doi.org/10.1083/jcb.200603013>
- Vogel, S. K., Wölfer, C., Ramirez-Diaz, D. A., Flassig, R. J., Sundmacher, K., Schwille, P. (2020). Symmetry Breaking and Emergence of Directional Flows in Minimal Actomyosin Cortices. *Cells*, 9(6), 1432.
- Weems, A.D., Welf, E.S., Driscoll, M.K., Zhou, F.Y., Mazloom-Farsibaf, H., Chang, B.J., Murali, V.S., Gihana, G.M., Weiss, B.G., Chi, J., Rajendran, D., Dean, K.M., Fiolka, R., Danuser, G. (2023). Blebs promote cell survival by assembling oncogenic signalling hubs. *Nature*, 615(7952), 517–525. <https://doi.org/10.1038/s41586-023-05758-6>
- Wegner, A. & Isenberg, G. (1983). 12-fold difference between the critical monomer concentrations of the two ends of actin filaments in physiological salt conditions. *PNAS USA*, 80, 4922–25.
- Wolf, K., Mazo, I., Leung, H., Engelke, K., von Andrian, U. H., Deryugina, E. I., Strongin, A. Y., Bröcker, E. B., Friedl, P. (2003). Compensation mechanism in tumor cell migration: mesenchymal-amoeboid transition after blocking of pericellular proteolysis. *JCB*, 160(2), 267–277.
- Wu, C., Asokan, S. B., Berginski, M. E., Haynes, E. M., Sharpless, N. E., Griffith, J. D., Gomez, S. M., Bear, J. E. (2012). Arp2/3 is critical for lamellipodia and response to extracellular matrix cues but is dispensable for chemotaxis. *Cell*, 148(5), 973–987. <https://doi.org/10.1016/j.cell.2011.12.034>
- Xu, B., Kang, H.-W., Jilkine, A. (2019). Comparison of Deterministic and Stochastic Regime in a Model for Cdc42 Oscillations in Fission Yeast. *Bulletin of Mathematical Biology*, 81, 1268–1302.
- Yamada, K.M. & Sixt, M. (2019). Mechanisms of 3D cell migration. *Nature Reviews Molecular Cell Biology*, 20, 738–752. <https://doi.org/10.1038/s41580-019-0172-9>
- Yoshida, K., & Soldati, T. (2006). Dissection of amoeboid movement into two mechanically distinct modes. *JCS*, 119(Pt 18), 3833–3844. <https://doi.org/10.1242/jcs.03152>
- Young, L. E., Heimsath, E. G., Higgs, H. N. (2015). Cell type-dependent mechanisms for formin-mediated assembly of filopodia. *MBoC*, 26(25), 4646–4659. <https://doi.org/10.1091/mbc.E15-09-0626>
- Yu, Q., Li, J., Murrell, M.P., Kim, T. (2018). Balance between Force Generation and Relaxation Leads to Pulsed Contraction of Actomyosin Networks. *Biophysical Journal*, 115, 2003–2013.
- Zaidel-Bar, R., Cohen, M., Addadi, L., Geiger, B. (2004). Hierarchical assembly of cell-matrix adhesion complexes. *Biochemical Society transactions*, 32(3), 416–420.
- Zaidel-Bar, R., Ballestrem, C., Kam, Z., Geiger, B. (2003). Early molecular events in the assembly of matrix adhesions at the leading edge of migrating cells. *JCS*, 116(22), 4605–4613.
- Zamir, E., & Geiger, B. (2001). Molecular complexity and dynamics of cell-matrix adhesions. *JCS*, 114(20), 3583–3590. <https://doi.org/10.1242/jcs.114.20.3583>
- Zhang, J., Kong, C., Xie, H., McPherson, P. S., Grinstein, S., Trimble, W. S. (1999). Phosphatidylinositol polyphosphate binding to the mammalian septin H5 is modulated by GTP. *Current biology*, 9(24), 1458–1467. [https://doi.org/10.1016/s0960-9822\(00\)80115-3](https://doi.org/10.1016/s0960-9822(00)80115-3)
- Zhang, N., Liu, L., Fan, N., Zhang, Q., Wang, W., Zheng, M., Ma, L., Li, Y., Shi, L. (2016). The requirement of SEPT2 and SEPT7 for migration and invasion in human breast cancer via MEK/ERK activation. *Oncotarget*, 7(38), 61587–61600. <https://doi.org/10.18632/oncotarget.11402>
- Zhao, X., Lei, Y., Zheng, J., Peng, J., Li, Y., Yu, L., Chen, Y. (2019). Identification of markers for migrasome detection. *Cell Discovery*, 5, 1–4. <https://doi.org/10.1038/s41421-019-0093-y>
- Zhovmer, A., Manning, A., Smith, C., Yashavantha, L., Wang, J., Saez, P. J., Cartagena-Rivera, A. X., Singh, R. K., Dokholyan, N. V., Tabdanov, E. D. (2022). Septin-Mediated Mechanobiological Reprogramming of T Cell Transmigration and 3D Motility. *bioRxiv*, 476840.

## VITA

The author, Asia Paguntalan, was born in Greenwood, SC on February 22, 1998 to Carol and John Paguntalan. Her enthusiasm for science began in 2003 when her brother, Tim, was born with Down's Syndrome, a genetic disorder caused by trisomy of the 21<sup>st</sup> chromosomal pair. From 2014 to 2016, Asia attended the South Carolina Governor's School for Science and Mathematics, where she specialized in molecular genetics and contributed to the foundation of an in-house research program that continues to find success today. While at the Governor's School, Asia conducted research with the Wang Lab in the Center for Genome Sciences and Systems Biology at Washington University in St. Louis, leading to her first publication.

Following high school, Asia attended Clemson University Honors College, where she earned a Bachelor of Science degree in Biochemistry, with minors in Genetics and Spanish Language Arts. At Clemson, Asia conducted research in the Birtwistle Lab, working towards a Departmental Honors thesis in Chemical and Molecular Engineering. After graduating in 2020, during the first lockdown of the COVID-19 pandemic, she spent one year teaching remotely as an adjunct biology instructor at Piedmont Technical College and volunteering as a math and science tutor for local high school students.

In the fall 2021, Asia matriculated into the Loyola University Chicago Stritch

School of Medicine Master's Program, and began her graduate education in Biochemistry and Molecular Biology under the mentorship of Dr. Patrick Oakes and Dr. Jordan Beach in the Department of Cell and Molecular Physiology. After completion of her graduate studies, she will remain in the Chicago area, working as a research assistant before pursuing a career in the biotechnology industry.

